8-HYDROXYQUINOLINE BASED SMALL MOLECULE INHIBITORS OF THE ENDOPROTEASE RAS CONVERTING ENZYME

by

ROBERT A. KUTLIK

(Under the Direction of Timothy M. Dore)

ABSTRACT

Ras converting enzyme (Rce1p) has been the focus of research due to the prevalence of Ras mutants in cancerous tissues. In vivo studies have shown inactivation of Rce1p causes the mislocalization of Ras; therefore inhibition of Rce1p might have applications in cancer treatment. Several inhibitors of Rce1p have been identified, including 4-((8-hydroxyquinolin-7-yl)(phenyl)methylamino)benzoic acid. The 8-hydroxyquinoline motif found in this molecule has been used extensively for its metal binding properties. The mechanism of Rce1p has been the subject of some debate, although, it is likely a zinc metalloprotease. Described here are several analogous molecules that display stronger Rce1p inhibition and looser zinc binding.

INDEX WORDS: Ras converting enzyme, Rce1, 8-hydroxyquinoline, small molecule inhibition

8-HYDROXYQUINOLINE BASED SMALL MOLECULE INHIBITORS OF THE ENDOPROTEASE RAS CONVERTING ENZYME

by

ROBERT A. KUTLIK

BSCHEM, University of Georgia, Athens Ga, 2007

A Thesis Submitted to the Graduate Faculty of The University of Georgia in Partial Fulfillment of the Requirements for the Degree

MASTER OF SCIENCE

ATHENS, GEORGIA

2010

8-HYDROXYQUINOLINE BASED SMALL MOLECULE INHIBITORS OF THE ENDOPROTEASE RAS CONVERTING ENZYME

by

ROBERT A. KUTLIK

Major Professor:	Timothy M. Dore
Committee:	Robert S. Phillips
	Walter K. Schmidt

Electronic Version Approved:

Maureen Grasso
Dean of the Graduate School
The University of Georgia
May 2010

DEDICATION

I would like to dedicate this work to my family and the memory of my younger brother.

May the joy that he brought to others while he suffered with cancer serve as a reminder:

No matter how bad things are, there is always something to be happy about.

ACKNOWLEDGEMENTS

I would like to thank my advisory committee for their support, especially my major advisor Dr. Timothy M. Dore whose continued encouragement and insistence helped drive my research forward. I would also like to thank Dr. George Majetich who offered advice and encouragement cheerfully whenever it was asked of him. I would also like to acknowledge Dr. Grant Walkup for his help with the suggestion of methodology for the metal-binding experiments and his help with the derivation of equations. Many thanks to Dr. Surya Manandhar who assisted me with the fluorescence based assay and performed many of the assays.

I would like to thank the University of Georgia and the Department of Chemistry for giving me the opportunity to perform this research. Last but not least I would like to thank all of my labmates. It is very fortunate when you can enjoy your work and the people who work with you.

TABLE OF CONTENTS

Page

CHAPTER 1

INTRODUCTION

RCE1P AND RAS: INHIBITION OF THE MATURATION OF RAS

Many proteins are translated from RNA in an inactive form which requires further modification to become biologically active. This post-translational modification enables spatio-temporal control within the cell. In some cases, the post-translation modification is necessary to remove a portion of the protein that prevents activity. In other cases, the protein modification allows for proper cellular localization. The processes by which inactive protein precursors are modified have become interesting targets for drug development.[1-2]

Cancer therapeutics and cancer drug targets are in high demand. One target is the Ras GTPase, a membrane bound signaling protein, found on the cytosolic side of the plasma membrane.[3-4] The high frequency with which Ras mutations are found in cancerous cells can be attributed to its structure and function.[3] As an integral part of intercellular signaling, Ras helps mediate the cell cycle, and the loss of this control can lead to oncogenesis. Specifically, Ras binds and activates the Raf kinase which turns on gene expression through the action of MAP kinase cascade.[5] The MAP kinase cascade involves the sequential phosphorylation of proteins, including nucleus localized transcription factors. Once activated these transcription factors induce the expression of their respective genes.

Ras proteins belong to a superfamily of small GTPases known as G proteins.[6] G proteins mediate the amplification of signal in response to extracellular stimuli. G proteins exist in two

states; a GDP-bound inactive form, and a GTP-bound active form.[5, 7] In its GDP-bound state Ras is associated with Grb and Sos proteins that bridge it to a transmembrane receptor tyrosine kinase (RTK) protein (Figure 1).[5] Upon binding of a stimulus to the extracellular portion of a receptor tyrosine kinase (RTK), the GDP-bound Ras is converted to a GTP-bound Ras, and thus activated.[5] The mechanism by which Ras exchanges GDP for GTP is analogous with other G proteins and is well understood.[7] Once in its GTP bound active form, Ras activates several downstream proteins that regulate the cell cycle.[5]

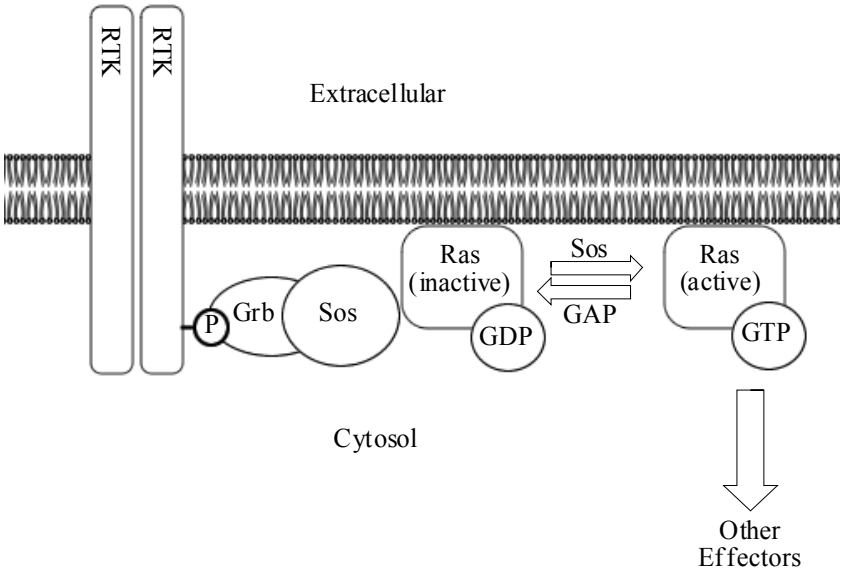

Figure 1. Ras activation pathway. Ras is activated by the action of Sos, which exchanges the bound GDP for GTP. Sos and Grb bridge Ras to a receptor tyrosine kinase (RTK) which receives extracellular signals.

The naturally occurring hydrolysis of GTP to GDP in Ras is approximately fifty times slower than other G proteins.[8] The slower rate of GTP hydrolysis by Ras gives the effect of a constitutively active state. Mutagenesis of Ras has revealed essentially two residues that can be linked to the constitutively active state, Gly^{12} and Gln^{61}.[8-9] Gly^{12}, when mutated to alanine, causes enough steric repulsion that Ras GTPase activating protein binding is not favorable. With the mutation of Ras Gly^{12} to alanine, the constitutively active state of Ras can lead to

oncogenesis.[8] Given these findings, the prevalence of Ras in human cancers is unsurprising.[8] To effectively target Ras both its structure and function must be better understood.

Ras also belongs to a large family of proteins known as CaaX proteins. CaaX proteins are named for their characteristic "CaaX box" at the C-terminus.[3-4, 10-11] The CaaX box is comprised of a cysteine residue "C," typically followed by two aliphatic residues "aa," and one of several amino acid residue "X."[3-4, 10-11] In the case of H-Ras the CaaX sequence is CVLS.[12] In N-Ras (CVVM) and both K-Ras variants (CIIM or CVIM) "X" is methionine.[12] The CaaX box is modified post-translationally in three sequential steps that enable the proper localization of Ras (Figure 2).[13-17] Ras is first isoprenylated by one of two enzymes farnesyl transferase (FTase) or geranylgeranyl transferase (GGTase), which attach either farnesyl or geranylgeranyl to the sulfur of the cysteine residue of the CaaX box, respectively.[13] In an ER-localized process Ras converting enzyme (Rce1p) cleaves the aaX portion of CaaX proteins.[14-15] In a final step isoprenylcysteine methyltransferase (ICMT) methylates the isoprenylated cysteine carboxylate residue.[16-17] Ras is then transported to the cytosolic side of the plasma membrane by an unknown mechanism.[18-20]

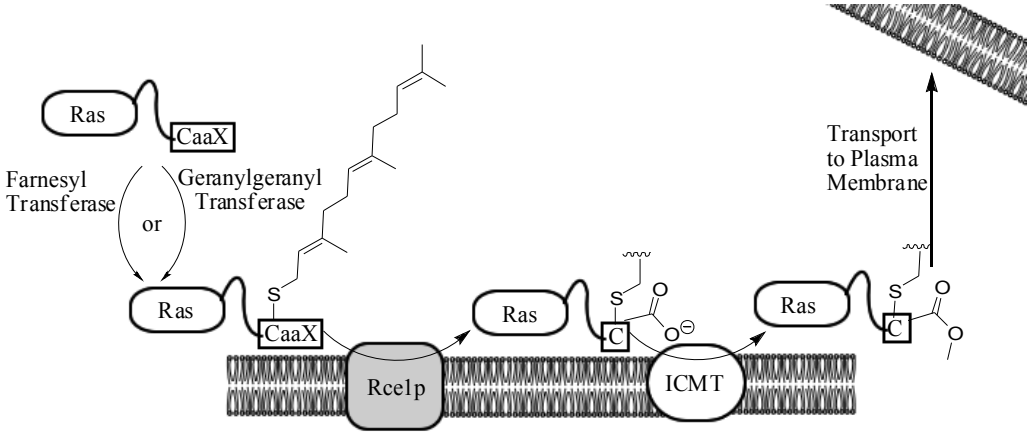

Figure 2. The post-translation modification of Ras is necessary for the proper localiztion of Ras. The mechanism by which Ras is transported to the plasma membrane is not well understood.

The reliance of Ras proteins on isoprenylation has led to the development of farnesyl transferase inhibitors (FTI).[21] However, in the absence of farnesyl transferase, K-Ras and N-Ras are geranylgeranylated by GGTase and remain active.[12] In response to this discovery, dual prenylation inhibitors (DPI) that inhibit both FTase and GGTase have been developed.[21] However, there are other CaaX proteins that require isoprenylation for full activity and complete inhibition of isoprenylation can lead to unwelcome side effects.[22-24] For instance, FTI's also inhibit prelamin A processing, and loss of lamin A expression has been linked to muscular dystrophy.[22-24] Nonetheless, FTI's and DPI's have proven value as potential therapeutics as demonstrated by some phase two and three clinical trials.[2, 21, 25] The use of FTI's and DPI's will be limited due to the inhibition of other proteins such as prelamin A.

ICMT is the only known isoprenyl carboxymethyl transferase and its inhibition would be expected to produce similar side effects to FTI's due to its lack of substrate specificity.[11, 16-17, 26] In yeast, the activity of ICMT is not necessary for cell viability.[27] Genetic manipulation studies have shown that the lack of ICMT function prevents the localization of a number of essential CaaX proteins such as Rac, Rho, and lamin B.[3-4, 28] Studies of ICMT inhibition have been limited to substrate mimetics, making it difficult to differentiate between ICMT inhibition and upstream inhibition, or a combination of the two.[3-4]

Rce1p is an interesting target for inhibition. Although Ste24p and Rce1p have some overlapping substrate specificity mammalian Ras maturation is likely due to Rce1p.[10, 14, 29-33] In Rce1p-deficient cells, Ras is partially mislocalized to the cytosplasm.[30, 34] Rce1p deficient cells have also been shown to be more sensitized to FTI's.[34] This observation has implications for the viability of mixed cancer therapies.

The development of Rce1p inhibitors has been complicated by several properties of Rce1p itself. First, as a transmembrane protein, it is a strenuous task to purify an active form of Rce1p.[35] Without a pure crystalline form of Rce1p it is difficult to solve the three-dimensional structure of Rce1p. Also, the mechanism for Rce1p is still uncertain, which complicates attempts at target oriented drug development.[36-38] As a result of these limitations progress in the development of Rce1p inhibitors has been slow.

Crystal structures can provide substantial insight into both the structure and mechanism of a protein and are often used as aids in the development of inhibitors.[39-40] Docking programs build off of the crystal structure and can enable screening of libraries of compounds in silico as well as the targeted refinement of lead compounds. In the case of Rce1p, a three-dimensional structure has yet to be obtained. This is partly due to the nature of Rce1p, which is a transmembrane protein with an active site presumably located on the cytosolic side of the ER of the cell.[35] Bioinformatics hydropathy plot based predictions suggest that Rce1p contains seven transmembrane helices.[35] The inclusion of several transmembrane spans is unusual for a protease.[35] Also, the proposed active site residues reside in proposed transmembrane spans, which is also atypical for a protease.[35] The uncertainty in the exact structure of Rce1p makes it difficult to determine the mechanism of action.[35-38, 41]

Rce1p was first hypothesized to function as a cysteine protease, and studies showing a highly conserved Cys^{251} residue in a proposed transmembrane helix supported this hypothesis.[36-38] The inhibition of Rce1p by classic cysteine protease inhibitors, discussed below, also supported this hypothesis.[37-38, 42] The lack of inhibition of Rce1p by metal chelators provided evidence that

Rce1p was not a metalloprotease.[38] So, for several years cysteine protease type inhibitors were developed for the inhibition of Rce1p.[37, 42-43]

Cysteine proteases have a well determined mechanism (Figure 3).[9] The classic type of cysteine protease inhibitors are substrate mimetics containing a halomethylketone.[9] These inhibitors take advantage of the nucleophilic nature of the active cysteine residue in order to form a covalent bond that results in irreversible inhibition (Figure 4). The halogen present is typically a chlorine, although some fluoromethylketones have been used. Such inhibitors have seen wide spread success as tools for studying cysteine proteases and other mechanistically related proteases.

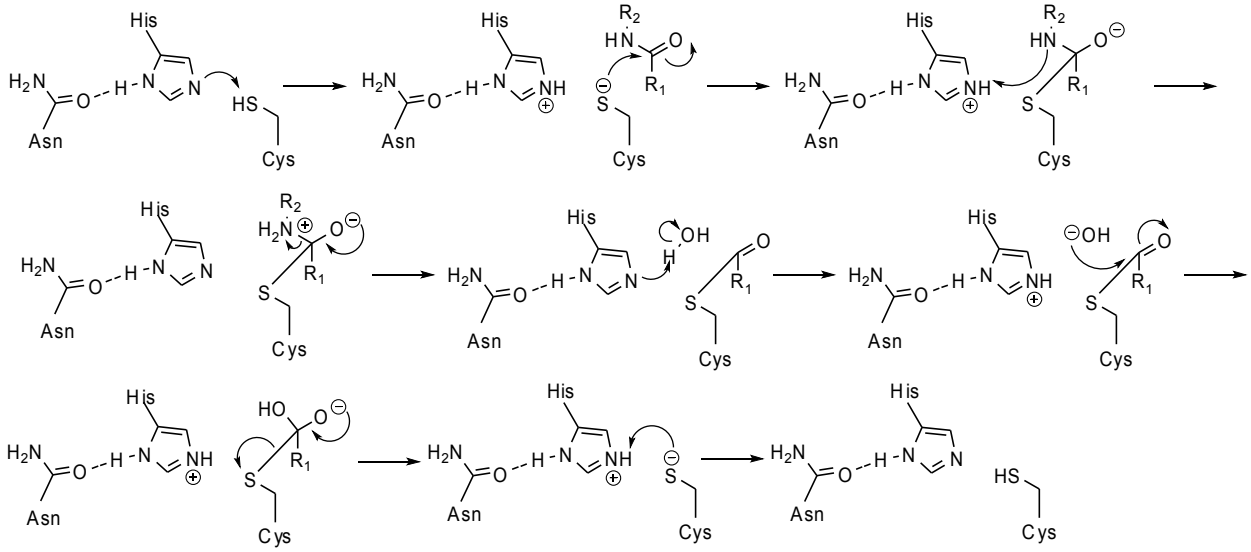

Figure 3. The known mechanism of cysteine proteases. The free thiol of the essential active site cysteine residue acts as a nucleophile and attacks the carbonyl carbon of the peptide substrate. Histidine and aspargine help to delocalize charge and stabilize the transition states.

More recent mutational studies have shown that the only conserved Cys^{251} is not necessary for the function of Rce1p.[35] Instead, it is proposed that a glutamate and two histidine residues (Glu^{156}, His^{194}, and His^{248}) are part of the active site.[35] The related metalloprotease

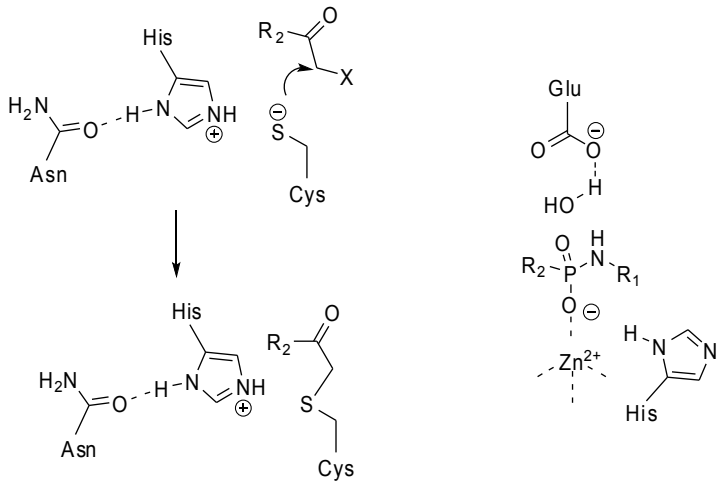

Figure 4. A halomethylketone(left) and a phosphonamidate(right) inhibiting a cysteine protease and a zinc metalloprotease respectively. The cysteine protease is irreversibly inhibited, while the zinc metalloprotease is competitively inhibited.

Ste24p also contains highly conserved histidine and glutamate residues, which are part of a putative HExxH zinc-coordinating motif.[14] Other residues thought to be necessary for optimal activity of Rce1p include Glu[157], Tyr[160], Phe[190], and Asn[252].[35] If the loss of activity from these mutations is due to a structural or conformational change and not the loss of a critical active site residue, could be determined by a crystal structure of the active enzyme.

The accepted mechanism of zinc metallo-proteases differs from that of cysteine proteases, mainly in that there is never a covalent bond formed between the enzyme and the substrate (Figure 5).[44] This lack of a covalently linked intermediate makes it unlikely that irreversible inhibition would be observed with a substrate mimetic. The covalently linked intermediate is essential for the inhibition of cysteine proteases by halomethylketones (Figure 4). Instead of a cysteine side chain acting as a nucleophile, a nucleophilic water molecule is present in the active site.

Inhibitors of zinc metallo-proteases have used substrate mimetics as inhibitors much like cysteine protease inhibitors.[1, 44-45] A typical substrate mimetic for a zinc metalloprotease contains

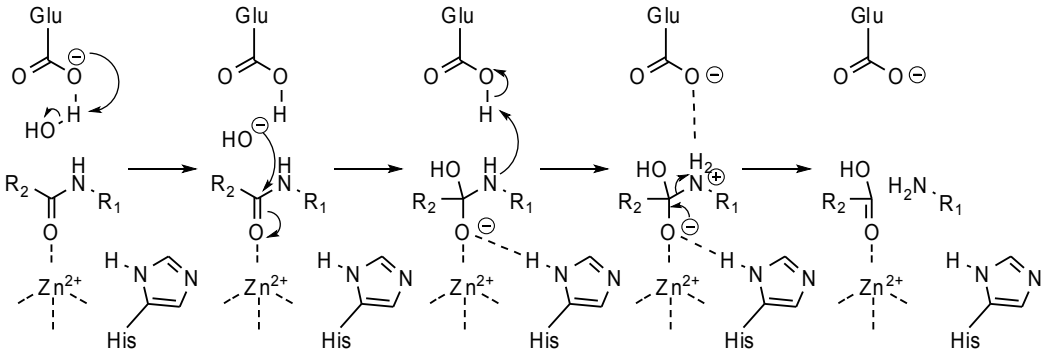

Figure 5. One of two proposed zinc metalloprotease mechanisms. The second proposed mechanism is similar to the one shown. Both mechanisms have zinc coordinating the carbonyl oxygen of the peptide substrate, with water acting as the nucleophile in both mechanisms. The mechanism not shown differs in the order of steps, and in the other enzyme residues (not shown) that coordinate with the substrate.

a strong metal binding moiety such as a phosphonamidate (Figure 4).[40, 44] Cysteine protease inhibitors take advantage of the nucleophilic cysteine to irreversibly inhibit the protease, whereas zinc metalloproteases cannot utilize this mechanism due to the lack of a covalently linked intermediate (Figure 4).[44] Instead, the substrate mimetics exploit the stability of a phosphonamidate oxygen to zinc bond.[44] This ionic interaction is strong enough for the phosphonamidate to be retained in the crystal structure of the zinc metalloprotease thermolysin from *Bacillus thermoproteolyticus*.[44]

Aside from substrate mimetics, small molecule inhibitors for zinc metalloproteases have been developed.[1, 46] Many metallo-protease inhibitors utilize a strong metal chelator.[1, 46] The design of many inhibitors is based on the hypothesis that the metal chelating moiety in the inhibitor will block the active site metal ion and prevent activity.[38] The non-chelating portions of the molecule bind to specific parts of the enzyme to increase inhibitor specificity.[1, 40, 44] Several metal chelators such as ethylenediaminetetraacetic acid (EDTA), ethylene glycol tetraacetic acid (EGTA), and tetrakis(2-pyridylmethyl)ethylenediamine (TPEN) have been shown to inhibit metalloproteases in vitro.[38] Rce1p is not inhibited by EDTA, EGTA, or TPEN; however, Rce1p

is inhibited by zinc and copper at micromolar concentrations.[38] As a metalloprotease, inhibition of Rce1p by known metal chelators was expected, but was not observed.[38] Previously identified inhibitors of Rce1p fall into two basic categories of small molecule inhibitors and peptidomimetic inhibitors (Figure 6).[36-38, 42-43, 47-50] Peptidomimetic inhibitors can be further divided into peptido (acyloxy)methyl ketones (AOMKs), farnesylated peptides, unnatural peptides, or a combination of the three.[36-38, 42-43, 48] TPCK, BFCCMK and UM96001 represent chloromethyl ketone inhibitors of Rce1p. Inhibition of Rce1p by TPCK is substrate dependent and when the substrate in the assay is altered there is no inhibition.[51] The inhibitors RPI and BFCCMK are farnesylated peptides. Barangcadoic acid A and rhopaloic acid A are natural product inhibitors of Rce1p which contain a farnesyl group. The other inhibitors (MSA, pHMB, pHMS, NPPI-A, NPPI-B, and NPPI-C) all contain metal binding motifs that may be responsible for their inhibition. Consistent reporting of inhibition constants for the listed inhibitors is not available, and IC_{50} values or single point inhibition data are available (Table 1). The specificity of the inhibitors also ranges.

Table 1. Inhibition data of previously described inhibitors.

Molecule	IC_{50}	% Activity, Inhibitior Conc.
TPCK	-	6 %, 300 μM
PHMB, pHMS	-	1 %, 22 μM
MSA	-	1%, 22 μM
AOMKs	-	10 – 100 %, 100 μM
RPI	103 nM	-
BFCCMK, UM96001	(5 μM), (5 μM)	-
Peptides **1-5**	3.3 – 17.6 μM	-
Barangcadoic acid A	~ 25 μM	-
Rhopaloic acid A	~ 25 μM	-
NPPI-A, NPPI-B, NPPI-C	14 μM, 7 μM, 7, μM	-

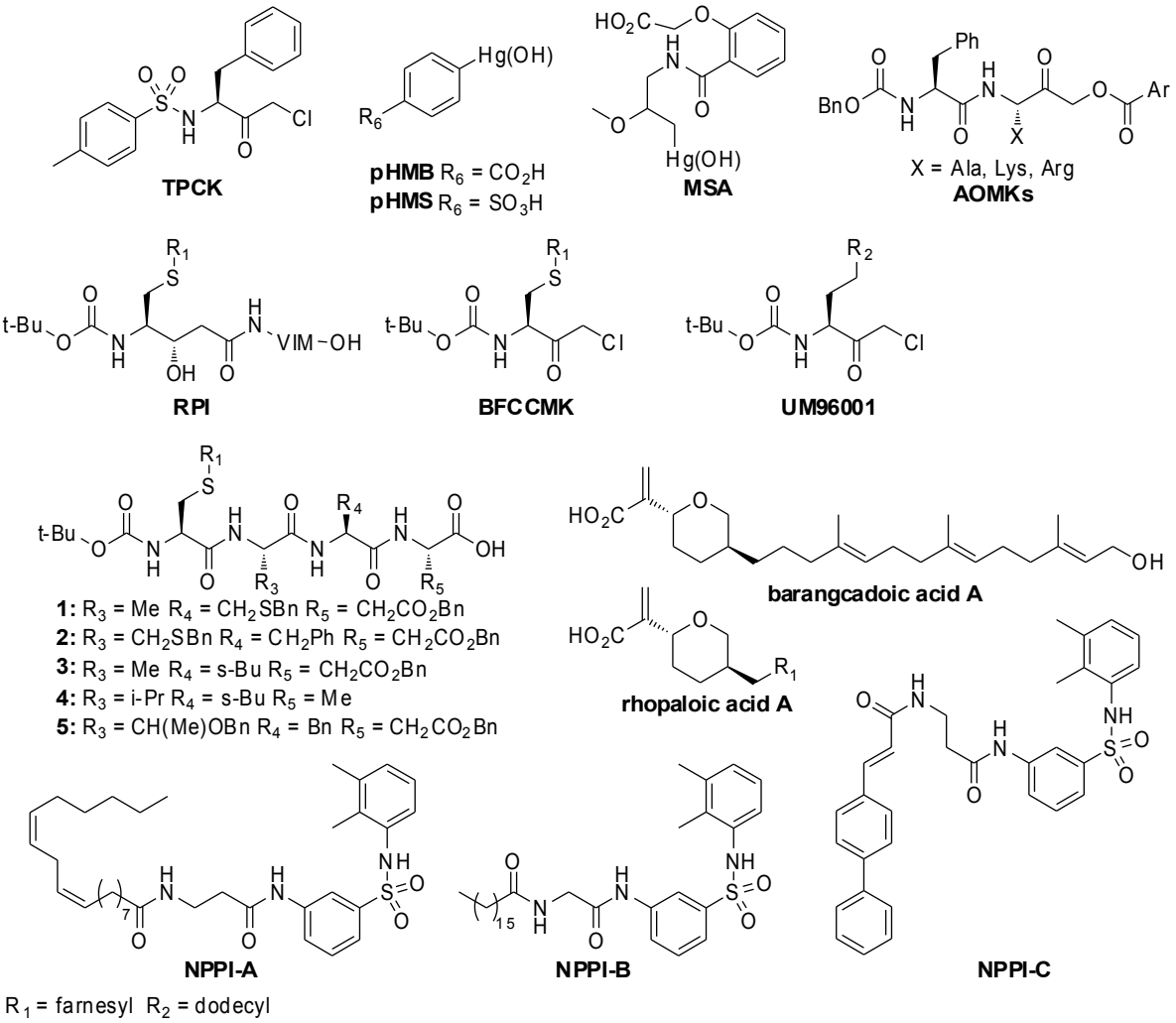

Figure 6. Small molecule and peptidomimetic inhibitors of Rce1p.

To enhance specificity, the development of small molecule inhibitors is more favorable than peptidomimetics.[47] A recent assay of the National Cancer Institutes (NCI) Developmental Therapeutics Program (DTP) diversity set library revealed nine small molecule inhibitors (Figure 7).[47] An initial fluorescence assay, the details of which will be discussed later, identified forty-six potential inhibitors; these compounds were then screened against an alternative substrate in an orthogonal assay revealing nine compounds to inhibit Rce1p.[47] The **a**-factor assay was used to limit the possibility that the inhibitors found were assay specific inhibitors as has been shown for

TPCK.[51] As would be expected for metalloprotease inhibitors, all but one (NSC 67485) of the nine compounds contained a metal binding motif.[47]

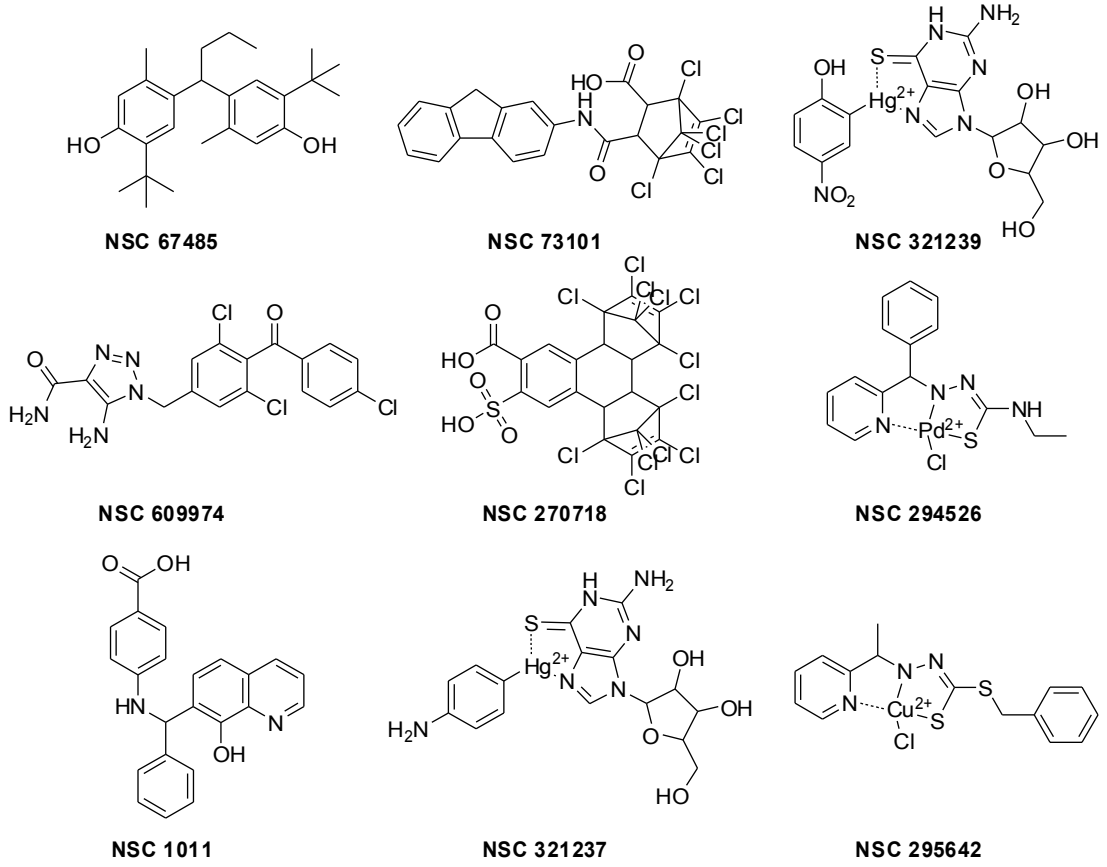

Figure 7. The structures of the nine inhibitors of Rce1p determined by the fluorescence and **a**-factor assays.

Of the nine inhibitors, four compounds (NSC 321239, NSC 294526, NSC321237, and NSC 295642) were deemed undesirable for further investigation for two primary reasons: first, the transition metals present in the molecules are likely toxic, and second, the same molecules have appeared in other unrelated high throughput screens.[47] This suggests that the molecules would be non-specific in vivo inhibitors and are thus poor candidates for the basis of drug design.[47]

Of the remaining five compounds, NSC 67485 was commercially available and was purchased in order to verify the assay hit. The remaining four molecules were to be re-synthesized in order to produce high purity samples to verify the hits from the initial assay. Another of the compounds, NSC 609974, was the target of "Synthesis of L-651582."[52] NSC 609974 has been the subject of several clinical trials for the treatment of tumors; however, adverse side effects have limited its use.[53-54] The anti-oncogenic mechanism of NSC 609974 is not clear; however, its activity in this assay suggests Rce1p might be involved. Inhibition of receptor-operated calcium channel-mediated calcium influx by NSC 609974 is known.[54-58] Two similar compounds, NSC 73101 and NSC 270718, were outside the scope of this research. NSC 73101 was also identified in a screen for inhibitors of poxvirus type I topoisomerase.[59] Thus the primary focus of this research was the synthesis of 4-((8-hydroxyquinolin-7-yl) (phenyl)methylamino)benzoic acid (NSC 1011) and analogous molecules (Figure 7).

In summary, the use of NSC 1011 for Rce1p inhibition can be improved in three ways. New NSC 1011 analogous molecules with better metal binding might lead to better inhibition of Rce1p. Protecting the free carboxylic acid of NSC 1011 will likely increase its cell permeability. The lengthy synthesis of NSC 1011 may be improved to enable the production of other analogous molecules for testing.

CHAPTER 2

RESULTS AND DISCUSSIONS

PART 1: SYNTHESIS OF INHIBITORS

Despite over sixty years since the original synthesis of NSC 1011 (**1**) by the Betti reaction (Figure 8), no alternate synthetic routes have been published.[60-63] The original synthesis requires thirty-five days in room temperature ethanol, an undesirable length of time.[60] Ethyl 3-(((8-hydroxyquinolin-7-yl)(phenyl)methyl)amino)benzoate was also synthesized at the same time as NSC 1011.[60] The analogous synthesis suggests that a less protic reactant and a higher pH solution could provide a faster reaction time.[60] Of the other known analogs of NSC 1011, the A-ring and C,D-ring analogs are among the most explored, with few modifications of the B-ring (Figure 8).[47]

NSC 1011 and a number of analogous structures can be synthesized by similar conditions to the original Betti reaction (Figure 9). Although initially low yielding, adding a large excess of 8-hydroxyquinoline to the reaction mixture improves yield and helps drive the reaction to completion. Nicotinaldehyde and picolinaldehyde react as much as seven times faster than other aromatic aldehydes. It is thus proposed that pyridinyl and other basic aldehydes should also yield faster reaction rates.

Based upon the original synthesis (Phillips, 1956) six analogs of NSC 1011 have been produced (Figure 10). These analogs include: 4-((8-hydroxyquinolin-7-yl)(pyridin-2-yl)methylamino)benzoic acid (**2**), 4-((4-cyanophenyl)(8-hydroxyquinolin-7-

yl)methylamino)benzoic acid (**3**), 4-((8-hydroxyquinolin-7-yl)(*p*-tolyl)methylamino)benzoic acid (**4**), 4-((4-bromophenyl)(8-hydroxyquinolin-7-yl)methylamino)benzoic acid (**5**), 4-((8-hydroxyquinolin-7-yl)(pyridin-3-yl)methylamino)benzoic acid (**6**), and 4-((4-fluorophenyl)(8-hydroxyquinolin-7-yl)methylamino)benzoic acid (**7**) (Figure 10). The first of these analogs isolated was **2** followed by **3**. The initial purification of **3** from other undesirable by-products required HPLC followed by recrystallization from ethanol. Reverse phase HPLC was used instead of the more common normal phase column chromatography because it was shown that **3** may decompose over TLC conditions. It is not clear why recrystallization was necessary and HPLC was unable to separate **3** from other compounds in the mixture.

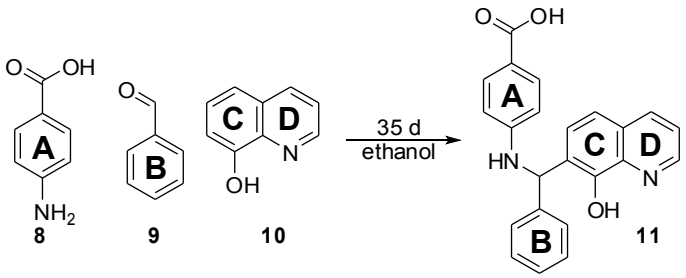

Figure 8. Original synthesis from Phillips, 1956. The rings have been labeled in both the starting materials and the products. Variation of the B-ring could be achieved via the use of different aldehydes.

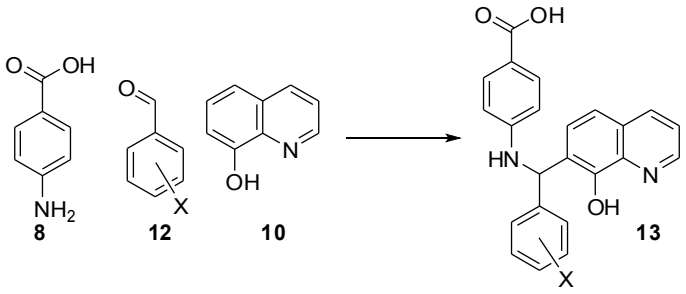

Figure 9. Synthetic pathway used for the production of analogs of NSC 1011.

The next two compounds were isolated from the filtrate of the reaction mixture several months after the filtering of the mixture. The filtrate contained excess unreacted 8-

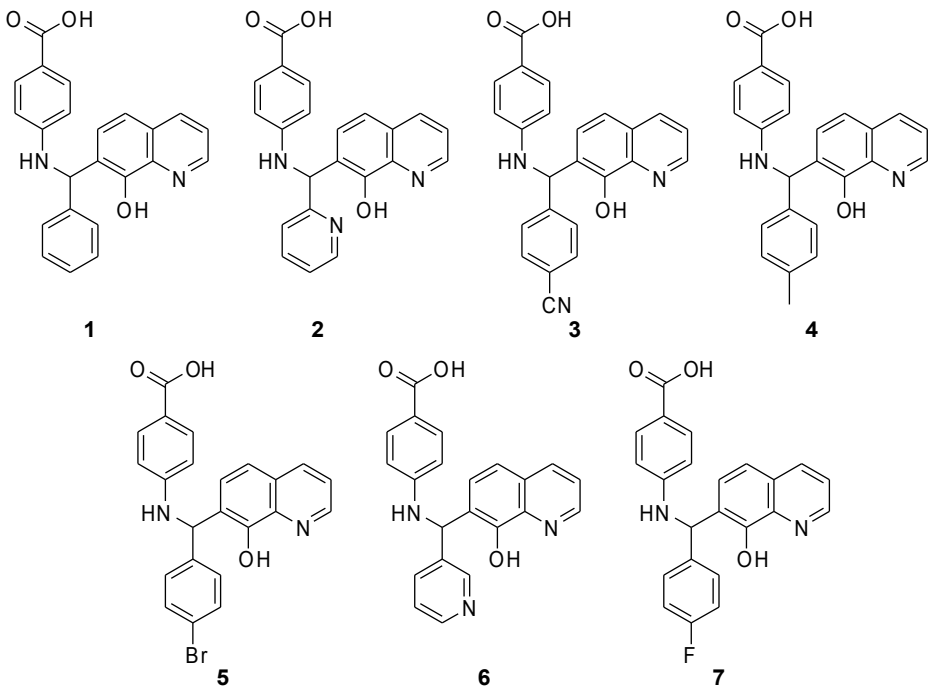

Figure 10. The structures of the analogs of NSC 1011 that were synthesized.

hydroxyquinoline and fewer equivalents of *p*-aminobenzoic acid and the corresponding aromatic aldehyde. The precipitate in these solutions was the desired compound and of high purity. To test the hypothesis that excess 8-hydroxyquinoline drives the Betti reaction to completion, several reactions were started with a large excess of 8-hydroxyquinoline. Three of the reactions showed products (**3**, **6**, and **7**) that required little or no purification beyond filtering and washing with ethanol. This supports the hypothesis that an excess of 8-hydroxyquinoline in a Betti reaction will drive the reaction further to completion. It has been shown that the excess reactant increases the reaction rate. The three products synthesized by this method include **3**, **6**, and **7**. In the case of both **3** and **7** recrystallization from acetonitrile was necessary to remove excess 8-hydroxyquinoline.

Although the Betti reaction was accomplished with nicotinaldehyde and picolinaldehyde to form **6** and **2** respectively, the reaction with isonicotinaldehyde has not been completed. The

Schiff base, *trans*-4-(pyridin-3-ylmethyleneamino)benzoic acid (**14**), and the NSC 1011 analogs **2** and **6** are all soluble in both methanol and dimethylsulfoxide (DMSO). However, the product from the reaction of isonicotinaldehyde and *p*-aminobenzoic acid is insoluble in both solvents. The product, *trans*-4-(pyridin-4-ylmethyleneamino)benzoic acid (**15**), is soluble in acidic DMSO, and an NMR obtained in deuterated DMSO with minimal hydrochloric acid shows resonances that are consistent with **15**. Based upon the solubility of **15**, the Betti reaction using isonicotinaldehyde may be incompatible with an ethanol solvent.

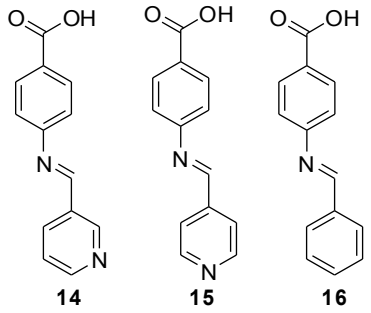

Figure 11. Structures of the Schiff Bases **14**, **15**, and **16**.

Other attempts to synthesize NSC 1011 or NSC 1008 via other synthetic pathways for a proof of concept have been attempted but not completed. Thus far there are two proposed methods (Figure 12) by which NSC 1011 and analogs could potentially be synthesized. The first uses the Schiff base intermediate, which can be readily formed, and is presumably present in the Betti reaction. The second pathway attempts to substitute 8-hydroxyquinoline at the seven position.

The formation of the Schiff base (**16**) of any of the aromatic aldehydes and *p*-aminobenzoic acid occurs readily and precipitates out of ethanol at room temperature. The problem with the synthetic pathway arises when trying to react the Schiff base with 8-hydroxyquinoline. Several attempts have been made using different conditions to form NSC

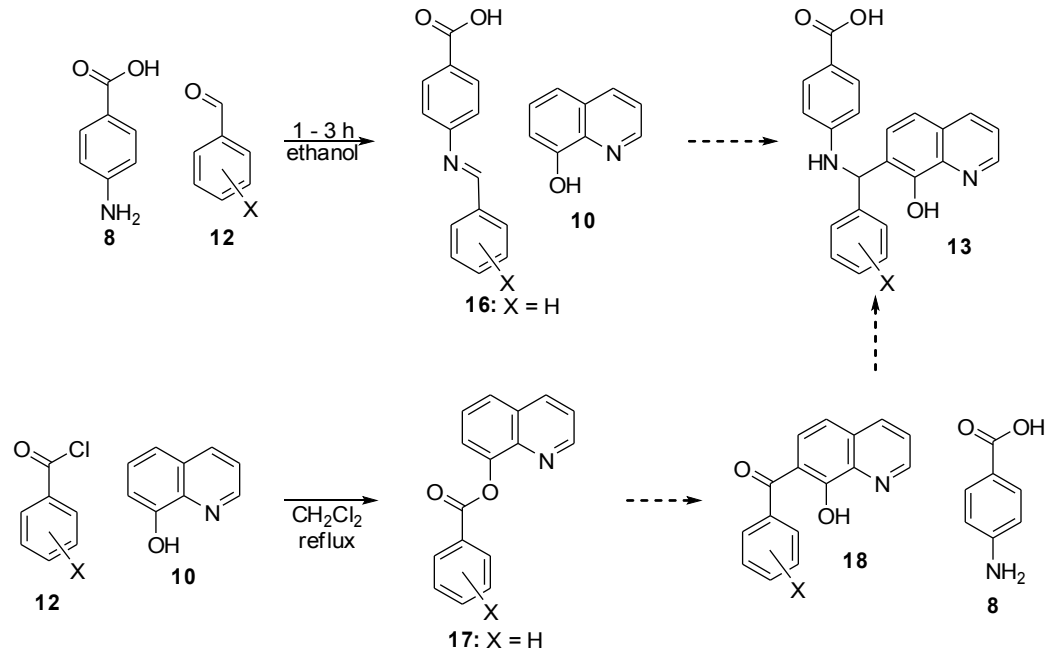

Figure 12. Possible alternate routes for the synthesis of NSC 1011 and analogs.

1011 and NSC 1008 by this method, with no success. Deprotonation of the oxygen of 8-hydroxyquinoline with sodium hydride followed by treatment with the corresponding Schiff base resulted in no reaction. Also, protected 8-hydroxyquinoline treated with excess strong base (*n*-butyl lithium or *t*-butyl lithium) followed by Schiff base yielded no desired product.

Attempts to substitute the seven position with a B-ring benzyl ketone have not yielded the desired products. Two methods to achieve the substitution include the Fries rearrangement and the photo-Fries rearrangement.[64-65] Both reactions require the quinolin-8-yl benzoate (**17**), which is formed in a reaction of benzoyl chloride and 8-hydroxyquinoline. Trouble arises when trying to complete either of the Fries reactions as neither reaction yielded the desired product.

PART 2: NSC 1011 AND ANALOGS AS METAL BINDING LIGANDS

Coordination chemistry is a branch of inorganic chemistry that deals with the interaction of transition metals and ligands. Ligands are molecules that "bind" metals via donation of

electrons into the d-orbitals of the metal atoms. The ability of a ligand to coordinate with a specific metal depends on several factors; including the geometry of the metal and the size of the ligand. NSC 1011 contains the well studied metal binding motif of 8-hydroxyquinoline.[66-69] Increasing the metal binding affinity in NSC 1011 analogs might also lead to increased inhibition of Rce1p provided that the inhibitor binds to the active site.

The metal binding properties of several molecules have been determined via titrations monitored by different means of spectroscopy.[70-72] The basis for this sort of analysis is that binding of a metal to a molecule significantly alters the electronic properties of that portion of the molecule.[70-72] If the metal coordinating portion of the molecule absorbs light in the UV-Vis region, then the changes in the electronic state of the molecule can be observed by UV-Vis spectroscopy.[70] It should also be possible to observe changes in a molecule by other spectroscopic methods given the structural and electrostatic changes that occur during metal binding. For instance, it has also been observed that metal chelation properties can be elucidated from changes in the ^{1}H-NMR spectra of organic molecules; however, this method would be significantly more expensive and time consuming.[71-72] Therefore, for the analysis of aromatic molecules, UV-Vis absorbance and fluorescence spectroscopy remain the methods of choice for measuring metal to ligand binding.

To minimize error in the concentration of the metal, it is common to use a competing metal ligand. The competing ligand, with a known metal binding dissociation constant, is used in excess of the ligand being measured to produce a more accurate measurement of the free metal concentration. Using this method, the exact binding dissociation constants for several compounds with a variety of different metals have been determined.[73]

Another important consideration for the study of metal binding via any method is the existence of only two states for the ligand.[74] The ligand must exist in only a metal-bound and a metal-free state, and with only one stoichiometric ratio.[74] The presence of an isosbestic point suggests that the measurements are dependent upon only two states. It is unlikely that more than two states would produce an isosbestic point.[74] Thus, the lack of an isosbestic point suggests either there are more than two binding states of the ligand, or something other than metal binding is being measured.[74]

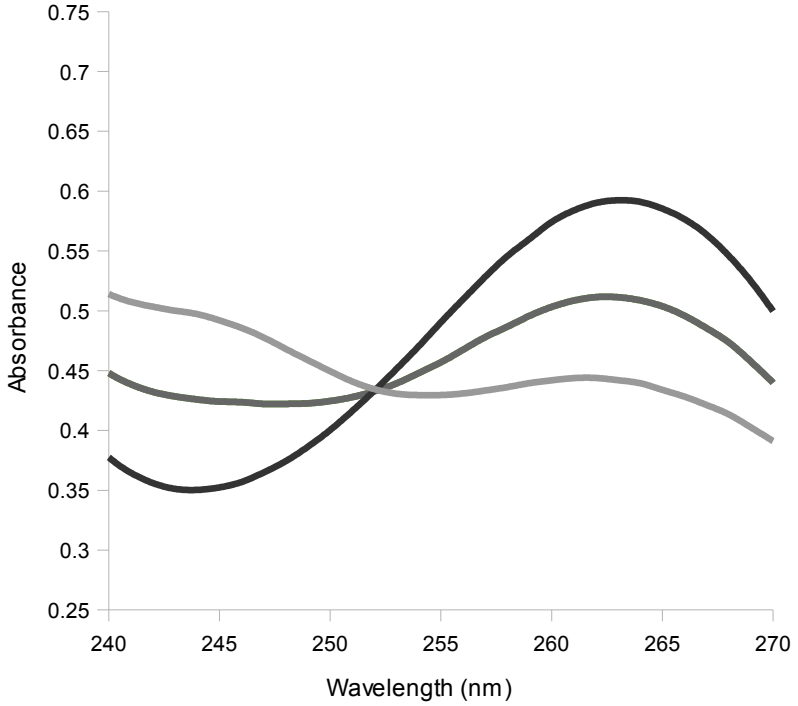

Figure 13. Example isosbestic point exhibited by three spectra. If no isosbestic point is observed and a spectral change is observed then a reaction occurred but either the stoichiometry of the reaction is not constant, or more than one reaction may have occurred.

Based upon the initial hypothesis that increased metal binding would increase the inhibition of Rce1p, the metal binding properties of NSC 1011 (**1**) and compounds **2 – 7** were determined. Using a UV-Vis spectrometer to monitor the changes in absorption during the

titration, several metals (zinc, calcium, magnesium, and manganese) were studied. As was expected the binding affinity of the analogs differed from analog to analog.

Plots of the percent change in absorbance (Equation 1) versus log of the concentration of free zinc were prepared for each sample from the UV-Vis absorbance data obtained.

$$Percent\,Change\,Absorbance = (A - A_o)/(A' - A_o) \qquad \text{Eq.1}$$

For the calculation of the percent change in absorbance at a chosen wavelength: A is the absorbance of the solution, A_o is the absorbance for the lowest absorbing solution, and A' is the absorbance for the highest absorbing solution. Zinc concentration was varied by combining a zinc containing solution and a metal free solution. Both working solutions contained identical concentrations of buffer solution, the competing ligand iminodiacetic acid (IDA), and the analog being studied. The concentration of free zinc in the solution could be determined based upon the total free zinc and the competing ligand concentration (Equation 2).

$$M_f = M_t - \left[\frac{(K_d + M_t + L_t) - \sqrt{(K_d + M_t + L_t)^2 - 4\mathrm{M}_t L_t}}{2} \right] \qquad \text{Eq.2}$$

Where M_f is the free metal in solution, M_t is the total metal in solution, K_d is the apparent binding dissociation constant for the competing ligand, L_t and is the total competing ligand concentration. The apparent binding dissociation constant for IDA could be determined given the pK_as of IDA and the binding dissociation constant (Equation 3).

$$pK_{d\,(app)} = -\log[(1 + 10^{logK_1 - pH + 0.11} + 10^{logK_1 + logK_2 - 2\mathrm{pH} + 0.22}) \cdot 10^{-logK_M}] \qquad \text{Eq.3}$$

Where p$K_{d(app)}$ is the apparent binding dissociation constant at the desired pH, K_M is the binding dissociation constant of the competing ligand, K_1 is the first K_a of the competing ligand, and K_2 is the second K_a of the competing ligand. The p$K_{d(app)}$ of IDA is 4.79 (Equation 3). From the plot of

the percent change in absorbance versus the log of the concentration of free zinc the $K_{d(app)}$ of the compounds can be found (Figure 14).

The zinc binding data revealed a wide range in the metal binding affinities of the analogs studied (Table 2). As was expected, B-ring analogs **2** and **6** were better metal binders than NSC 1011. The pyridinyl B-ring is probablly involved in helping the ligand bind zinc. Analogs **4** and **7** exhibited similar binding dissociation constants of 2.64 mM and 1.08 mM respectively. The zinc binding could not be determined for the cyano derivative **3** because there was not enough material. Binding data for four compounds from the DTP library (NSC 1008, NSC 1013, NSC 84093, and NSC 84097 (Figure 15)) were also determined. The binding dissociation constant for the *p*-pyridinyl B-ring analog (NSC 84097) was tighter (2.70 μM) than the other DTP library analogs that displayed millimolar range binding dissociation constants.

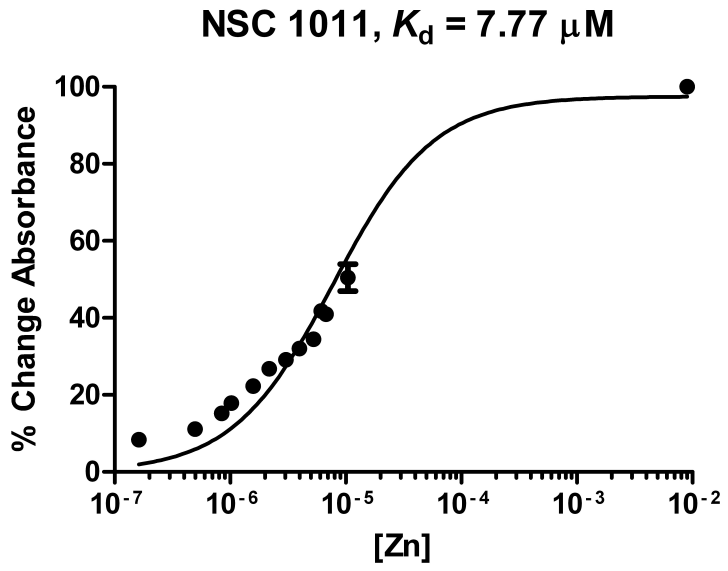

Figure 14. Zinc binding dissociation constant determination for NSC 1011 (**1**).

The metal binding properties of NSC 1011 and analogs were also explored for other biologically relevant metals using a similar method. Neither calcium nor magnesium gave

proper isosbestic points for any of the compounds tested (**1**, **2**, **4**, and **5**). The lack of observable binding is possibly due to the inaccessible d-orbitals of calcium and magnesium. Addition of calcium to **1**, **2**, or **5** resulted in no change in the absorption spectra but methyl derivative **4** did bind calcium, though it is unclear why it does and the others do not.

The binding spectra of magnesium are complicated by the change in the spectra of the blank when titrated with magnesium. To correct for the change in the baseline spectra, two baseline solutions were made, one containing magnesium and one without metal. New baseline spectra of the appropriate magnesium concentration were obtained before the acquisition of a spectrum. Using this method, no isosbestic point was found for any of the analogs when titrated with magnesium. This indicates that although magnesium is interacting with the compounds being studied, the stoichiometry and geometry of the reactions are non-specific.

Manganese binding dissociation constants were determined using a similar method to that used for zinc. Binding dissociation constants indicate twenty to thirty times looser binding for manganese than for zinc. The K_d for **1** and **2** were determined to be 531 μM and 289 μM respectively.

The study of how NSC 1011 and analogous molecules interact with other biologically relevant metals has yet to be completed. Other metals of interest include, cobalt(III), multiple oxidation states of iron, and copper(II). The data collected for the metals studied is summarized in Table 1.

The metal-binding data collected so far suggests that steric bulk at the *para*-position of the B-ring weakens the ligand-metal interaction. Also, electron withdrawing groups likely produce weaker metal binders. More studies will aid in the determination of trends based upon

Table 2. The binding dissociation constants of the analogs of NSC 1011 that were synthesized. Where NA means that a value could not be obtained from the experiment performed; and NB means that there was no spectral change observed when the molecule was titrated. Measurements for zinc(II), calcium(II), magnesium(II), and manganese(II) were taken at pH 7.0.

Molecule	IC_{50} (μM)	Zn^{2+} K_d (μM)	Ca^{2+} K_d (μM)	Mg^{2+} K_d (μM)	Mn^{2+} K_d (μM)
NSC 1011 (1)	20.12	7.77	NB	NA	531
o-pyridinyl **(2)**	66.85	0.86	NB	NA	289
p-cyano **(3)**	26.83	NA			
p-methyl **(4)**	7.8	2640	2490	NA	
p-bromo **(5)**	10.4	NA	NB	NA	
m-pyridinyl **(6)**	34.24	1.3			
p-fluoro **(7)**	11.21	1080			
NSC 1008	8.54	2160			
NSC 1013	4.91	3190			
NSC 84093	9.73	2880			
NSC 84097	16.34	2.78			

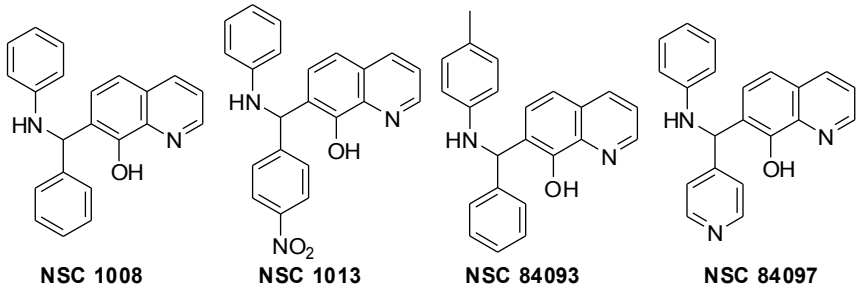

NSC 1008 **NSC 1013** **NSC 84093** **NSC 84097**

Figure 15. Structures of NCI samples NSC 1008, NSC 1013, NSC 84093, and NSC 84097.

the substitution of the B-ring. The effect of *ortho*- or *meta*-substituted B-ring analogs on the metal binding properties might also be investigated.

PART 3: INHIBITION OF RCE1P

Three main assays have been used for the determination of inhibition of Rce1p by small molecules.[47] Of these, the in vitro fluorescence assay and the fluorescence in vivo study in yeast culture cells were used in the present work. The **a**-factor assay was used as a secondary screen in identifying the nine inhibitors from the DTS library.[47] There are a number of reasons for the use

of the fluorescence assay over the **a**-factor assay for the studies, but the primary one is that it is a direct assay, whereas the **a**-factor assay is an indirect assay.

The fluorescence assay functions by providing Rce1p with a synthetic farnesylated peptide substrate (ABZ-KSKTKC(farnesyl)K(DNP)IM-OH) (Figure 16). Within the substrate, there is an ABZ fluorphore on the N-terminus and a DNP on a lysine in the CaaX box. The membrane bound active Rce1p is first incubated with the inhibitor to be studied before addition of the substrate. Upon initial addition of the substrate, little fluorescence is observed. After cleavage of the substrate, the fluorophore and the quencher are separated and increased fluorescence can be observed. By incubating Rce1p with differing concentrations of inhibitor, a dose response curve can be obtained (Figure 17). From the dose response curves, the IC_{50}'s of the inhibitors can be determined.

The IC_{50} for synthetic **1** was found to be lower than the NSC 1011 sample provided by NCI. For **1** the lower IC_{50} might be due in part to the purity of the sample. MS data for the original NSC 1011 sample received from the NCI did not display a molecular ion peak indicating that NSC 1011 might not have been present. Conversely, resynthesized **1** has been fully characterized, and both low-resolution MS and high-resolution MS have identified the molecular ion. Also, the purity of synthetic **1** has been determined via ^{1}H-NMR. The IC_{50} of each analog was determined using the fluorescence based assay (Table 2) and compared with the various metal K_d's.

The hypothesis that better metal-binders would be better Rce1p inhibitors can be tested from comparison of the data in Table 2. It is interesting that both *p*-methyl analog **4** and *p*-bromo analog **5** show near double or greater inhibition of Rce1p by the fluorescence assay relative to **1**.

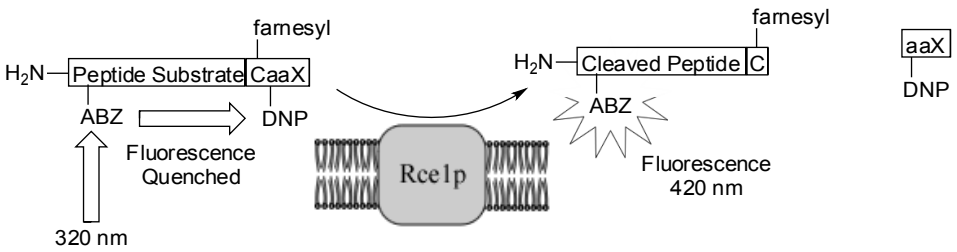

Figure 16. The fluorescence assay functions by providing Rce1p with a small synthetic peptide substrate. Upon removal of the CaaX box by Rce1p, the fluorophore is no longer quenched, and a change in fluorescence is observed.

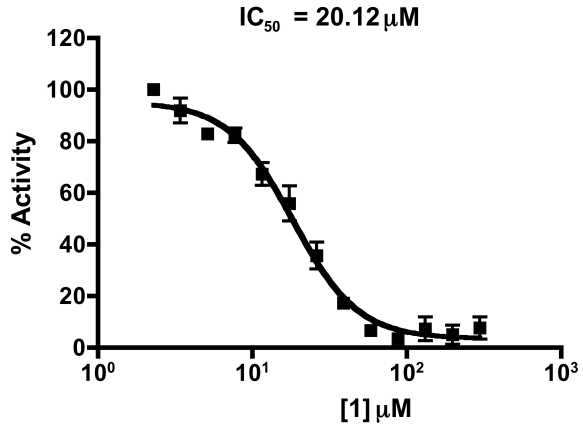

Figure 17. Dose response curve for **1** determined using the fluorescence assay (assay performed by Dr. Surya Manandhar).

Also, the tighter zinc binding observed for pyridinyl derivative **2** correlates to an IC_{50} that was close to double the value measured for **1**. *p*-Cyano analog **3** and the *p*-fluoro analog **7** had similar IC_{50} values to NSC 1011 with **3** being slightly less potent and **7** derivative being slightly more potent. This trend is the inverse of what was expected for a correlation between metal binding and Rce1p inhibition.

PART 4: CELL PERMEABILITY OF NSC 1011 ANALOGS

Yeast cells with over expressed green fluorescent protein (GFP) labeled Ras have been used to observe the mislocalization of Ras due to the inhibition of certain post-translation

processes, including Rce1p inhibition.[47] Inhibitors of Rce1p that are also cell permeable display mislocalization of GFP labeled Ras to the cytoplasm. It was determined that NSC 1011 (**1**) was not completely cell permeable due to the low frequency of the mislocalization phenotype displayed.[47] Based upon this observation more cell permeable analogs of NSC 1011 are needed.

All of the synthesized analogs (**1**-**7**) were incubated with the yeast cells to test their cell permeability. For analogs **1-4**, **6**, and **7** to achieve Rce1p inhibition in yeast cells a non-toxic amount of detergent sodium dodecyl sulfate (SDS) was required.[47] However, approximately twenty percent of the cells from the in vivo assay with **5** showed a mislocalization of GFP labeled Ras to the cytoplasm without the addition of SDS. This supports the conclusion that **5** is more cell permeable than the other analogs. Also, upon addition of SDS to cells treated with **5** during the in vivo test, almost 100% of the cells displayed the mislocalized Ras phenotype. Improvements to the cell permeability of NSC 1011 are required.

A known method to increase cell permeability is to attach an acetoxymethyl (AM) protecting group to any free carboxylic acids, to form the AM-ester (Figure 18).[75] The AM-ester is later cleaved in the cytosol by non-specific esterases.[75] Thus, the active non-protected molecule is released inside the cell. It has also been shown that the de-protection of carboxylic acids in the cytosol prevents diffusion of the molecule to the extracellular space.[75] By protecting the carboxylic acid of the A-ring, the cell permeability issues observed in NSC 1011 and analogous compounds might be addressed.

The AM-ester of NSC 1011 was synthesized yielding the carboxylate protected AM-ester (Figure 19), acetoxymethyl 4-((8-hydroxyquinolin-7-yl)(phenyl)methylamino)benzoate (**19**). The carboxylate protected AM-ester, **19**, and not the phenolate or amine protected AM-ester was

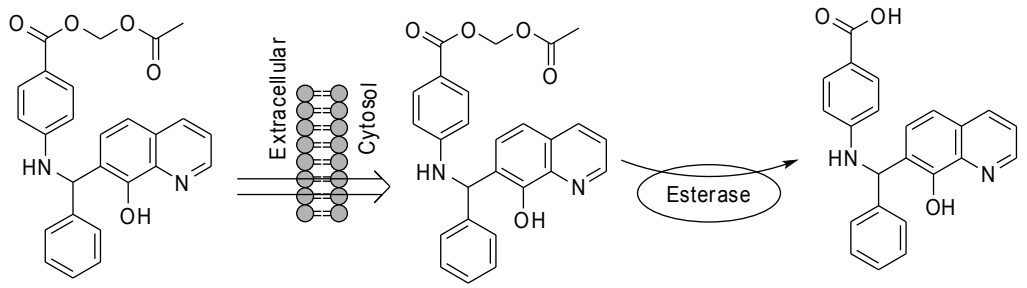

Figure 18. An AM-ester protected carboxylate increases compound cell permeability and the desired compound is released in vivo by the action of non-specific esterases.

found to be the product of the reaction based upon analysis of the ^{1}H-NMR spectra of **19**, **1**, and 8-hydroxyquinoline (**10**). Specifically the absence of the carboxylic acid proton peak of **1** at 12 ppm, the presence of the phenol proton of **10** at 10 ppm, and the presence of the amine proton suggest that the carboxylate protected AM-ester is the isolated product. In addition to the ^{1}H-NMR, the mass spectrum of **19** contains a fragment peak for the loss of the AM-ester protected A-ring, and no fragment for the loss of the A-ring without the AM-ester.

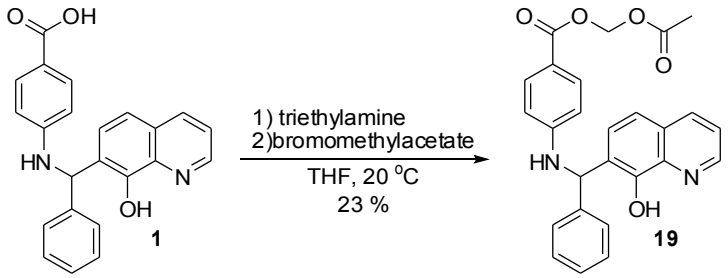

Figure 19. The AM-ester protection of NSC 1011 to form the AM-ester protected **19**.

AM-ester **19** was tested in the in vivo Ras localization assay. Unfortunately, no mislocalization of GFP labeled Ras was observed in the yeast cells (Figure 20). The lack of phenotype expression with the addition of detergent SDS suggests that the AM-ester protection of **1** might be inactivating, and the AM-ester might not be cleaved in vivo. Testing of AM-ester **19** in different cell lines might display the desired phenotype and thus confirm that the reason for no phenotype expression in yeast is due to a lack of AM-ester cleavage.

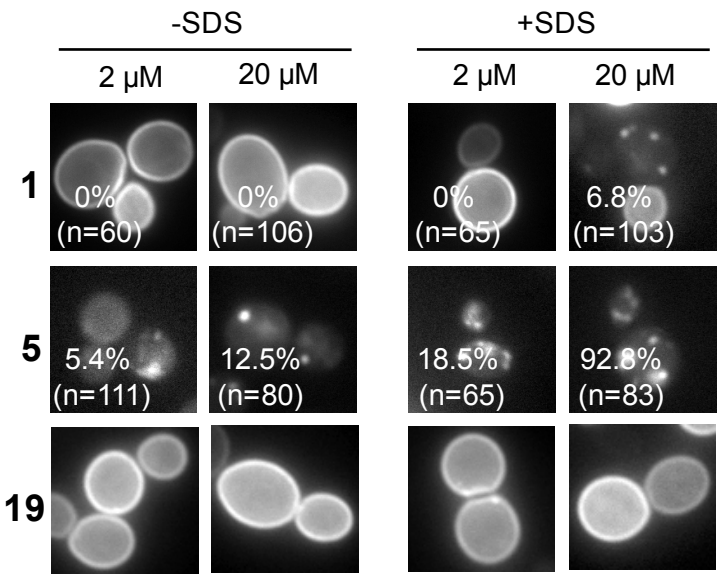

Figure 20. In vivo assay results for non-protected **1**, *p*-bromo analog **5**, and AM-ester protected NSC 1011 **19** (Assay performed by Dr. Surya Manandhar).

CONCLUSIONS

Several analogs of NSC 1011 were synthesized to explore the effect of B-ring substituents on the metal binding and Rce1p inhibition properties. The hypothesis that increased metal-binding would result in increased Rce1p inhibition was incorrect. Conversely, the weaker the metal-binding properties of the NSC 1011 analog, the lower the IC_{50} value. The cell permeability of NSC 1011 may still be improved by protection of the A-ring carboxylate; however, further testing is required. Testing of AM-esters of NSC 1011 and other analogs in other cell lines might determine that the AM-esters are more cell permeable. The development of other analogs of the B-ring is still needed to fully explore the effect of steric bulk, electron withdrawing groups, and *ortho*- and *meta*-substitution.

CHAPTER 3

MATERIALS AND METHODS

^{1}H-NMR and ^{13}C-NMR spectrometry: All NMR spectra were obtained using a Varian Mercury Plus 400 MHz NMR spectrometer except where denoted that a Varian Unity Inova 500 MHz NMR spectrometer was used.

Mass spectrometry: All low-resolution mass spectra were obtained using a Perkin Elmer Sciex API I plus quadrupole mass spectrometer. All high-resolution mass spectra were obtained using a Fourier transform ion cyclotron resonance mass spectrometer with a 4.7 T magnet.

High-pressure liquid chromatography (HPLC): All HPLC methods used a Varian ProStar Chromatography Workstation with either a 25 cm x 4.6 mm column and analytical size flow cell for analytical methods, or a 25 cm x 21.4 mm column and preparatory size flow cell for preparatory methods.

Determination of pH: The pH of aqueous solutions was determined using a Accumet BASIC pH probe.

Flourescence based bioassay: The fluorescence of the bioassay samples was measured using a BioTek Synergy HT microplate fluorometer and 340/420 excitation/emission filter set.

UV/Vis Spectroscopy: A Cary 300 Bio UV-Vis spectrometer was used to gather all UV-Vis absorbance spectra.

Materials used: Normal phase (standard grade), C18 capped silica gel, TLC plates (with UV 254), and C18 capped TLC plates (with UV) were purchased from Sorbent Technologies

(Atlanta, GA). NSC 1008, NSC 1011, NSC 1013, NSC 84093, and NSC 84097 samples were provided by the NCI-DTP program. All reagents were of reagent grade, and purchased from Acros Chemicals, Alfa Aesar, J.T. Baker, Sigma-Aldrich, Fisher Scientific, or OmniSolv and used without further purification. All dry solvents were obtained by passing the solvent through an activated alumina column and stored under a nitrogen atmosphere. Membrane-bound Rce1p was isolated as previously described.[51] Internally quenched fluorgenic peptide substrate was purchased from AnaSpec.

4-((8-hydroxyquinolin-7-yl)(phenyl)methylamino)benzoic acid (NSC 1011) (1):

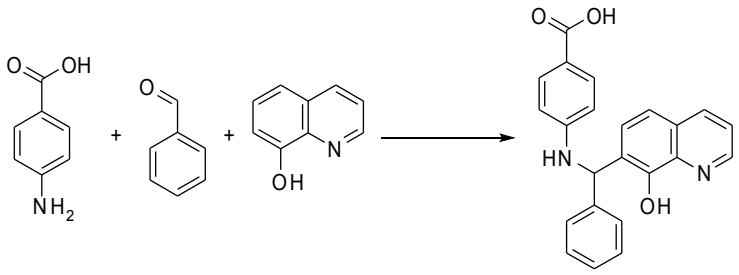

In enough ethanol for complete solvation, 8-hydroxyquinoline (0.750 g, 5.17 mmol), *p*-aminobenzoic acid (0.709 g, 5.17 mmol), and benzaldehyde (0.548 g, 5.17 mmol) were dissolved. The solution was stirred for 59 d at room temperature. NSC 1011 (**1**) was isolated as an off white precipitate (0.535 g, 1.44 mmol, 27.9%) via vacuum filtration. No further purification was necessary. ^{1}H NMR (400 MHz DMSO-d_6, δ): 8.87 (dd, 1H, J = 1.3 Hz, 3.3 Hz), 8.29 (dd, 1H, J = 1.3 Hz, 3.3 Hz), 7.63 (d, 2H, J = 8.8 Hz), 7.55 (m, 2H), 7.41, (d, 3H J = 6.8 Hz), 7.3 (m, 4H), 6.68 (d, 2H, J = 8.8 Hz), 6.26 (d, 1H, J = 7 Hz); ^{13}C NMR (DMSO-d_6, δ): 185.3, 168.1, 152.3, 150.6, 149.0, 142.6, 138.7, 136.7, 131.6, 129.1, 128.3, 128.1, 127.7, 126.8, 125.2, 122.5, 118.3, 112.4, 54.6; HRMS-ESI (*m/z*): $[M + H]^+$ calcd for $C_{23}H_{18}N_2O_3$ 371.1390; found, 371.1392. COSY-NMR and gHSQC-NMR are shown.

NSC 1011 (**1**) could be synthesized in a shorter period of time using the following protocol: In enough ethanol for complete solvation, 8-hydroxyquinoline (1.365 g, 9.4 mmol), *p*-aminobenzoic acid (0.129 g, 0.94 mmol), and benzaldehyde (0.100 g, 0.94 mmol) were dissolved. Pyridine (0.2 mL, 2.5 mmol) was added to the solution, which was subsequently stirred for 10 d. NSC 1011 (**1**) was isolated as a white precipitate (57 mg, 0.15 mmol, 16.4%) via vacuum filtration.

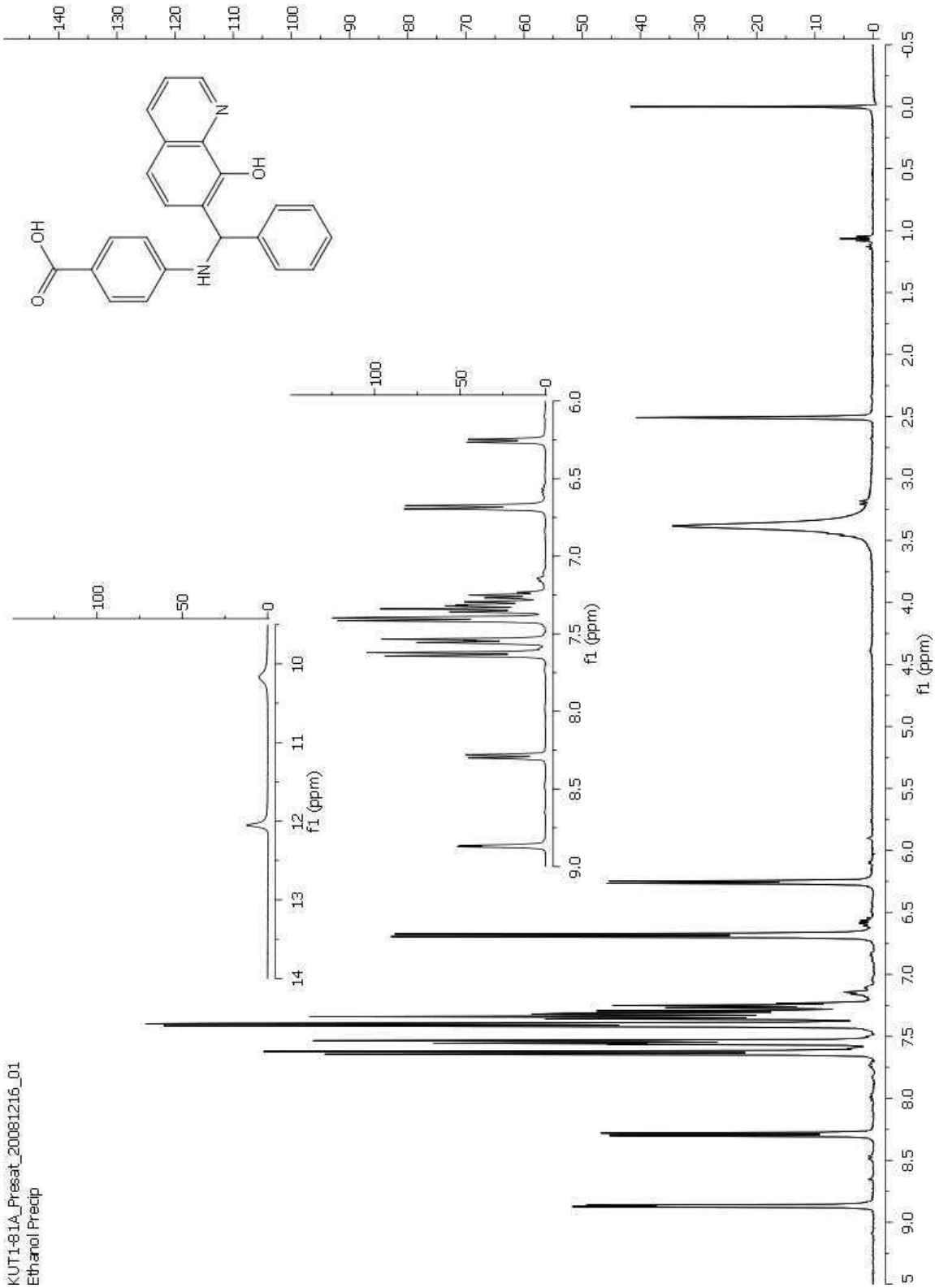
KUT1-81A_Presat_20081216_01
Ethanol Precip
OH
O
HN
N
OH
f1 (ppm)

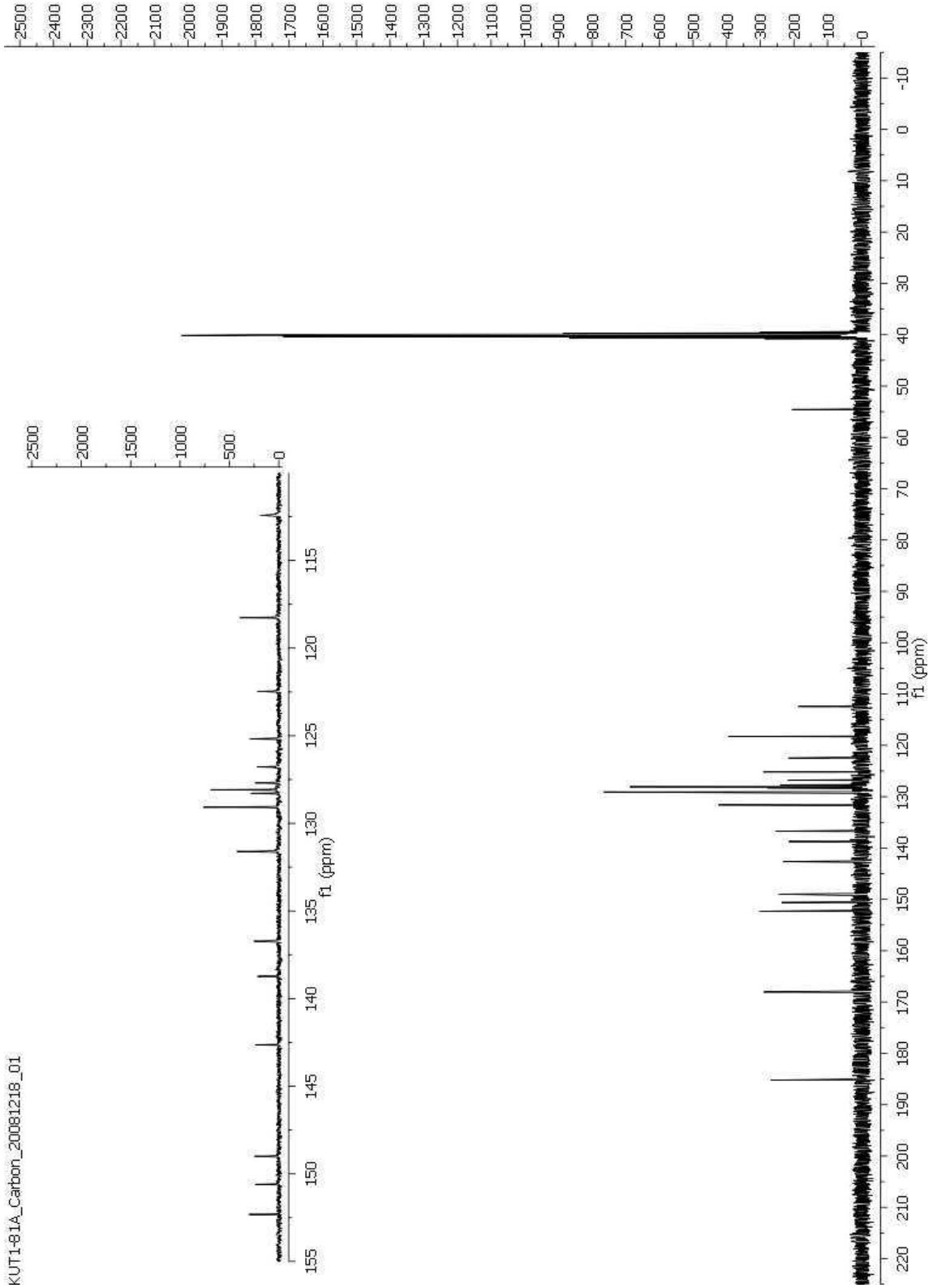
KUT1-81A_Carbon_20081218_01
f1 (ppm)
f1 (ppm)

KUT1-81A_Gcosy_20081218_01
f2 (ppm)
f1 (ppm)

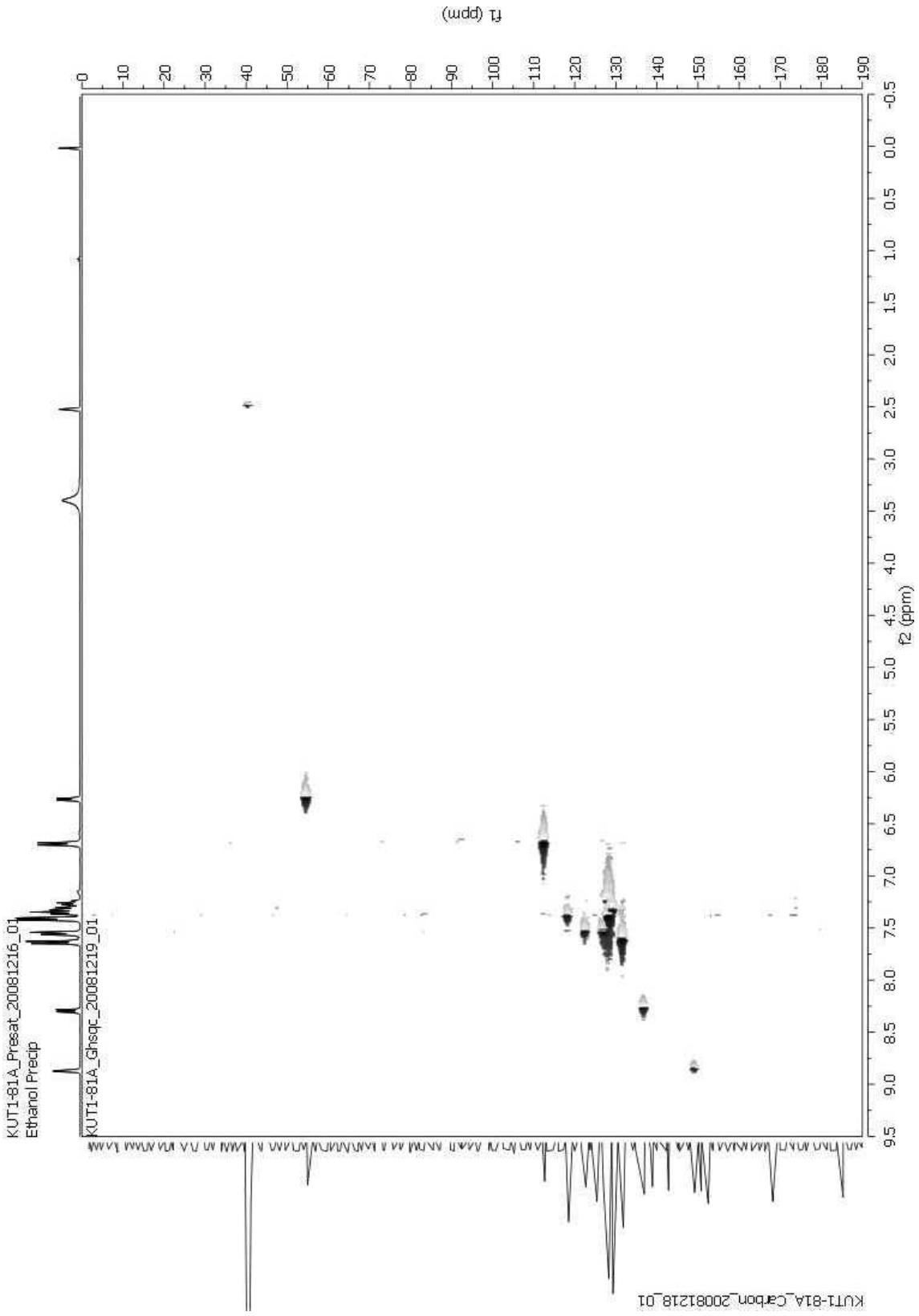
f1 (ppm)
KUT1-81A_Presat_20081216_01
Ethanol Precip
KUT1-81A_Ghsqc_20081219_01
KUT1-81A_Carbon_20081218_01
f2 (ppm)

4-((8-hydroxyquinolin-7-yl)(pyridin-2-yl)methylamino)benzoic acid (2):

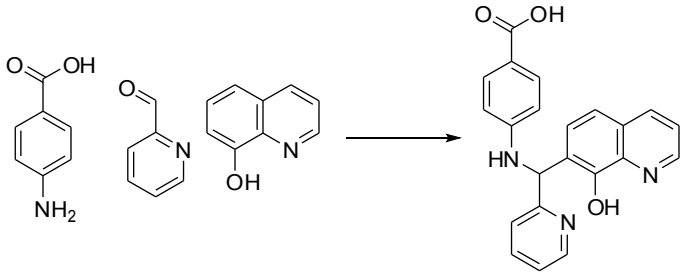

2-Pyridine-carboxyaldehyde (0.250 g, 2.33 mmol), 8-hydroxyquinoline (0.339 g, 2.33 mmol), and *p*-aminobenzoic acid (0.320 g, 2.33 mmol) were stirred in a minimal volume of ethanol at room temperature for 42 d. A miniature workup (~2 mL) of the reaction mixture was performed by filtering the mixture through a pipette filter. The filtrate was collected, and the filtrant placed in an NMR tube. The remainder of the precipitate was isolated via gravity filtration to afford 0.5615 g (1.513 mmol, 64.9%). ^{1}H NMR (400 MHz DMSO-d_6, δ): 12.04 (br s, 1H), 10.25 (br s, 1H), 8.87 (d, 1H), 8.57 (d, 1H), 8.27 (d, 1H), 7.78 (dt, 1H), 7.62 (d, 2H), 7.52, (m, 3H), 7.33 (m, 3H), 6.72 (d, 2H), 6.34 (d, 1H); ^{13}C NMR (DMSO-d_6, δ): 194.1, 168.1, 160.6, 151.9, 150.8, 149.6, 138.8, 137.8, 136.7, 131.6, 131.4, 128.4, 126.9, 124.7, 123.2, 122.8, 122.5, 118.4, 118.3, 55.5; HRMS-ESI (*m/z*): $[M + H]^+$ calcd for $C_{22}H_{17}N_3O_3$ 372.1343; found, 372.1349.

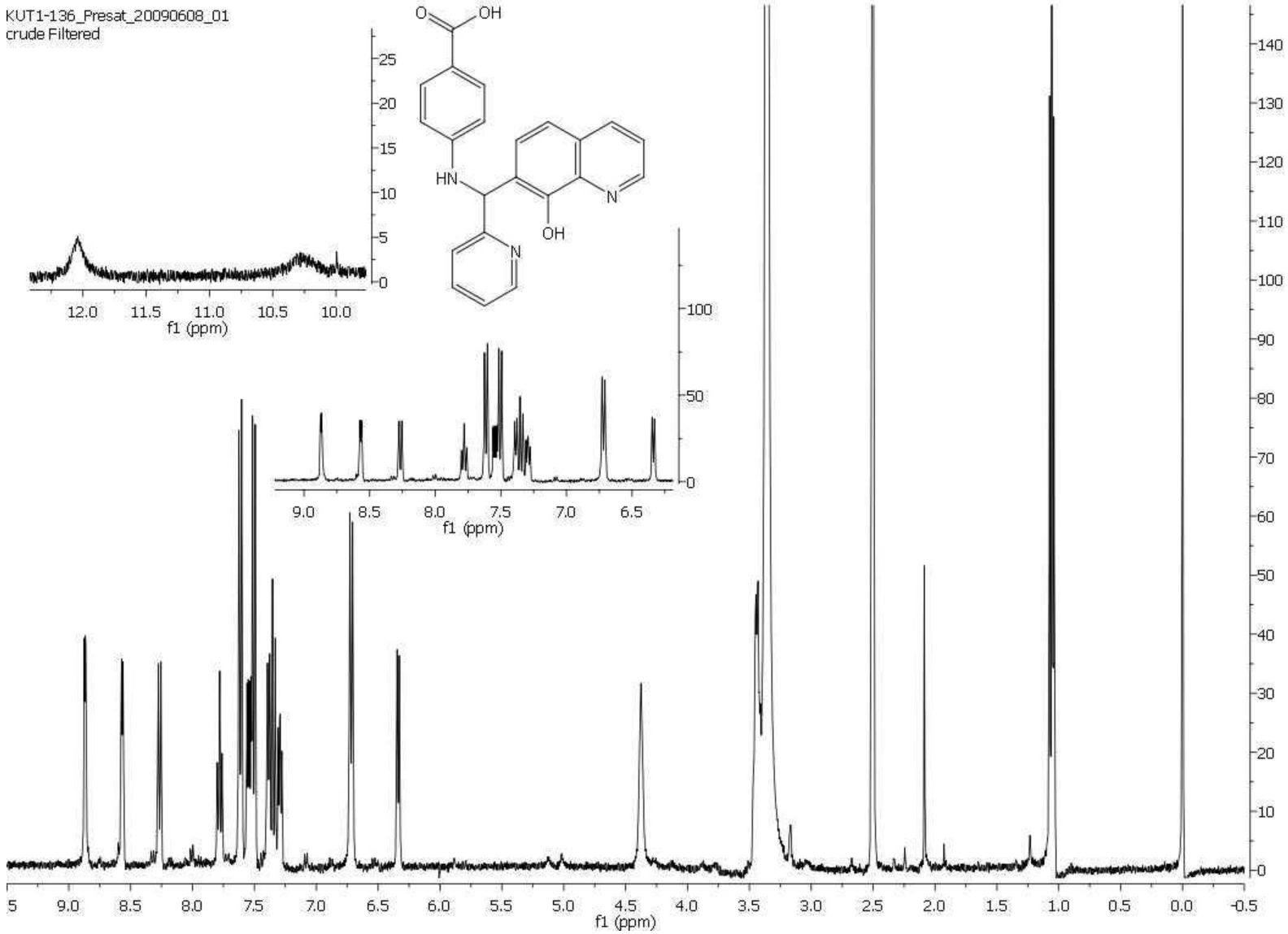
KUT1-136_Presat_20090608_01
crude Filtered
O
OH
HN
N
OH
N
12.0
11.5
11.0
10.5
10.0
f1 (ppm)
9.0
8.5
8.0
7.5
7.0
6.5
f1 (ppm)
f1 (ppm)

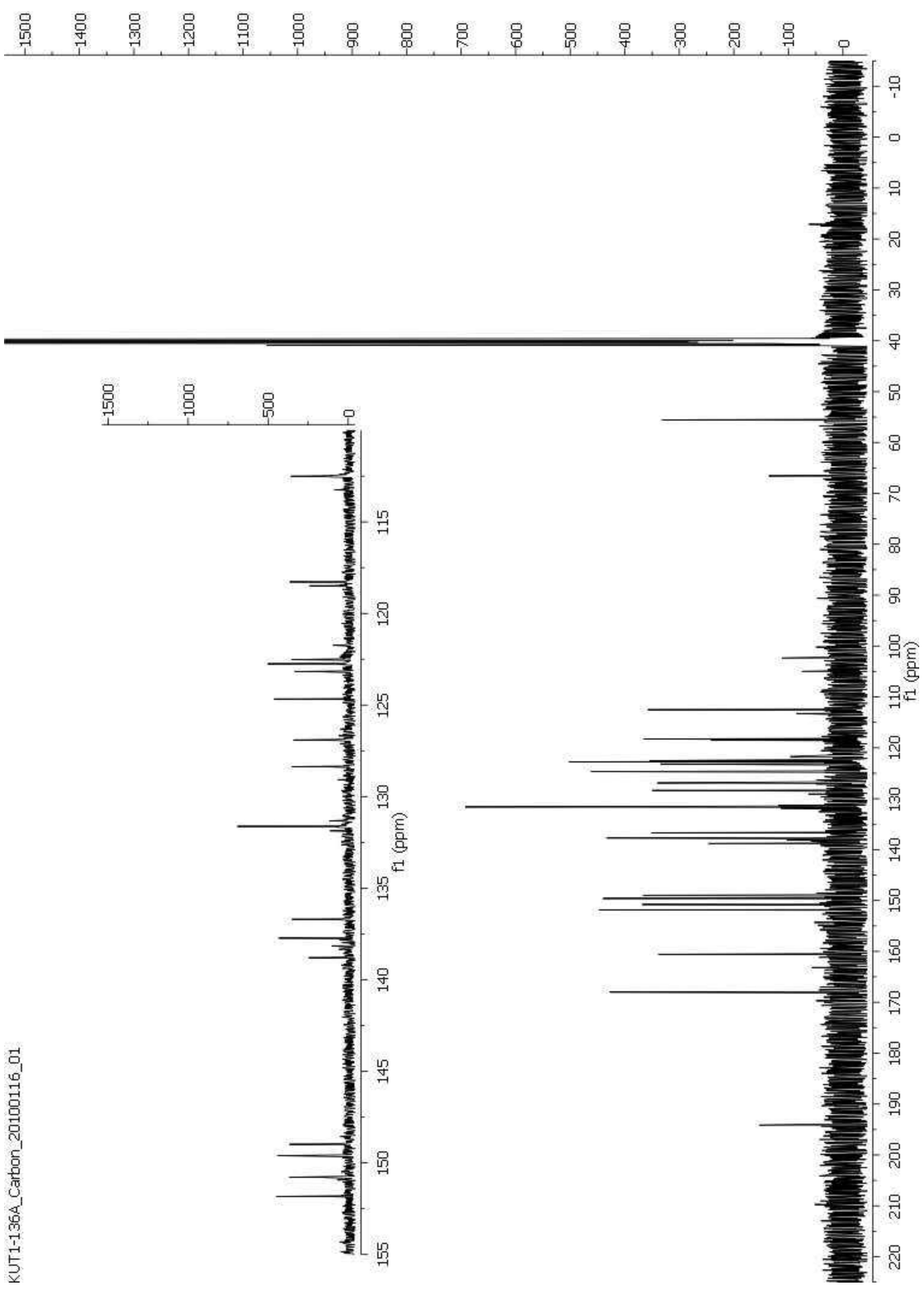
KUT1-136A_Carbon_20100116_01
f1 (ppm)
f1 (ppm)

4-((4-cyanophenyl)(8-hydroxyquinolin-7-yl)methylamino)benzoic acid (3):

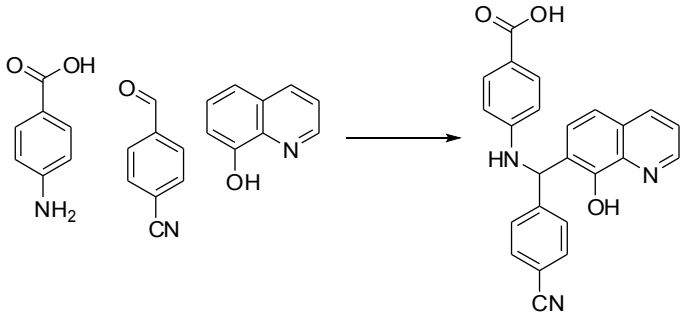

p-Cyanobenzaldehyde (0.250 g, 1.91 mmol), 8-hydroxyquinoline (0.277 g, 1.91 mmol), and *p*-aminobenzoic acid (0.261 g, 1.91 mmol) were stirred in a minimal volume of ethanol at room temperature. A miniature workup (~2 mL) of the reaction mixture was performed by filtering the mixture through a pipette filter after 43 d. The filtrate was collected, and the filtrant placed in an NMR tube. After 84 d a small portion of the reaction mixture was removed, vacuum filtered, and washed with small portions of fresh ethanol. Analyzing the solid via TLC shows decomposition of the crude solid. Reverse phase TLC analysis was performed with 3:2 acetonitrile:water. An analytical HPLC method was developed empirically. The final method used for purification consisted of: 3:7 acetonitrile:water with 0.1% TFA isocratic for 16.5 min, 6.5 min ramp to 100% acetonitrile, and 4 min flush with 100% acetonitrile. Three visible peaks at 3.8 min, 12.5 min, and 14 min. The peak at 14 min contained the desired product, recrystallization from ethanol and vacuum filtration using 2 micron filter paper yielded 7.0 mg (0.02 mmol, 0.9%) desired product. ^{1}H NMR (400 MHz DMSO-d_6, δ): 8.87 (d, 1H), 8.31 (d, 1H), 7.82 (d, 2H), 7.60 (m, 5H), 7.48, (d, 1H), 7.41 (d, 1H), 7.35 (d, 1H), 6.67 (d, 2H), 6.32 (d, 1H); ^{13}C NMR (DMSO-d_6, δ): 194.1, 168.0, 152.0, 150.8, 149.2, 148.4, 138.8, 136.8, 133.1, 131.7, 129.0, 128.5, 124.2, 122.7, 118.8, 118.6, 112.6, 110.5, 102.4, 54.6; HRMS-ESI (*m/z*): $[M + H]^+$ calcd for $C_{24}H_{17}N_3O_3$ 396.1343; found, 396.1365.

Compound **3** could be synthesized in a shorter period of time using the following protocol: *p*-Cyanobenzaldehyde (0.100 g, 0.73 mmol), 8-hydroxyquinoline (1.060 g, 7.3 mmol), and *p*-aminobenzoic acid (0.096 g, 0.73 mmol) were stirred in a minimal volume (~25 mL) of ethanol at R.T for 15 d. The precipitate was removed via vacuum filtration and recrystallized from acetonitrile to afford the desired product (1.7 mg, 0.004 mmol, 0.59 %).

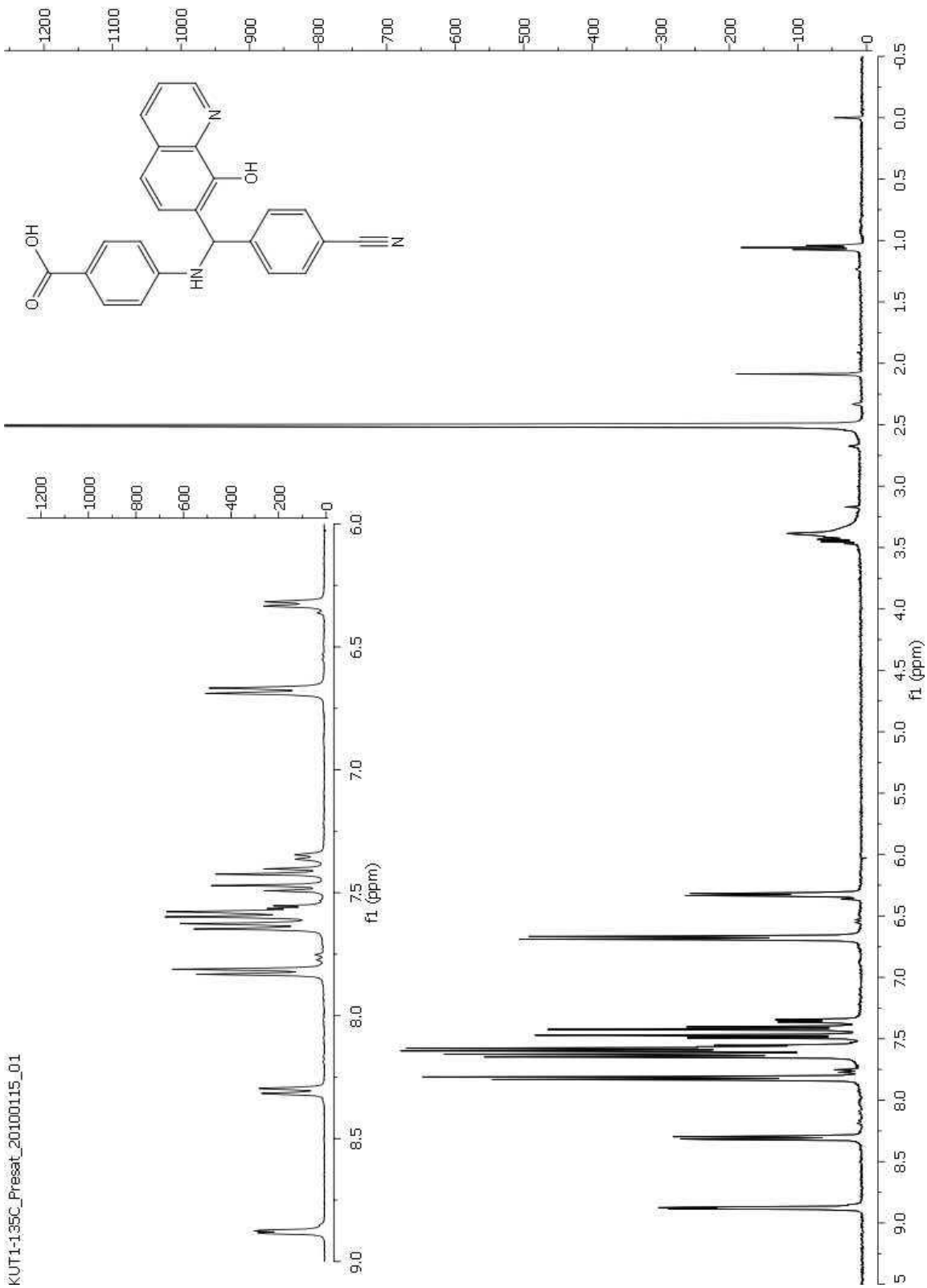
KUT1-135C_Presat_20100115_01
f1 (ppm)
f1 (ppm)
OH
O
HN
OH
N
N

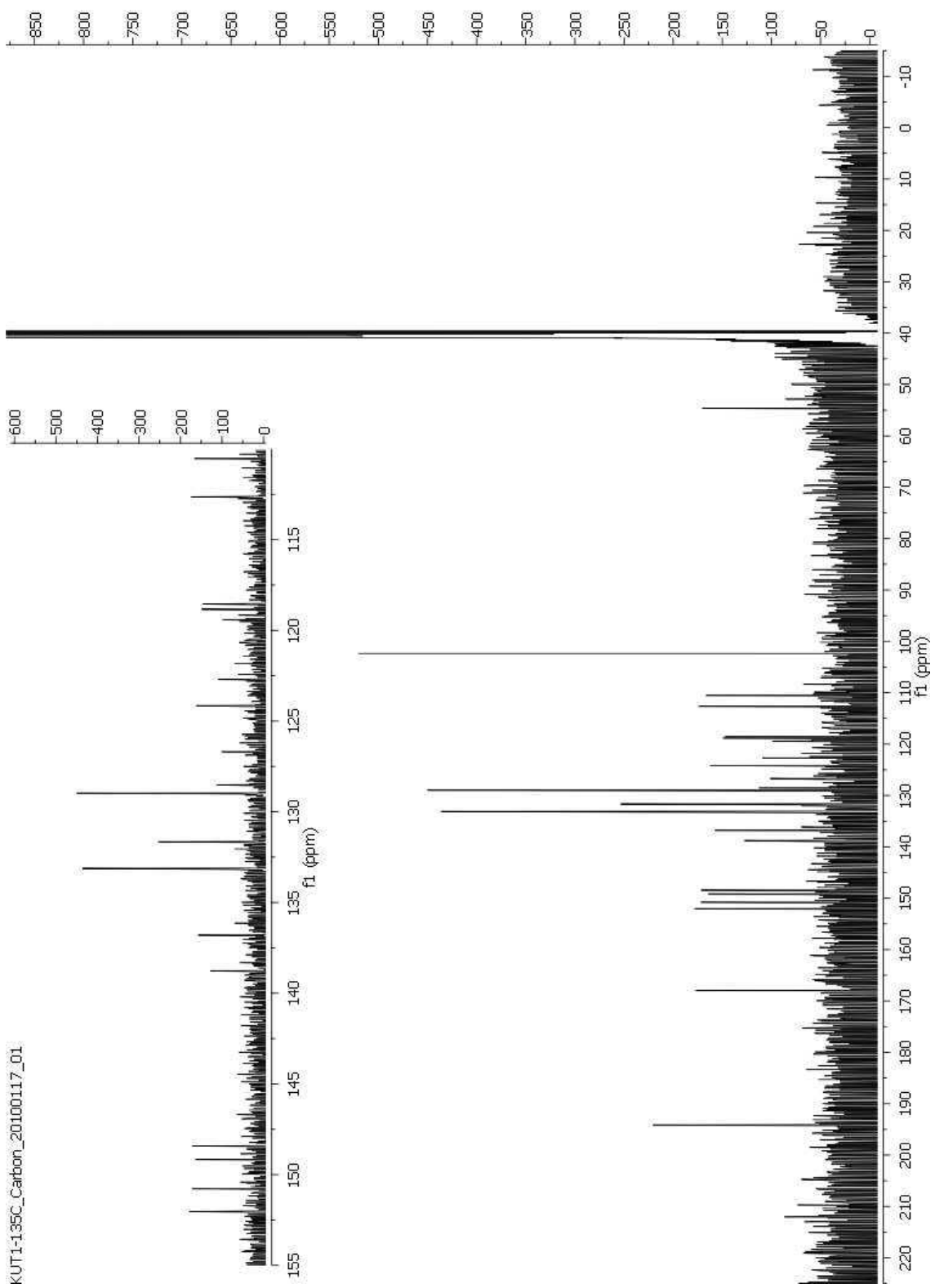
KUT1-135C_Carbon_20100117_01
f1 (ppm)
f1 (ppm)

4-((8-hydroxyquinolin-7-yl)(p-tolyl)methylamino)benzoic acid (4):

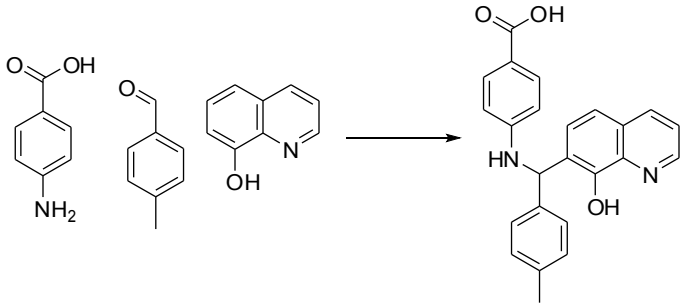

p-Tolualdehyde (0.250 g, 2.08 mmol), 8-hydroxyquinoline (0.339 g, 2.08 mmol), and *p*-aminobenzoic acid (0.320 g, 2.08 mmol) were stirred in a minimal volume of ethanol at room temperature. After 69 d a small portion of the reaction mixture was removed and analyzed by HPLC. After 88 d the reaction mixture was vacuum filtered and the filtrant was dissolved in DMSO for HPLC purification. 103 d after filtering there was visible precipitate in the filtrate which upon inspection was the desired product (49.1 mg, 0.10 mmol, 4.8 %). ^{1}H NMR (400 MHz DMSO-d_6, δ): 8.84 (d, 1H), 8.26 (d, 1H), 7.58 (d, 2H), 7.50 (m, 2H), 7.36, (d, 1H), 7.25 (m, 3H), 7.11 (d, 2H), 6.63 (d, 2H), 6.17 (d, 1H), 2.23 (s, 3H); ^{13}C NMR (DMSO-d_6, δ): 194.2, 168.1, 152.4, 150.6, 149.0, 139.7, 138.8, 136.8, 131.6, 129.6, 128.3, 128.0, 126.9, 125.4, 122.5, 118.2, 112.4, 54.2, 21.3; HRMS-ESI (*m/z*): $[M + K]^+$ calcd for $C_{24}H_{20}N_2O_3$ 423.1106; found, 423.1003.

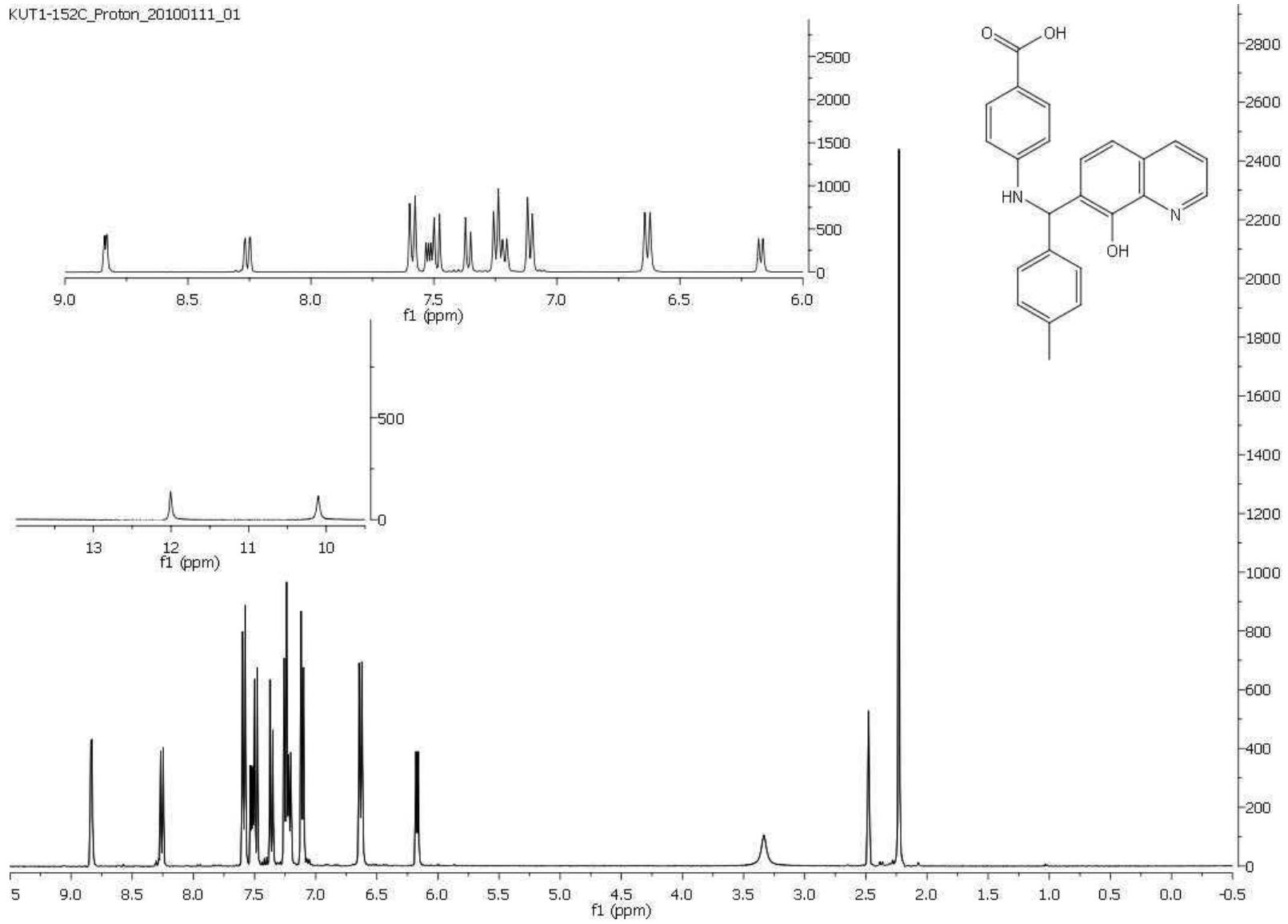
KUT1-152C_Proton_20100111_01
O
OH
HN
N
OH
f1 (ppm)
f1 (ppm)
f1 (ppm)

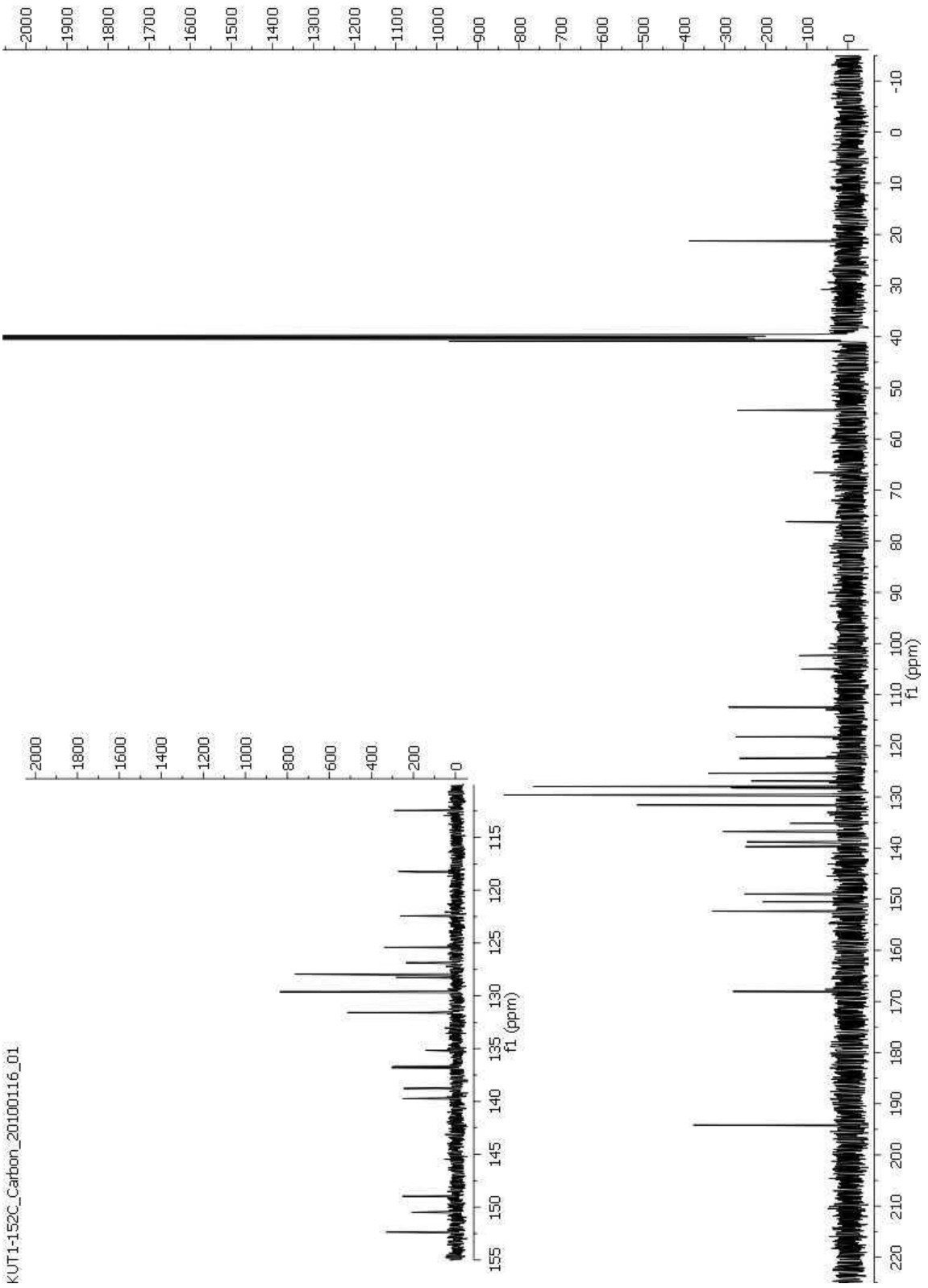
KUT1-152C_Carbon_20100116_01
f1 (ppm)
f1 (ppm)

4-((4-bromophenyl)(8-hydroxyquinolin-7-yl)methylamino)benzoic acid (5):

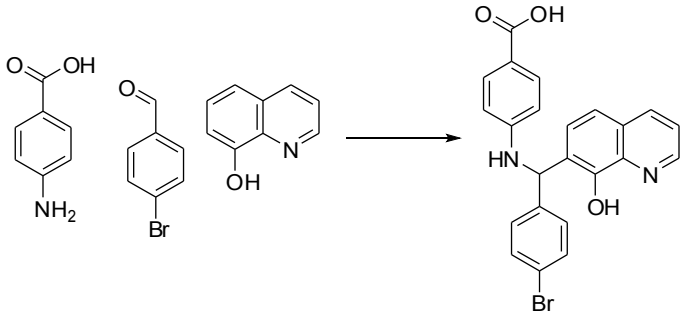

p-Bromobenzaldehyde (0.250 g, 1.91 mmol), 8-hydroxyquinoline (0.277 g, 1.91 mmol), and *p*-aminobenzoic acid (0.261 g, 1.91 mmol) were stirred in a minimal volume of ethanol at room temperature. A miniature workup (~2 mL) of the reaction mixture was performed by filtering the mixture through a pipette filter after 43 d. The filtrate was collected, and the filtrant placed in an NMR tube. At 113 d a small portion of the reaction mixture was removed and vacuum filtered. The filtrant was used to develop an HPLC method for separation. At 136 d the reaction mixture was filtered and the filtrant was dissolved in 2.5 mL of DMSO, filtered with a 2.2 micron filter, and separated using the developed HPLC method. From the filtrate obtained on day 136, a precipitate was visible, and was separated via vacuum filtration to afford **5** as a white solid (10.0 mg, 0.02 mmol, 1.6%). ^{1}H NMR (400 MHz DMSO-d_6, δ): 8.84 (d, 1H), 8.27 (d, 1H), 7.60 (d, 2H), 7.50 (m, 4H), 7.38, (d, 1H), 7.28 (m, 3H), 6.63 (d, 2H), 6.19 (d, 1H); ^{13}C NMR (DMSO-d_6, δ): 194.2, 168.0, 152.2, 150.7, 149.1, 142.2, 138.8, 136.8, 132.0, 131.6, 130.3, 128.4, 126.7, 124.7, 122.6, 120.8, 118.5, 118.4, 112.5, 54.2; HRMS-ESI (*m/z*): $[M - C_7H_6NO_2]^+$ calcd for $C_{23}H_{17}BrN_2O_3$ 312.0024 and 314.0004; found, 312.0019 and 314.0017.

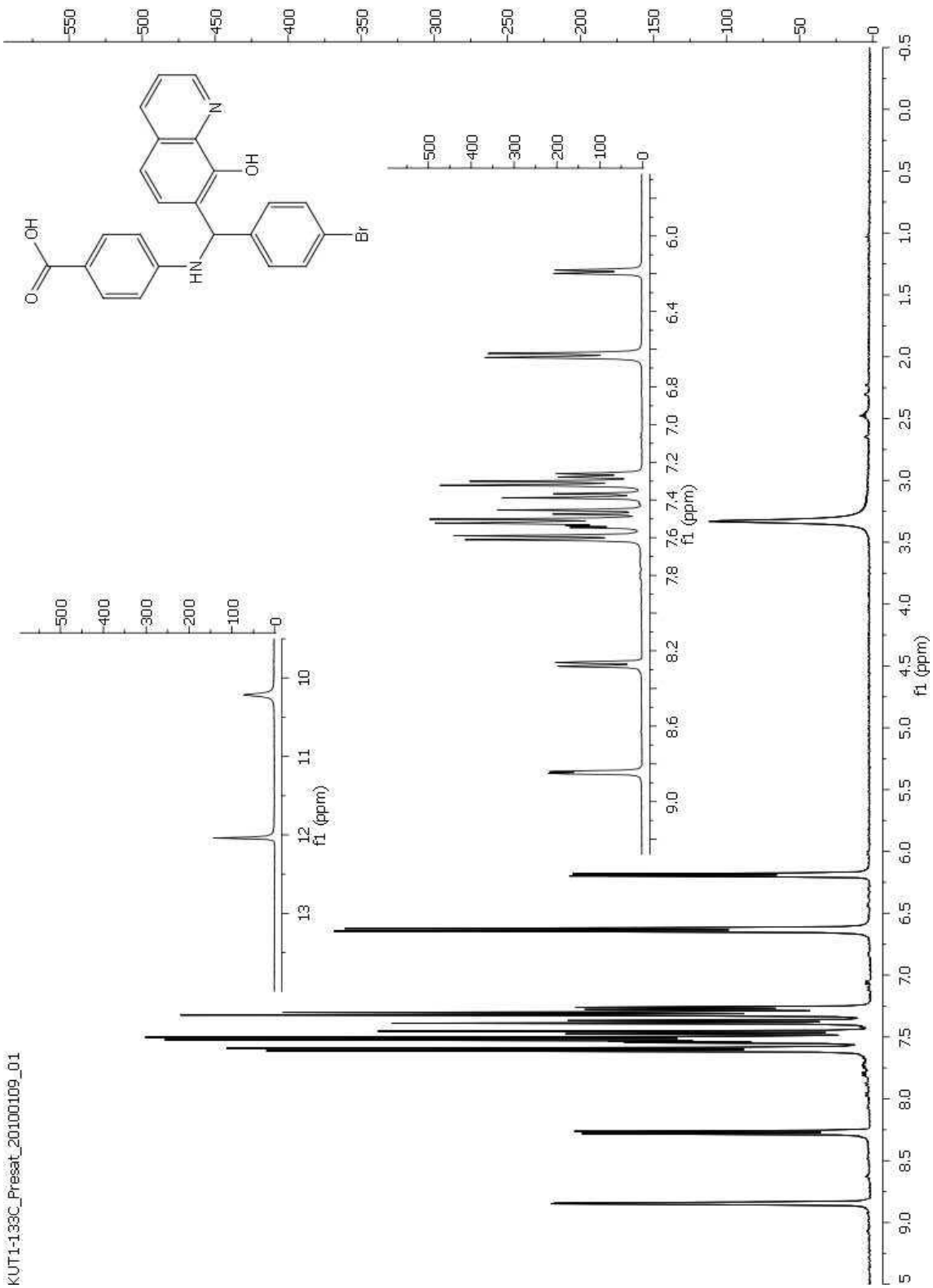
KUT1-133C_Presat_20100109_01
f1 (ppm)
OH
O
HN
N
OH
Br

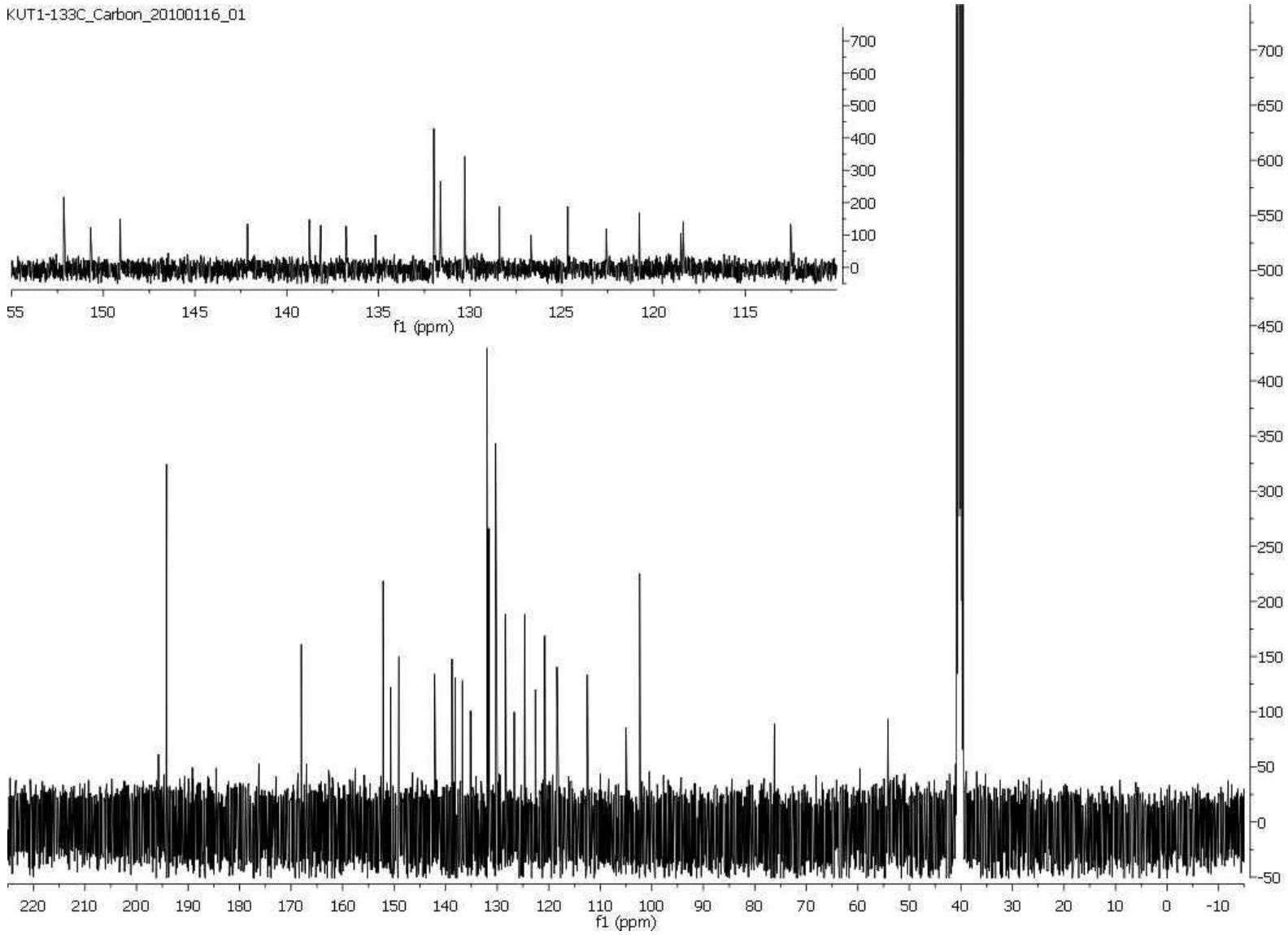
KUT1-133C_Carbon_20100116_01
f1 (ppm)
f1 (ppm)

4-((8-hydroxyquinolin-7-yl)(pyridin-3-yl)methylamino)benzoic acid (6):

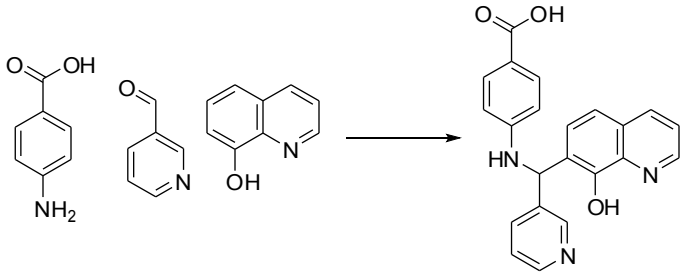

3-Pyridine-carboxaldehyde (0.100 g, 0.93 mmol), 8-hydroxyquinoline (1.35 g, 9.30 mmol), and *p*-aminobenzoic acid (0.128 g, 0.93 mmol) were stirred in sufficient ethanol to completely dissolve 8-hydroxyquinoline. The reactants were allowed to stir for 8 d with monitoring the reaction by ^{1}H-NMR. The precipitate was removed via vacuum filtration, washed with fresh ethanol, and dried under reduced pressure to afford 84.2 mg (0.227 mmol, 24%) of a pink-white solid. ^{1}H NMR (400 MHz DMSO-d_6, δ): 8.83 (d, 1H), 8.61 (s, 1H), 8.44 (d, 1H), 8.26 (d, 1H), 7.72 (d, 1H), 7.62 (d, 2H), 7.53 (m, 2H), 7.38, (m, 3H) 6.66 (d, 2H), 6.26 (d, 1H); ^{13}C NMR (DMSO-d_6, δ): 194.2, 168.0, 152.1, 150.8, 149.7, 149.1, 138.8, 138.1, 136.8, 135.7, 131.7, 128.5, 126.4, 124.3, 124.2, 122.6, 118.8, 118.5, 112.6, 53.0; HRMS-ESI (*m/z*): $[M + H]^+$ calcd for $C_{22}H_{17}N_3O_3$ 372.1343; found, 372.1341.

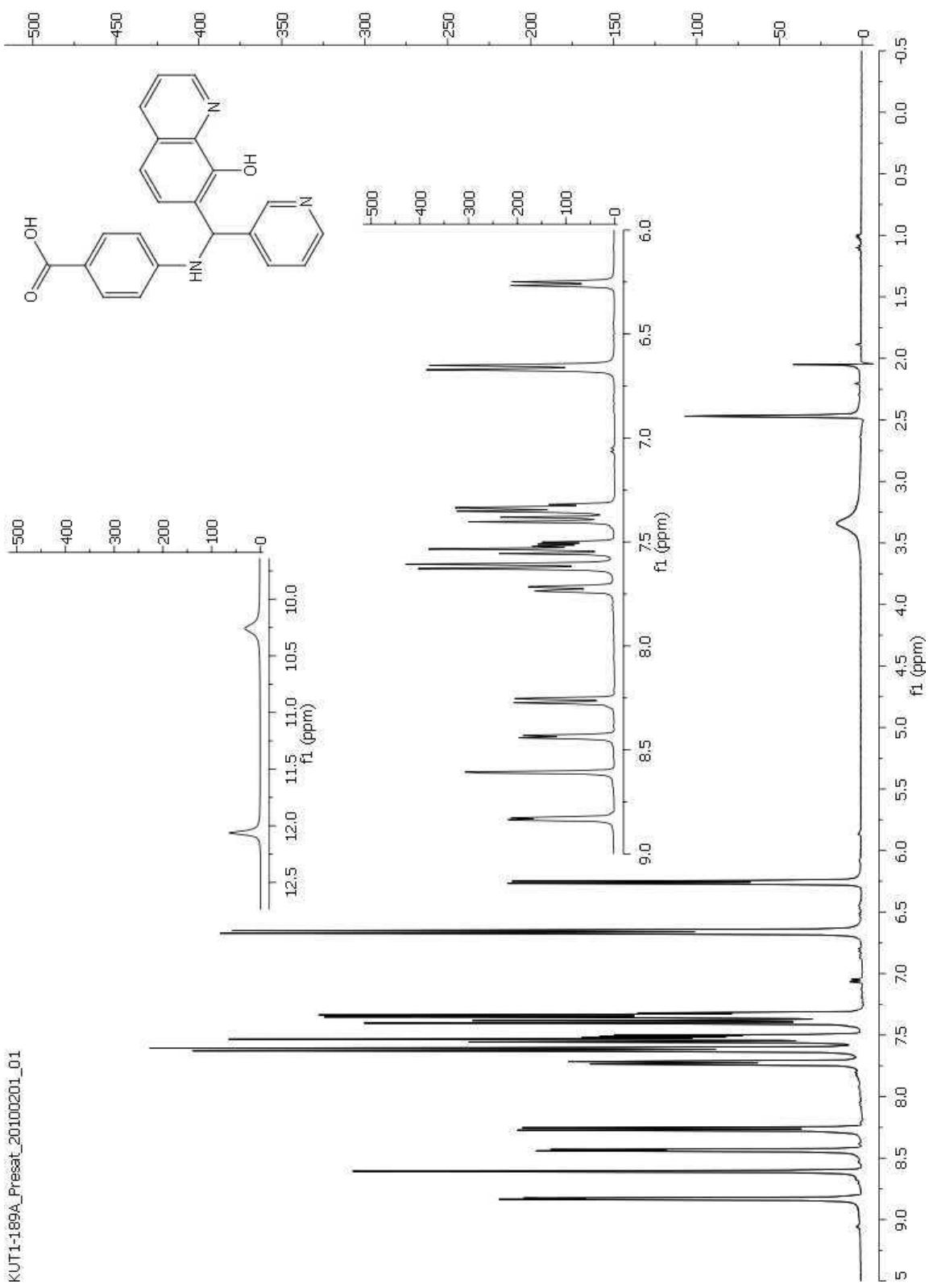
KUT1-189A_Presat_20100201_01
f1 (ppm)
OH
HN
N
O

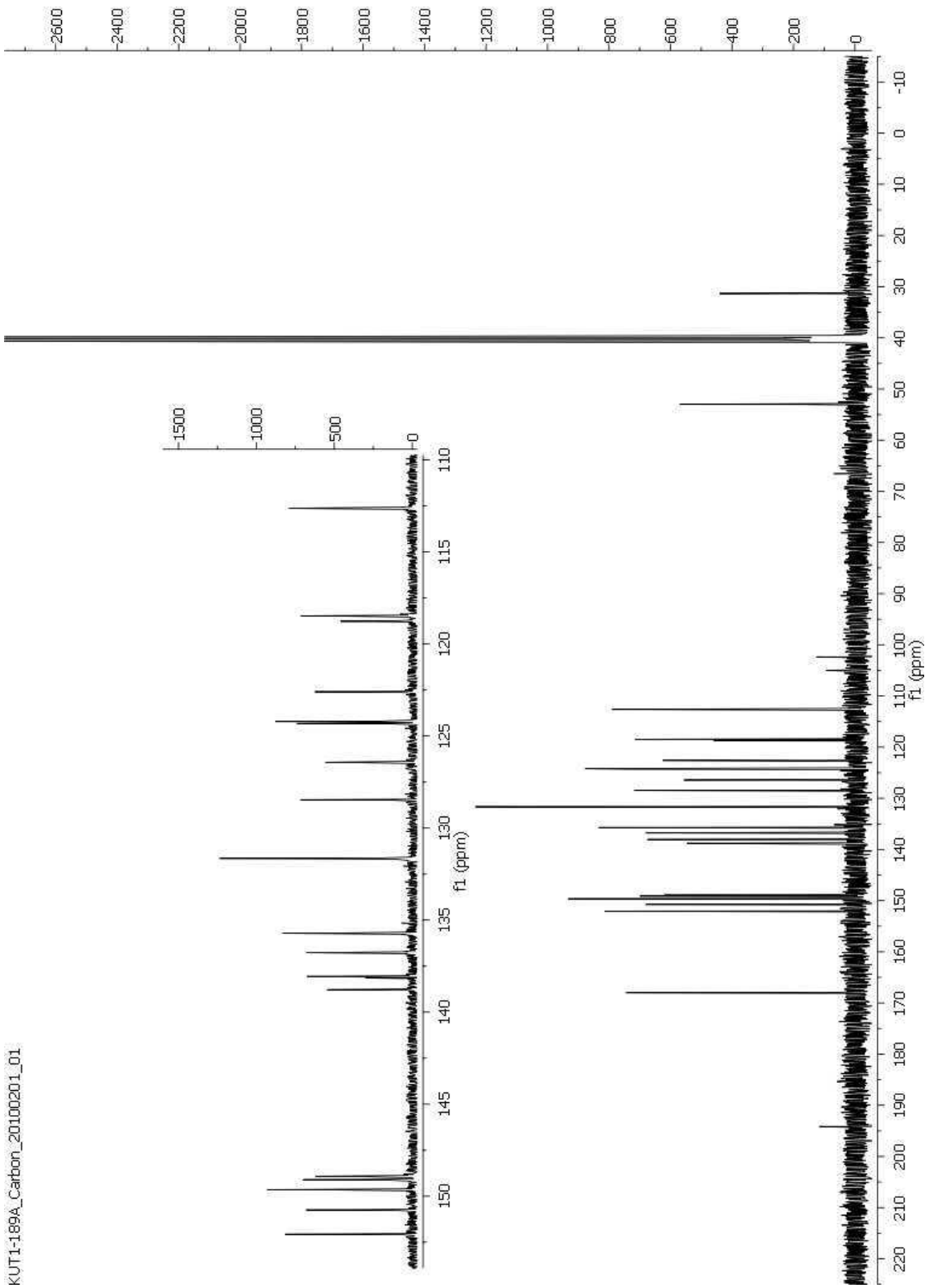
KUT1-189A_Carbon_20100201_01
f1 (ppm)
f1 (ppm)

4-((4-fluorophenyl)(8-hydroxyquinolin-7-yl)methylamino)benzoic acid (7):

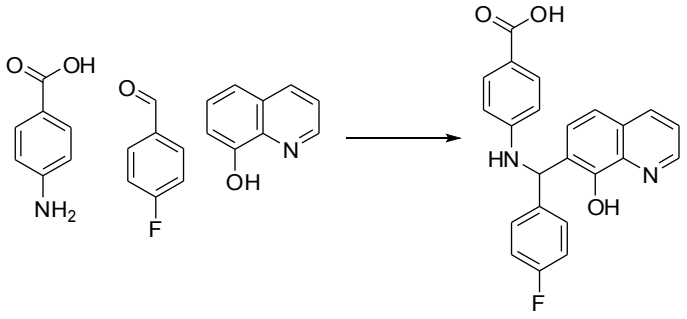

p-Fluorobenzaldehyde (0.250 g, 2.01 mmol), 8-hydroxyquinoline (2.95 g, 20.01 mmol), and *p*-aminobenzoic acid (0.276 g, 2.01 mmol) were stirred in sufficient ethanol to completely dissolve 8-hydroxyquinoline. The solution was allowed to stir for 26 d. The precipitate was removed via vacuum filtration and recrystallized from acetonitrile to afford 144.6 mg (0.37 mmol, 18.4 %) of a white powder. ^{1}H NMR (400 MHz DMSO-d_6, δ): 8.85 (d, 1H), 8.27 (d, 1H), 7.60 (d, 2H), 7.50 (m, 2H), 7.39, (m, 3H), 7.27 (d, 1H), 7.15 (t, 2H), 6.64 (d, 2H), 6.21 (d, 1H); ^{13}C NMR (DMSO-d_6, δ): 194.2, 168.0, 152.2, 150.6, 149.1, 138.8, 136.8, 131.6, 130.1, 130.0, 128.4, 126.7, 125.0, 122.5, 118.5, 118.4, 115.9, 115.7, 112.5, 54.1; HRMS-ESI (*m/z*): $[M - C_7H_6NO_2]^+$ calcd for $C_{23}H_{17}FN_2O_3$ 252.0819; found, 252.0822.

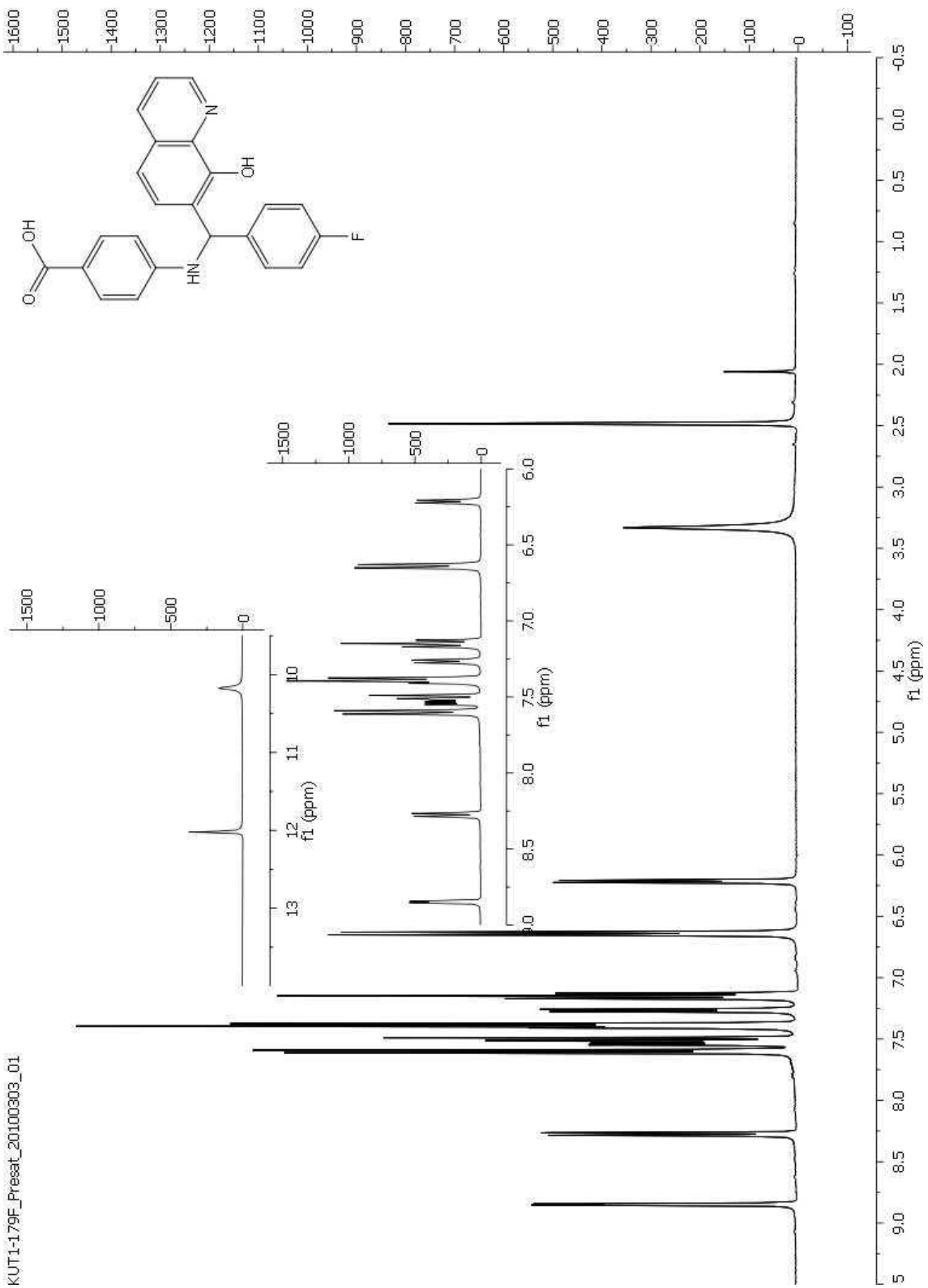
KUT1-179F_Presat_20100303_01
f1 (ppm)
OH
HN
F
N
O

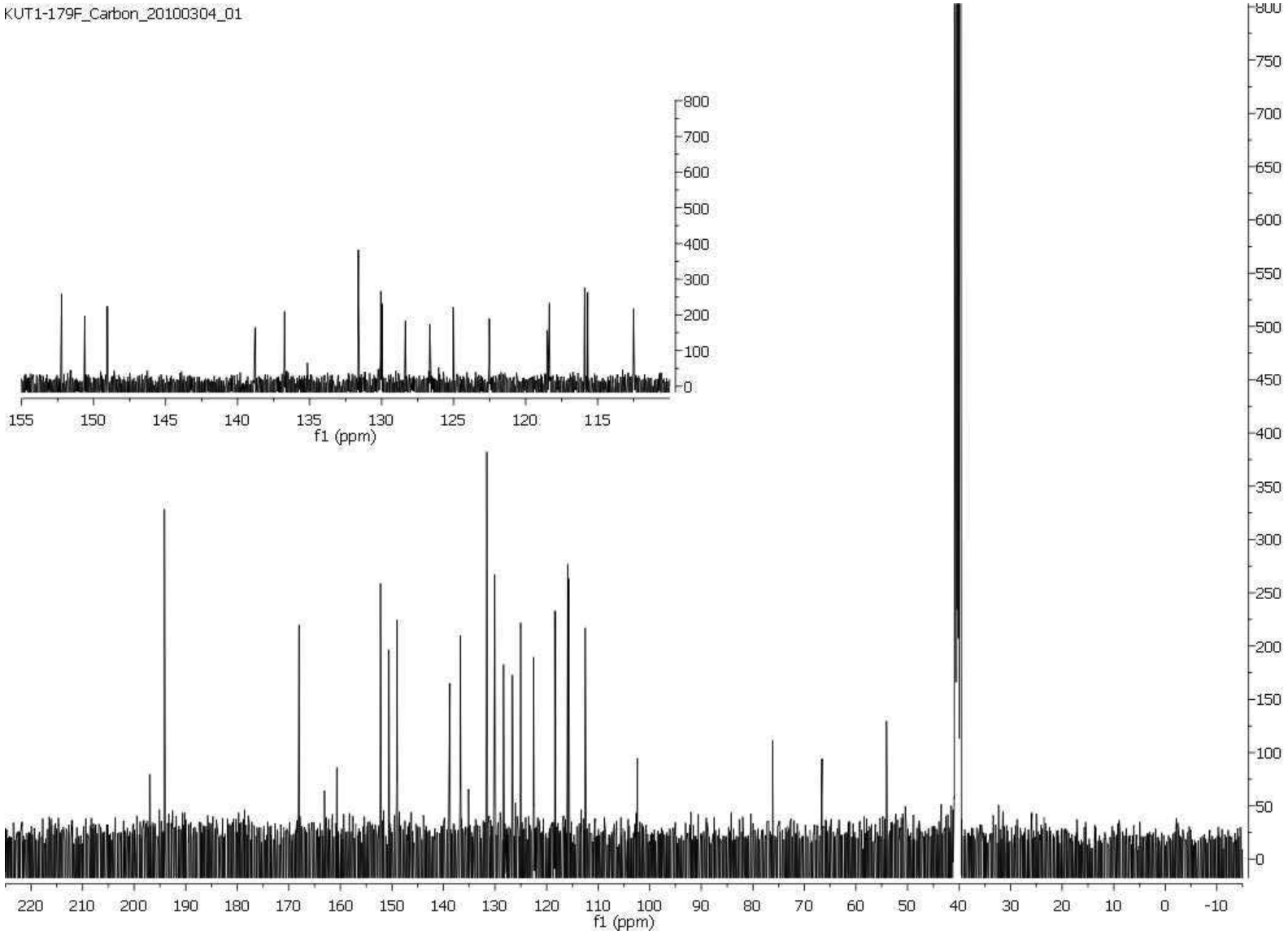
KUT1-179F_Carbon_20100304_01
f1 (ppm)
f1 (ppm)

***trans*-4-(pyridin-3-ylmethyleneamino)benzoic acid (14):**

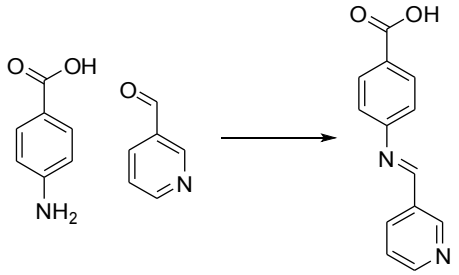

p-Aminobenzoic acid (0.32 g, 2.3 mmol) and 3-pyridine-carboxaldehyde (0.250 g, 2.3 mmol) were combined in enough ethanol to completely solvate both reactants. A precipitate is visible immediately after the addition of both reactants. The light yellow solid (0.430 g, 82.6%) was isolated via vacuum filtration. ^{1}H NMR (400 MHz DMSO-d_6, δ): 9.06 (s, 1H), 8.7 (s, 2H), 8.31 (d, 1H), 7.98 (d, 2H), 7.56 (dd, 1H), 7.34 (d, 2H).

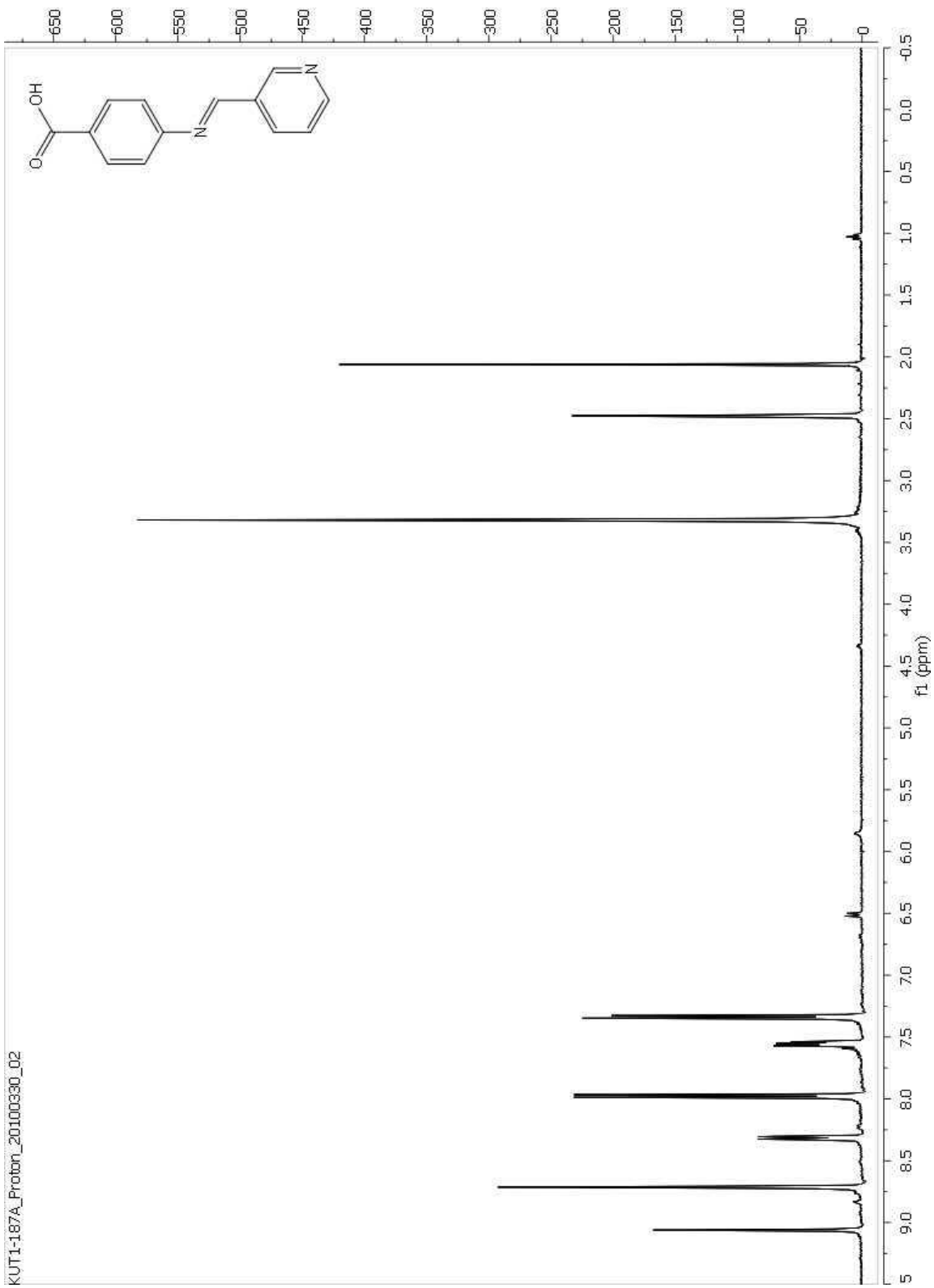
KUT1-187A_Proton_20100330_02
f1 (ppm)
OH
O
N
N

***trans*-4-(benzylideneamino)benzoic acid (16):**

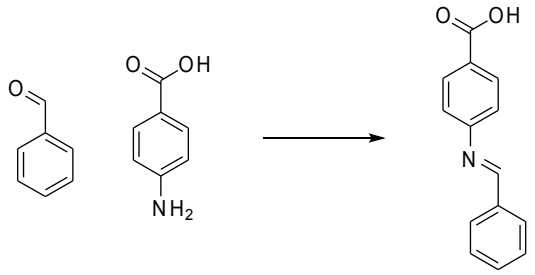

4-Aminobenzoic acid (4.061 g, 29.6 mmol) and benzaldehyde (3.141 g, 29.6 mmol) were dissolved in a minimal amount of ethanol and stirred for 4h at room temperature. The reaction mixture was cooled to 0 °C, and the resulting white precipitate was collected via vacuum filtration yielding 2.9664 g of a white solid (13.2 mmol, 44.5%). No further purification was necessary. ^{1}H NMR (400 MHz DMSO-d_6, δ): 12.73 (br s, 1H, -CO_2H), 8.65 (s, 1H, -NC*H*-), 8.00 (m, 4H, C*H*), 7.56 (m, 3H, C*H*), 7.31 (d, 2H, J = 8.4 Hz, C*H*)

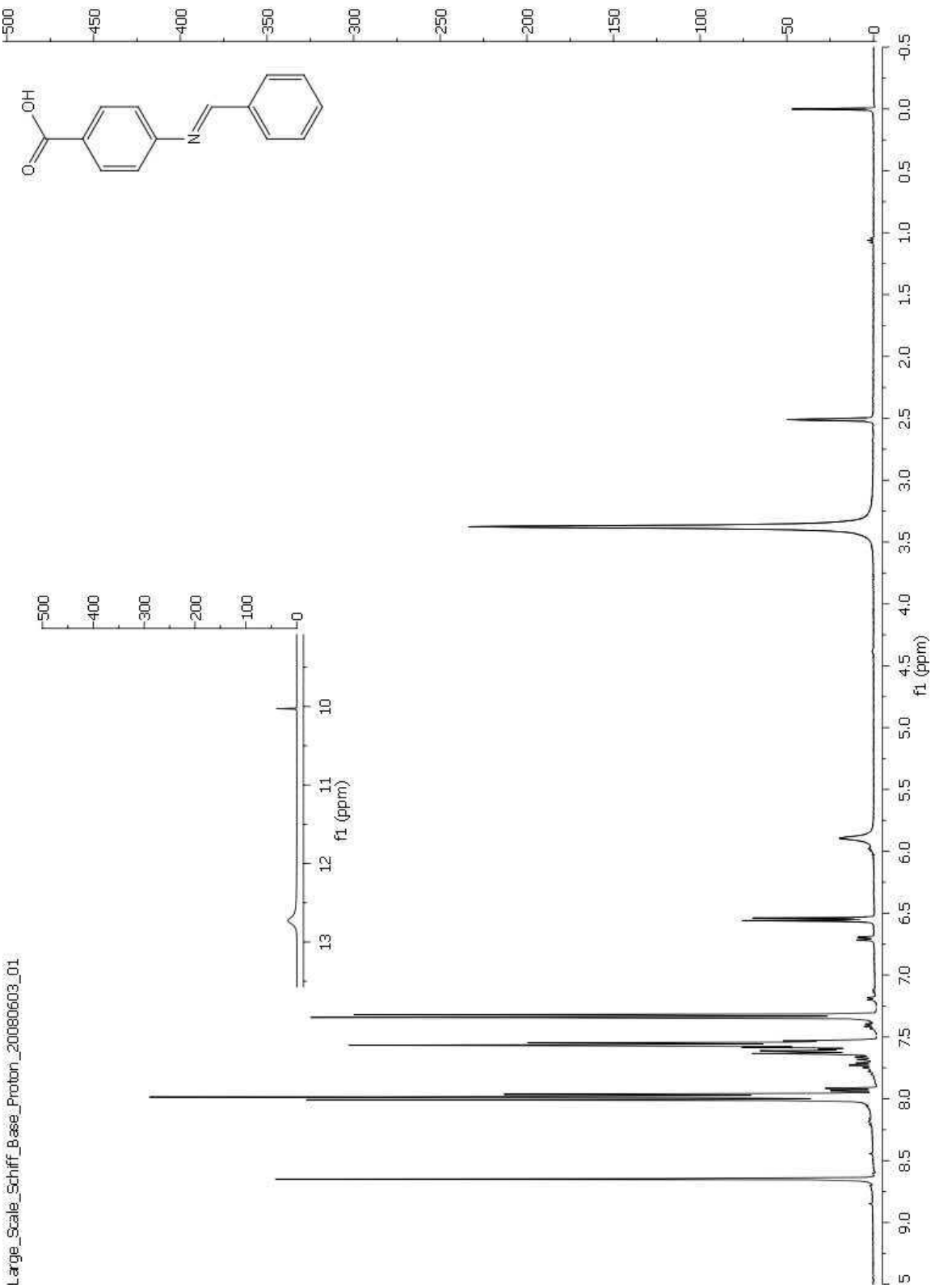
Large_Scale_Schiff_Base_Proton_20080603_01
OH
O
N
f1 (ppm)
f1 (ppm)

quinolin-8-yl benzoate (17):

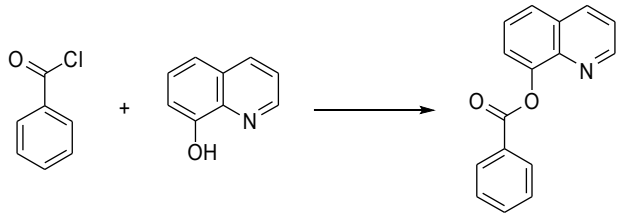

Freshly distilled benzoyl chloride (0.230 mL, 2.0 mmol) and 8-hydroxyquinoline (0.290 g, 2.0 mmol) were combined in enough methylene chloride to achieve solvation. The solution was stirred and refluxed for 24 h. The solution was concentrated under reduced pressure and the solution reconstituted in fresh ethanol. The mixture was gravity filtered to afford 52.2 mg of solid. The filtrate was concentrated under reduced pressure and reconstituted in ethanol again. The recrystallization procedure was repeated three more times to afford another 309.4 mg of white solid, a total of 361.6 mg (1.45 mmol, 62.1%) were isolated. ^{1}H NMR (400 MHz DMSO-d_6, δ): 8.87 (d, 1H), 8.49 (d, 1H), 8.23 (d, 2H), 7.99, (dd, 1H), 7.80 (t, 1H), 7.66 (m, 4H).

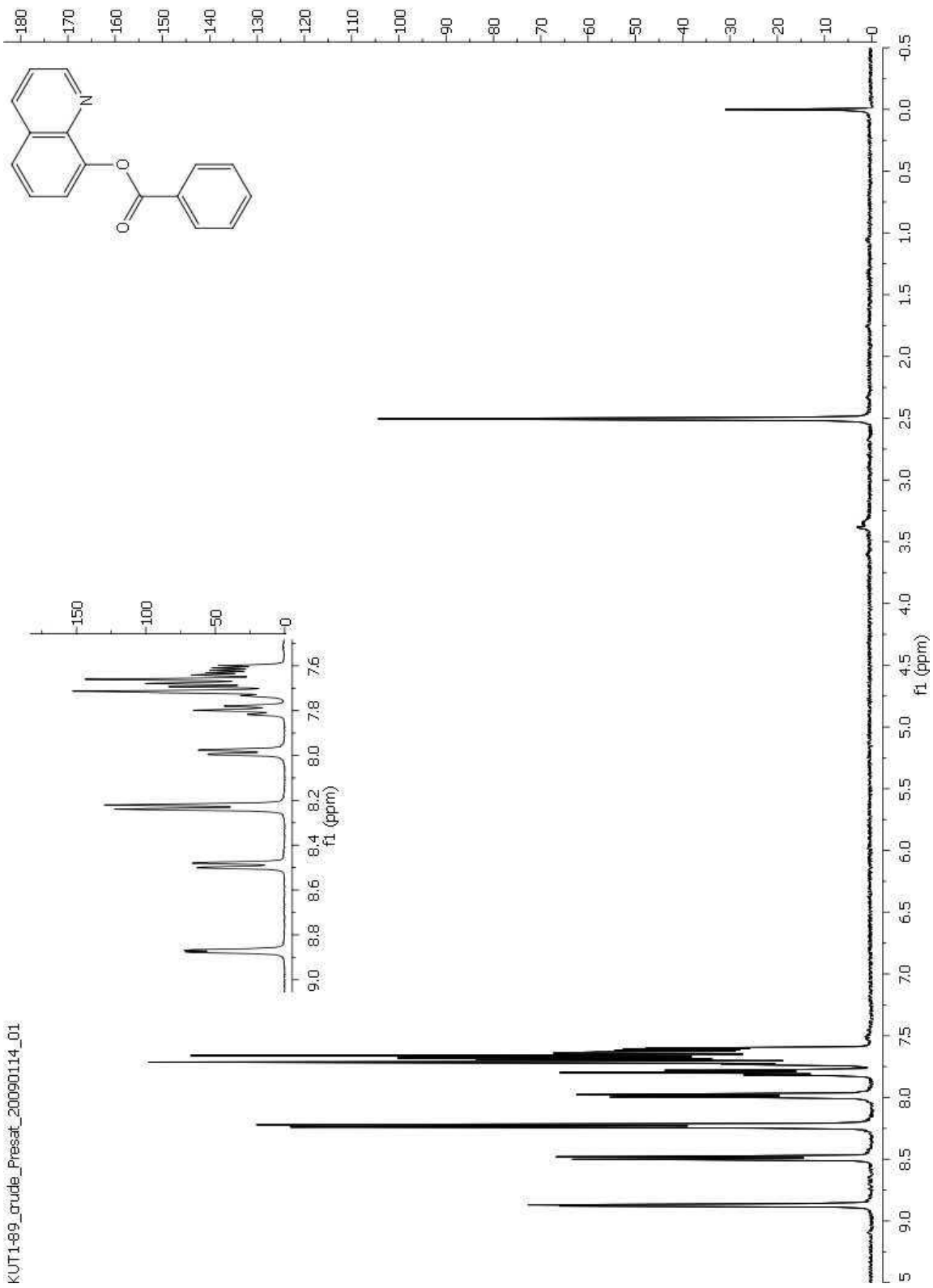
KUT1-69_crude_Presat_20090114_01
f1 (ppm)
f1 (ppm)

acetoxymethyl 4-((8-hydroxyquinolin-7-yl)(phenyl)methylamino)benzoate (19):

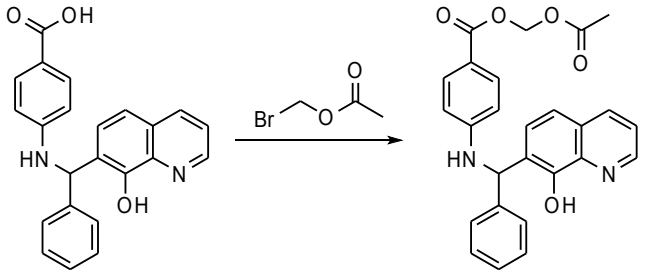

A solution of 4-((8-hydroxyquinolin-7-yl)(phenyl)methylamino)benzoic acid (0.100 g, 0.27 mmol) in dry THF and TEA (0.075 mL, 0.54 mmol) was stirred vigorously under a nitrogen atmosphere for 30 min. To the solution bromomethyl acetate was added drop-wise, and the solution allowed to stir for 36 h. The precipitate was removed via vacuum filtration and solvent removed from the filtrate under reduced pressure. TLC analysis of the crude product was performed, and the product was purified via flash column chromatography with 1:1 ethyl acetate:hexanes eluent. The top spot (R_f = 0.38) was isolated affording 27.3 mg (0.06 mmol, 22.9% yield) of a clear-white oily residue. ^{1}H NMR (400 MHz DMSO-d_6, δ): 8.85 (d, 1H), 8.27 (d, 1H), 7.63 (d, 2H), 7.53 (m, 3H), 7.36 (m, 5H), 7.23, (t, 1H) 6.69 (d, 2H), 6.24 (d, 1H), 5.78 (s, 2H), 2.02 (s, 3H); ^{13}C NMR (DMSO-d_6, δ): 170.1, 165.1, 153.3, 150.7, 149.1, 142.4, 138.8, 136.8, 132.0, 129.2, 128.4, 128.1, 127.8, 126.8, 124.9, 122.6, 118.3, 115.6, 79.8, 54.6, 21.2; HRMS-ESI (*m/z)*: $[M - C_{10}H_{10}NO_4]^+$ calcd for $C_{26}H_{22}N_2O_5^+$ 234.0913; found, 234.0912.

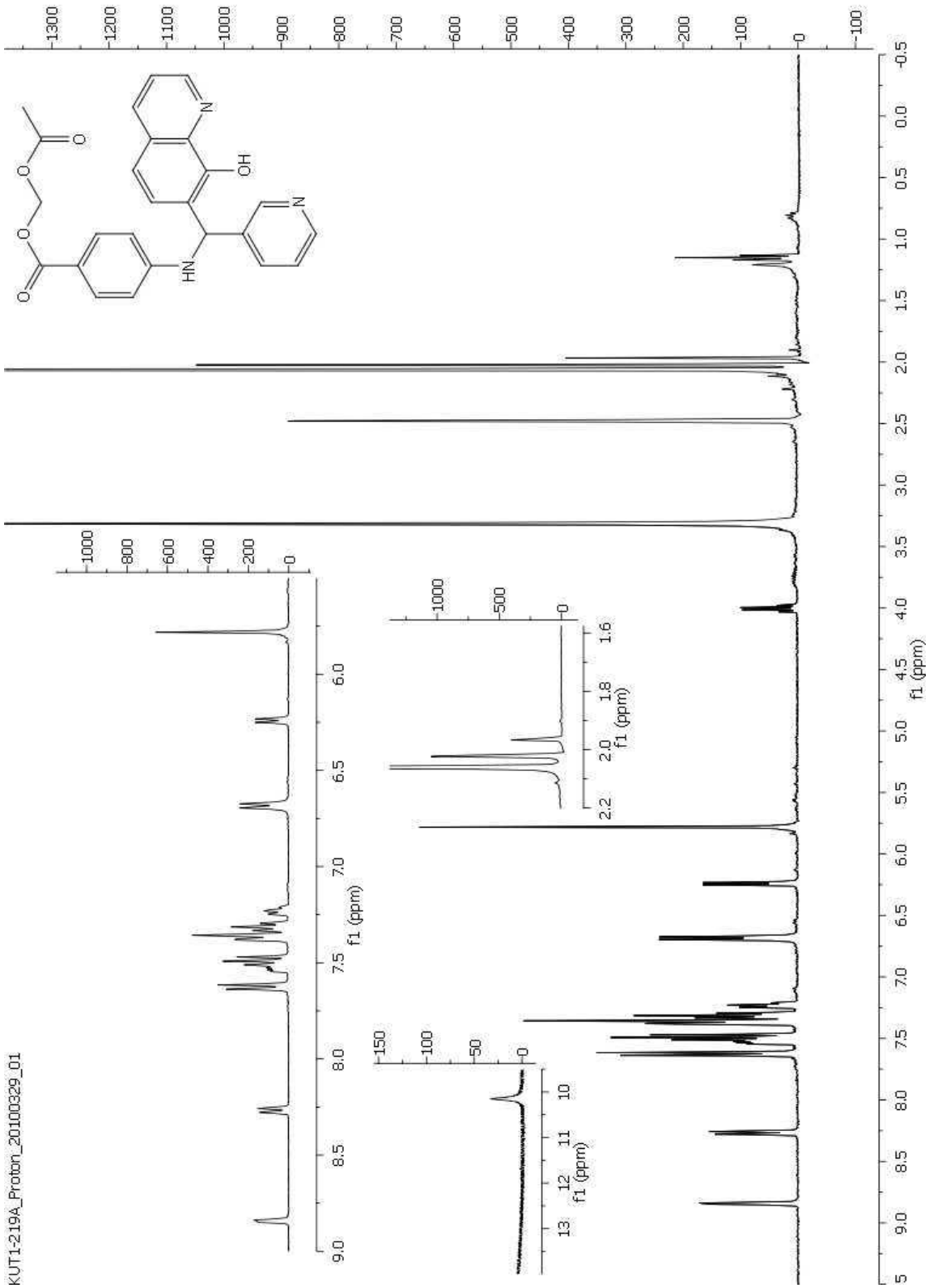
KUT1-219A_Proton_20100329_01
f1 (ppm)

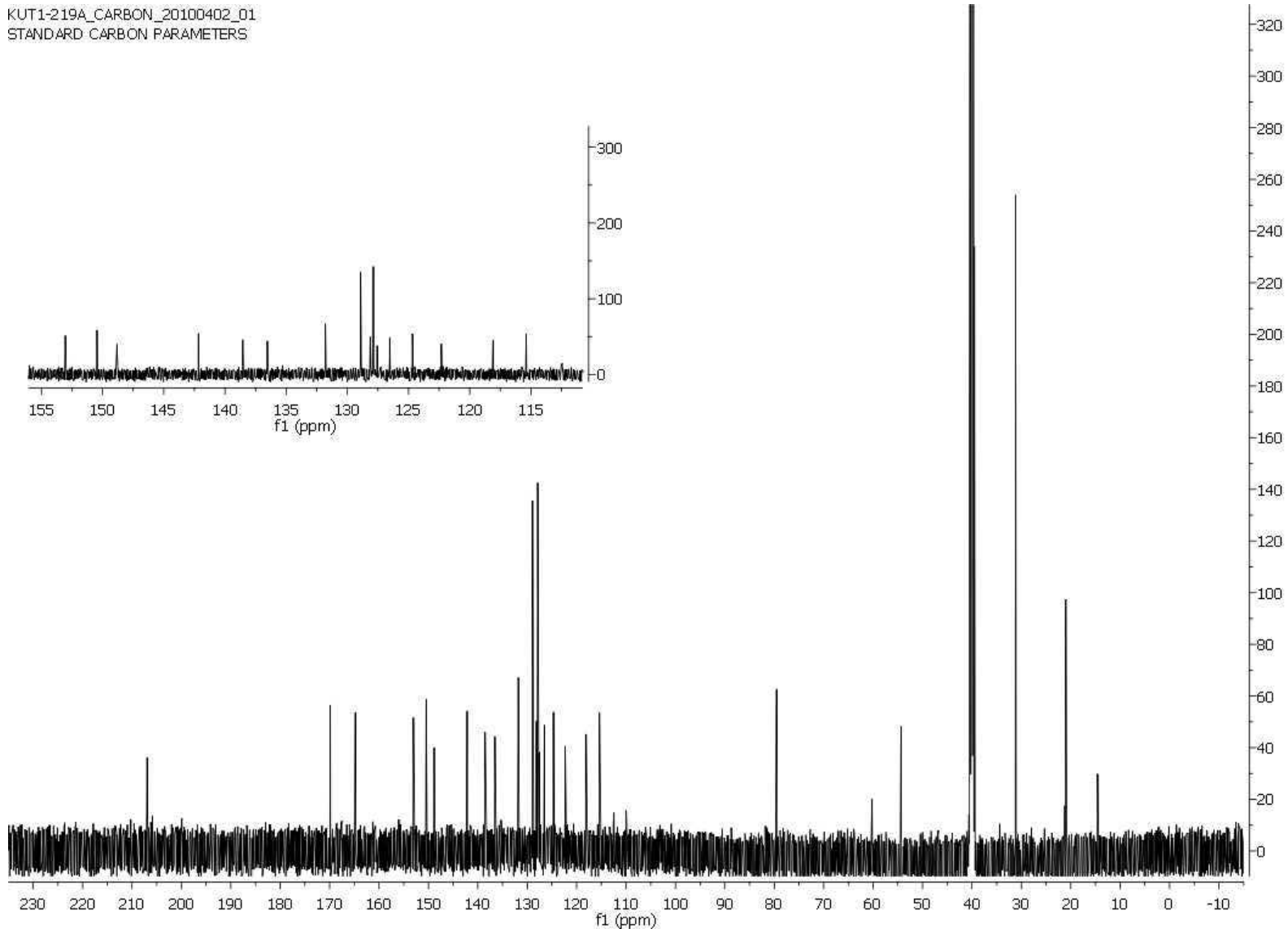
KUT1-219A_CARBON_20100402_01
STANDARD CARBON PARAMETERS
f1 (ppm)
f1 (ppm)

General procedure for fluorescence-based in vitro proteolysis assay:

The fluorescence-based in vitro assay was performed as previously described.[47, 51, 76] Yeast membrane fractions containing Rce1p were incubated with a range of inhibitor concentrations for 10 m at 30 °C in a black, flat, clear bottom, 96-well microtiter plate with two replicates. Synthetic internally quenched fluorescent peptide substrate was then added to the wells to form a final substrate concentration of 50 μM. The fluorescence of the samples was then monitored every 30 s for 1 h at 30 °C. The assay for compounds **1-6** was performed by Dr. Surya Manandhar. This procedure was repeated once with **7** for a total of 4 trials.

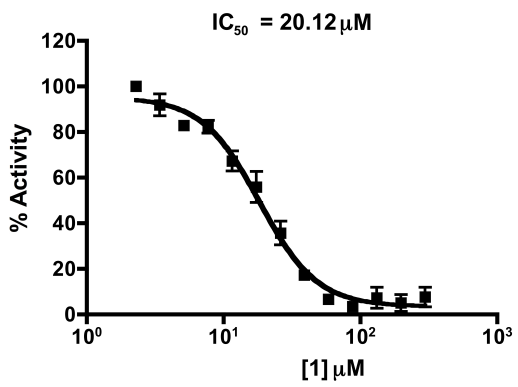

Assay performed by Dr. Surya Manandhar

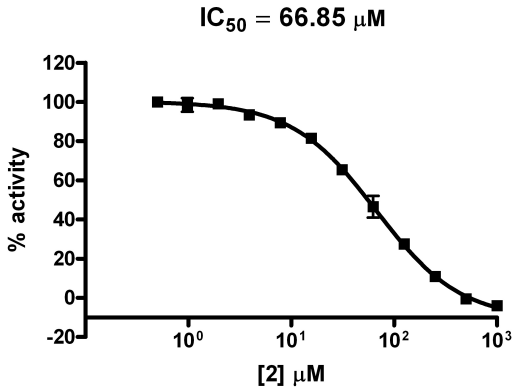

Assay performed by Dr. Surya Manandhar

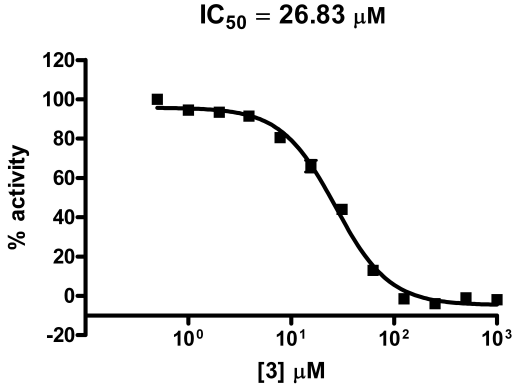

Assay performed by Dr. Surya Manandhar

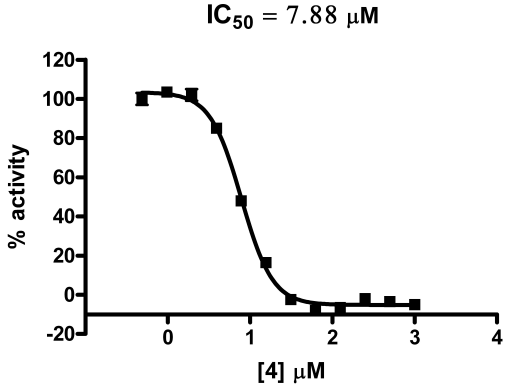

Assay performed by Dr. Surya Manandhar

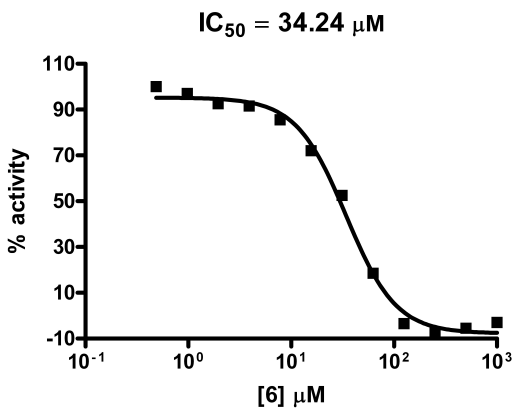

Assay performed by Dr. Surya Manandhar

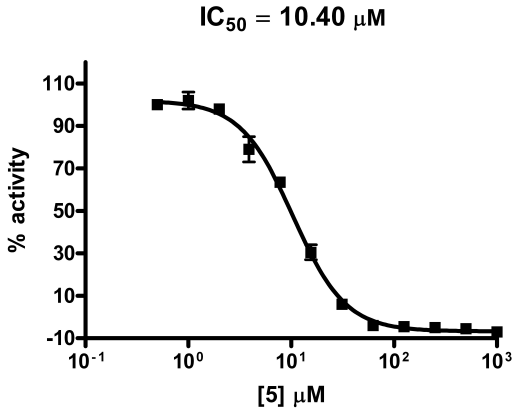

Assay performed by Dr. Surya Manandhar

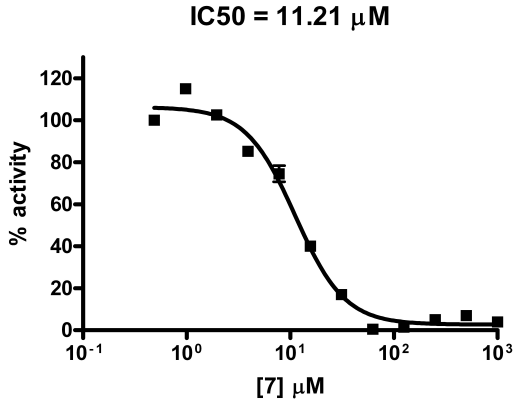

Assay performed by Robert Kutlik

Method for determing zinc binding dissociation constants (K_d): The free concentration of zinc dication in solution was determined (Equation 2). The total concentration of zinc in a measured solution was varied by combining different ratios of zinc-containing solution and those without zinc. The UV-Vis absorption spectrum from 350 – 200 nm was obatined for each solution. The wavelength displaying the largest absorbance change was converted to percent change in absorbance and plotted versus the log of the concentration of free zinc. The K_d of the analog was then determined from the inflection point of the curve.

Solutions used for determination of zinc binding dissociation constant (K_d):

Stock solutions of zinc: A stock solution of freshly purified zinc chloride (1.363 g, 10.0 mmol) was made in 7.0 pH HEPES buffer (250.0 mL) to form a zinc chloride concentration of 0.04 M. A concentrated zinc chloride stock solution was made from freshly purified zinc chloride (6.58 g, 48.3 mmol) with IDA (0.644 g, 4.83 mmol) in 250 mL HEPES buffer and 25 mL methanol to form a 0.176 M zinc chloride 0.0176 M IDA solution.

7.0 pH HEPES buffer solution: The 7.0 pH HEPES buffer was made from enzyme grade HEPES (23.83 g, 0.1 mol) in nano-pure water (1.0 L). The pH of the HEPES buffer was adjusted with sodium hydroxide (5.0 M) to 7.0 pH. The pH was measured using a probe, calibrated with 4.0 pH stock buffer solutions and 6.88 pH stock buffer solutions.

Iminodiacetic acid solution: A solution of iminodiacetic acid (IDA, 133.3 mg, 1.00 mmol) was made in 7.0 pH HEPES buffer (100.0 mL) solution to form a IDA concentration of 10.0 mM.

Solutions of 4-((8-hydroxyquinolin-7-yl)(phenyl)methylamino)benzoic acid (1): A stock solution of **1** (9.3 mg, 25 μmol) was made in methanol (25.0 mL) to form a 1.0 mM concentration. From this stock solution two working solutions were prepared via dilutions. For

the 10.0 μM **1**, 1.0 mM IDA, and 10.0 mM $ZnCl_2$ solution, 1.0 mL of stock **1** solution, 10.0 mL of stock IDA solution, 25.0 mL of stock 0.04 M $ZnCl_2$ solution, and 9.0 mL of methanol were combined in a 100 mL volumetric flask. The solution was then dilute with 7.0 pH HEPES buffer to fill. The working solution containing 10.0 μM NSC **1** and 1.0 mM IDA was made in the same fashion excluding the addition of any $ZnCl_2$ solution. For both working solutions a 1:9 ratio of methanol: HEPES aqueous solution was maintained.

Solutions of 4-((8-hydroxyquinolin-7-yl)(pyridin-2-yl)methylamino)benzoic acid (2): A stock solution of **2** (9.3 mg, 25 μmol) was made in methanol (25.0 mL) to form a 1.0 mM concentration. From this stock solution two working solutions were prepared via dilutions. For the 10.0 μM **2**, 1.0 mM IDA, and 10.0 mM $ZnCl_2$ solution, 1.0 mL of stock **2** solution, 10.0 mL of stock IDA solution, 25.0 mL of stock 0.04 M $ZnCl_2$ solution, and 9.0 mL of methanol were combined in a 100 mL volumetric flask. The solution was then dilute with 7.0 pH HEPES buffer to fill. The working solution containing 10.0 μM **2** and 1.0 mM IDA was made in the same fashion excluding the addition of any $ZnCl_2$ solution. For both working solutions a 1:9 ratio of methanol: HEPES aqueous solution was maintained.

Solutions of 4-((8-hydroxyquinolin-7-yl)(*p*-tolyl)methylamino)benzoic acid (4): A stock solution of **4** (9.6 mg, 25 μmol) was made in methanol (25 mL) to form a 1.0 mM concentration. From this stock solution two working solutions were prepared via dilutions. For the 10.0 μM **4**, 1.0 mM IDA, and 10.0 mM $ZnCl_2$ solution, 1.0 mL of stock **4** solution, 10.0 mL of stock IDA solution, 25.0 mL of stock 0.04 M $ZnCl_2$ solution, and 9.0 mL of methanol were combined in a 100 mL volumetric flask. The solution was then dilute with 7.0 pH HEPES buffer to fill. The working solution containing 10.0 μM **4** and 1.0 mM IDA was made in the same fashion

excluding the addition of any $ZnCl_2$ solution. For both working solutions a 1:9 ratio of methanol: HEPES aqueous solution was maintained.

Solutions of 4-((4-bromophenyl)(8-hydroxyquinolin-7-yl)methylamino)benzoic acid (5): A stock solution of **5** (8.2 mg, 18 μmol) was made in methanol (25.0 mL) to form a 0.73 mM concentration. From this stock solution two working solutions were prepared via dilutions. For the 7.3 μM **5**, 1.0 mM IDA, and 10.0 mM $ZnCl_2$ solution, 1.0 mL of stock **5** solution, 10.0 mL of stock IDA solution, 25.0 mL of stock 0.04 M $ZnCl_2$ solution, and 9.0 mL of methanol were combined in a 100 mL volumetric flask. The solution was then dilute with 7.0 pH HEPES buffer to fill. The working solution containing 7.3 μM **5** and 1.0 mM IDA was made in the same fashion excluding the addition of any $ZnCl_2$ solution. For both working solutions a 1:9 ratio of methanol: HEPES aqueous solution was maintained.

Solutions of 4-((8-hydroxyquinolin-7-yl)(pyridin-3-yl)methylamino)benzoic acid (6): A stock solution of **6** (9.3 mg, 25 μmol) was made in methanol (25 mL) to form a 1.0 mM concentration. From this stock solution two working solutions were prepared via dilutions. For the 10.0 μM **6**, 1.0 mM IDA, and 10.0 mM $ZnCl_2$ solution, 1.0 mL of stock **6** solution, 5.68 mL of stock 0.176 M $ZnCl_2$, 0.0176 M IDA solution, and 8.9 mL of methanol were combined in a 100 mL volumetric flask. The solution was then dilute with 7.0 pH HEPES buffer to fill. The working solution containing 10.0 μM **6** and 1.0 mM IDA was made from 1.0 mL of stock **6** solution, 10.0 mL of stock IDA solution, 25.0 mL of stock 0.04 M $ZnCl_2$ solution, and 9.0 mL of methanol in a 100 mL volumetric flask and diluted to fill with7.0 pH HEPES buffer. For both working solutions a 1:9 ratio of methanol: HEPES aqueous solution was maintained.

Solutions of 4-((4-fluorophenyl)(8-hydroxyquinolin-7-yl)methylamino)benzoic acid (7): A stock solution of **7** (9.7 mg, 25 μmol) was made in methanol (25 mL) to form a 1.0 mM concentration. From this stock solution two working solutions were prepared via dilutions. For the 10.0 μM **7**, 1.0 mM IDA, and 10.0 mM $ZnCl_2$ solution, 1.0 mL of stock **7** solution, 5.68 mL of stock 0.176 M $ZnCl_2$, 0.0176 M IDA solution, and 8.9 mL of methanol were combined in a 100 mL volumetric flask. The solution was then dilute with 7.0 pH HEPES buffer to fill. The working solution containing 10.0 μM **7** and 1.0 mM IDA was made from 1.0 mL of stock **7** solution, 10.0 mL of stock IDA solution, 25.0 mL of stock 0.04 M $ZnCl_2$ solution, and 9.0 mL of methanol in a 100 mL volumetric flask and diluted to fill with 7.0 pH HEPES buffer. For both working solutions a 1:9 ratio of methanol: HEPES aqueous solution was maintained.

Solutions of NSC 1008: From 25 μL of a stock solution of NSC 1008 (10 mM), 1.42 mL of stock 0.176 M $ZnCl_2$, 0.0176 M IDA solution, and 2.4 mL of methanol a 10.0 μM NSC 1008, 1.0 mM IDA, and 10.0 mM $ZnCl_2$ solution was made in a 25 mL volumetric flask. The solution was dilute with 7.0 pH HEPES buffer to fill. The working solution containing 10.0 μM NSC 1008 and 1.0 mM IDA was made from 25 μL of a stock solution of NSC 1008, 2.5 mL of stock IDA solution, and 2.5 mL of methanol in a 25 mL volumetric flask and diluted to fill with7.0 pH HEPES buffer. For both working solutions a 1:9 ratio of methanol: HEPES aqueous solution was maintained.

Solutions of NSC 1013: From 25 μL of a stock solution of NSC 1013 (10 mM), 1.42 mL of stock 0.176 M $ZnCl_2$, 0.0176 M IDA solution, and 2.4 mL of methanol a 10.0 μM NSC 1013, 1.0 mM IDA, and 10.0 mM $ZnCl_2$ solution was made in a 25 mL volumetric flask. The solution was dilute with 7.0 pH HEPES buffer to fill. The working solution containing 10.0 μM NSC 1013

and 1.0 mM IDA was made from 25 μL of a stock solution of NSC 1013, 2.5 mL of stock IDA solution, and 2.5 mL of methanol in a 25 mL volumetric flask and diluted to fill with7.0 pH HEPES buffer. For both working solutions a 1:9 ratio of methanol: HEPES aqueous solution was maintained.

Solutions of NSC 84093: From 25 μL of a stock solution of NSC 84093 (10 mM), 1.42 mL of stock 0.176 M $ZnCl_2$, 0.0176 M IDA solution, and 2.4 mL of methanol a 10.0 μM NSC 84093, 1.0 mM IDA, and 10.0 mM $ZnCl_2$ solution was made in a 25 mL volumetric flask. The solution was dilute with 7.0 pH HEPES buffer to fill. The working solution containing 10.0 μM NSC 84093 and 1.0 mM IDA was made from 25 μL of a stock solution of NSC 84093, 2.5 mL of stock IDA solution, and 2.5 mL of methanol in a 25 mL volumetric flask and diluted to fill with7.0 pH HEPES buffer. For both working solutions a 1:9 ratio of methanol: HEPES aqueous solution was maintained.

Solutions of NSC 84097: From 25 μL of a stock solution of NSC 84097 (10 mM), 1.42 mL of stock 0.176 M $ZnCl_2$, 0.0176 M IDA solution, and 2.4 mL of methanol a 10.0 μM NSC 84097, 1.0 mM IDA, and 10.0 mM $ZnCl_2$ solution was made in a 25 mL volumetric flask. The solution was dilute with 7.0 pH HEPES buffer to fill. The working solution containing 10.0 μM NSC 84097 and 1.0 mM IDA was made from 25 μL of a stock solution of NSC 84097, 2.5 mL of stock IDA solution, and 2.5 mL of methanol in a 25 mL volumetric flask and diluted to fill with7.0 pH HEPES buffer. For both working solutions a 1:9 ratio of methanol: HEPES aqueous solution was maintained.

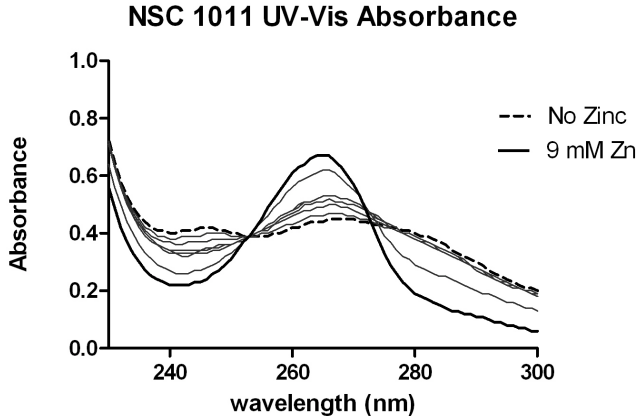
NSC 1011 UV-Vis Absorbance
Absorbance
wavelength (nm)
No Zinc
9 mM Zn

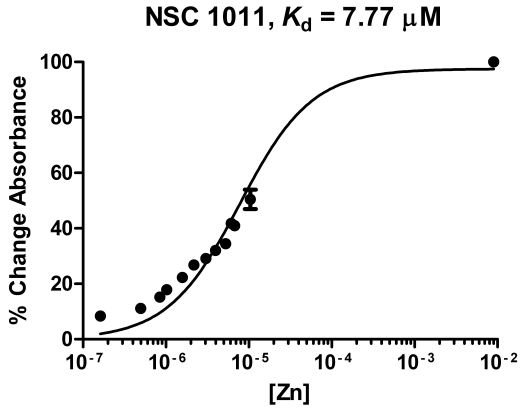
NSC 1011, K_d = 7.77 μM
% Change Absorbance
[Zn]

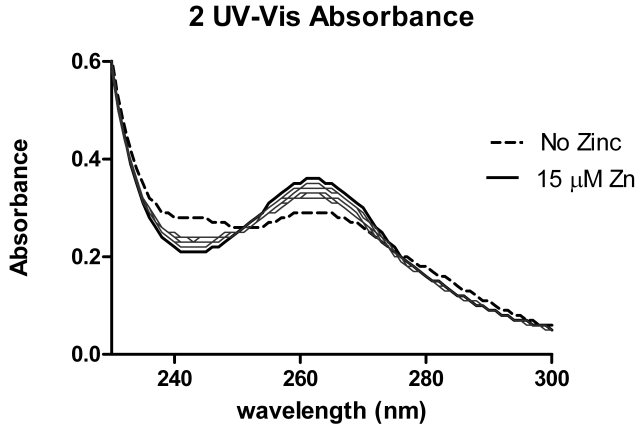
2 UV-Vis Absorbance
Absorbance
wavelength (nm)
No Zinc
15 μM Zn

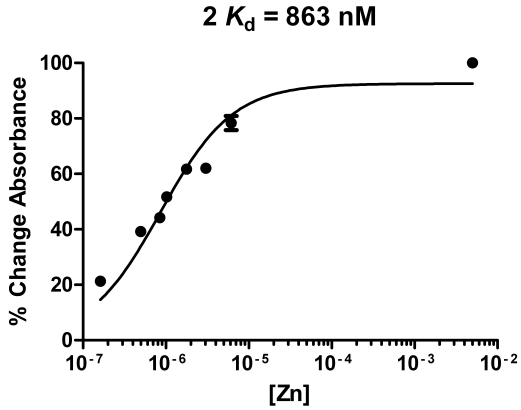
2 K_d = 863 nM
% Change Absorbance
[Zn]

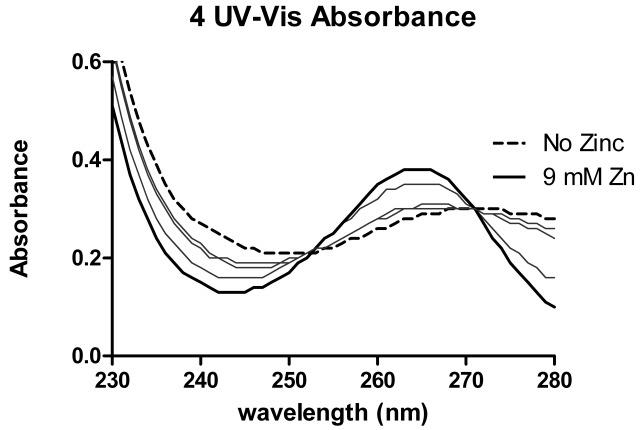
4 UV-Vis Absorbance
Absorbance
wavelength (nm)
No Zinc
9 mM Zn

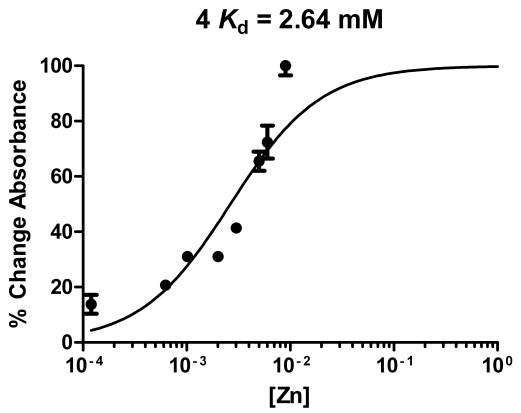
4 K_d = 2.64 mM
% Change Absorbance
[Zn]

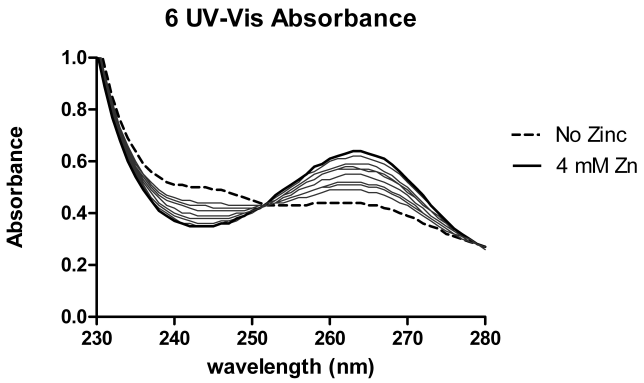
6 UV-Vis Absorbance
Absorbance
wavelength (nm)
No Zinc
4 mM Zn

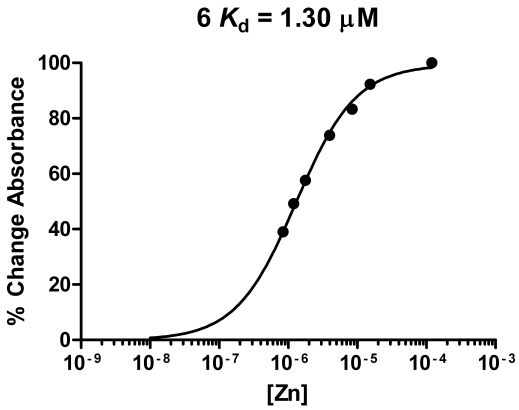
6 K_d = 1.30 μM
% Change Absorbance
[Zn]

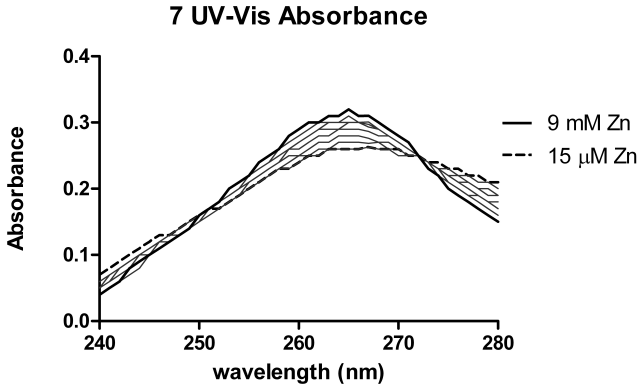
7 UV-Vis Absorbance
Absorbance
wavelength (nm)
9 mM Zn
15 μM Zn

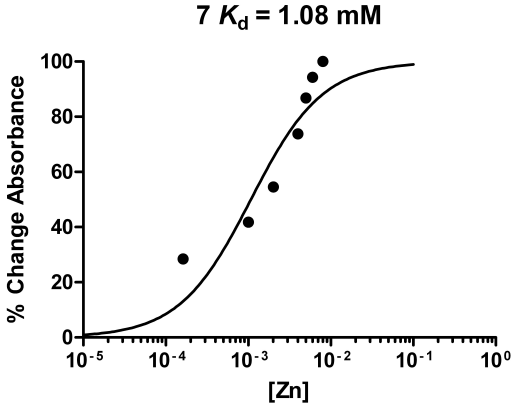
7 K_d = 1.08 mM
% Change Absorbance
[Zn]

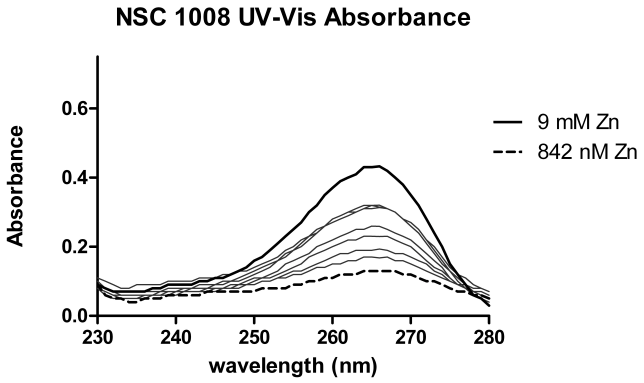
NSC 1008 UV-Vis Absorbance
Absorbance
wavelength (nm)
9 mM Zn
842 nM Zn

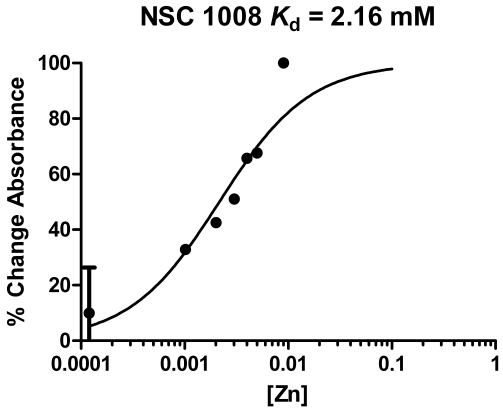
NSC 1008 K_d = 2.16 mM
% Change Absorbance
[Zn]

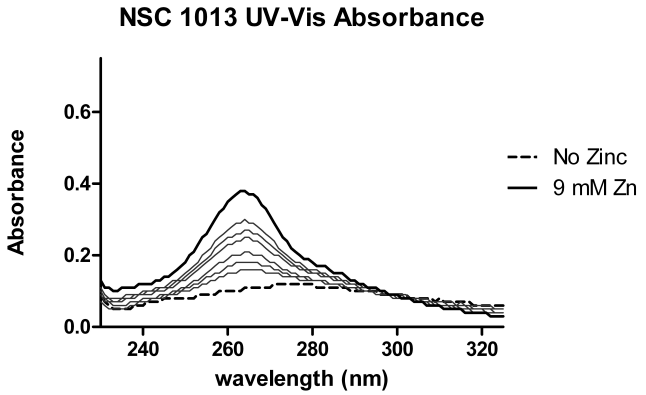
NSC 1013 UV-Vis Absorbance
Absorbance
0.0
0.2
0.4
0.6
240
260
280
300
320
wavelength (nm)
No Zinc
9 mM Zn

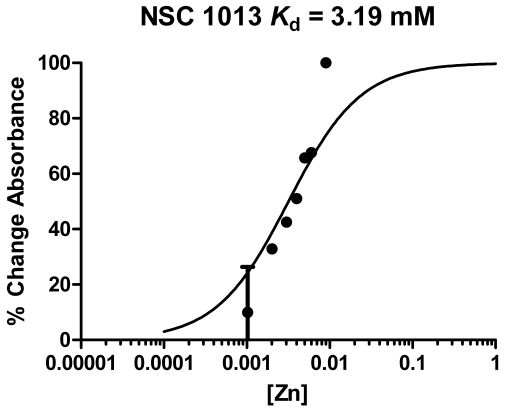
NSC 1013 K_d = 3.19 mM
% Change Absorbance
0
20
40
60
80
100
0.00001
0.0001
0.001
0.01
0.1
1
[Zn]

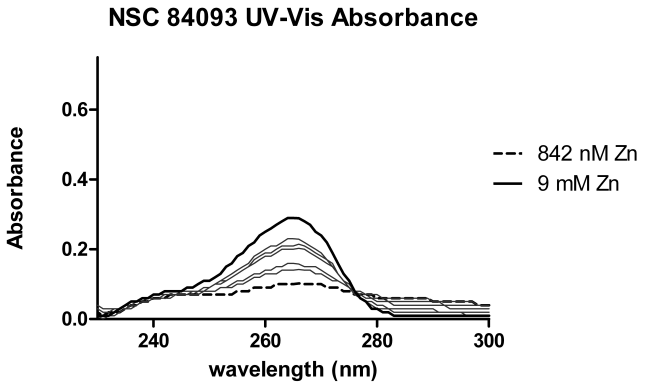
NSC 84093 UV-Vis Absorbance
Absorbance
0.0
0.2
0.4
0.6
240
260
280
300
wavelength (nm)
842 nM Zn
9 mM Zn

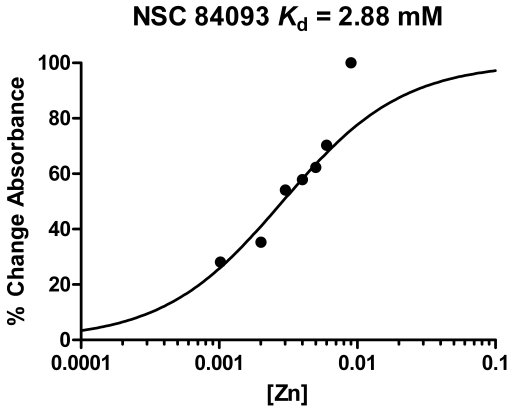
NSC 84093 K_d = 2.88 mM
% Change Absorbance
0
20
40
60
80
100
0.0001
0.001
0.01
0.1
[Zn]

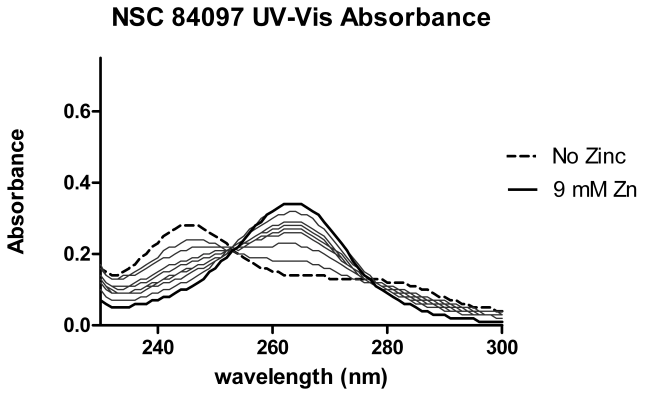
NSC 84097 UV-Vis Absorbance
Absorbance
0.0
0.2
0.4
0.6
240
260
280
300
wavelength (nm)
No Zinc
9 mM Zn

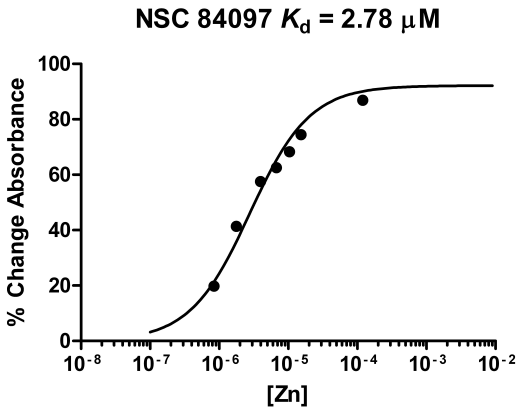
NSC 84097 K_d = 2.78 μM
% Change Absorbance
0
20
40
60
80
100
10^{-8}
10^{-7}
10^{-6}
10^{-5}
10^{-4}
10^{-3}
10^{-2}
[Zn]

Method for determining calcium binding dissociation constants (K_d): The free concentration of calcium dication in solution was determined (Equation 2). The total concentration of calcium in a measured solution was varied by combining different ratios of calcium-containing solution and those without calcium. The UV-Vis absorption spectrum from 350 – 200 nm was obatined for each solution. The wavelength displaying the largest absorbance change was converted to percent change in absorbance and plotted versus the log of the concentration of free zinc. The K_d of the analog was then determined from the inflection point of the curve.

Solutions used for determination of calcium binding dissociation constants (K_d):

Stock solution of calcium: A stock solution of calcium chloride dihydrate (1.470 g, 10.0 mmol) was made in 7.0 pH HEPES buffer (250.0 mL) to form a calcium chloride concentration of 0.04 M.

7.0 pH HEPES buffer solution: The 7.0 pH HEPES buffer was made from enzyme grade HEPES (23.83 g, 0.1 mol) in nano-pure water (1.0 L). The pH of the HEPES buffer was adjusted with sodium hydroxide (5.0 M) to 7.0 pH. The pH was measured using a probe, calibrated with 4.0 pH stock buffer solutions and 6.88 pH stock buffer solutions.

Solution of nitriloacetic acid: A solution of nitrilotriacetic acid (NTA, 181.1 mg, 1.00 mmol) was made in 7.0 pH HEPES buffer (100.0 mL) solution to form a NTA concentration of 10.0 mM.

Solutions of 4-((8-hydroxyquinolin-7-yl)(phenyl)methylamino)benzoic acid (1): A stock solution of NSC 1011 (9.3 mg, 25 μmol) was made in methanol (25.0 mL) to form a 1.0 mM concentration. From this stock solution two working solutions were prepared via dilutions. For the 10.0 μM **1**, 1.0 mM NTA, and 10.0 mM $CaCl_2$ solution, 1.0 mL of stock **1** solution, 10.0 mL

of stock NTA solution, 25.0 mL of stock 0.04 M $CaCl_2$ solution, and 9.0 mL of methanol were combined in a 100 mL volumetric flask. The solution was then dilute with 7.0 pH HEPES buffer to fill. The working solution containing 10.0 μM **1** and 1.0 mM NTA was made in the same fashion excluding the addition of any $CaCl_2$ solution. For both working solutions a 1:9 ratio of methanol: HEPES aqueous solution was maintained.

Solutions of 4-((8-hydroxyquinolin-7-yl)(pyridin-2-yl)methylamino)benzoic acid (2): A stock solution of **2** (9.3 mg, 25 μmol) was made in methanol (25.0 mL) to form a 1.0 mM concentration. From this stock solution two working solutions were prepared via dilutions. For the 10.0 μM **2**, 1.0 mM NTA, and 10.0 mM $CaCl_2$ solution, 1.0 mL of stock **2** solution, 10.0 mL of stock NTA solution, 25.0 mL of stock 0.04 M $CaCl_2$ solution, and 9.0 mL of methanol were combined in a 100 mL volumetric flask. The solution was then dilute with 7.0 pH HEPES buffer to fill. The working solution containing 10.0 μM **2** and 1.0 mM NTA was made in the same fashion excluding the addition of any $CaCl_2$ solution. For both working solutions a 1:9 ratio of methanol: HEPES aqueous solution was maintained.

Solutions of 4-((8-hydroxyquinolin-7-yl)(*p*-tolyl)methylamino)benzoic acid (4): A stock solution of **4** (9.6 mg, 25 μmol) was made in methanol (25mL) to form a 1.0 mM concentration. From this stock solution two working solutions were prepared via dilutions. For the 10.0 μM **4**, 1.0 mM NTA, and 10.0 mM $CaCl_2$ solution, 1.0 mL of stock **4** solution, 10.0 mL of stock NTA solution, 25.0 mL of stock 0.04 M $CaCl_2$ solution, and 9.0 mL of methanol were combined in a 100 mL volumetric flask. The solution was then dilute with 7.0 pH HEPES buffer to fill. The working solution containing 10.0 μM **4** and 1.0 mM NTA was made in the same fashion

excluding the addition of any $CaCl_2$ solution. For both working solutions a 1:9 ratio of methanol: HEPES aqueous solution was maintained.

Solutions of 4-((4-bromophenyl)(8-hydroxyquinolin-7-yl)methylamino)benzoic acid (5): A stock solution of **5** (8.2 mg, 18 μmol) was made in methanol (25.0 mL) to form a 0.73 mM concentration. From this stock solution two working solutions were prepared via dilutions. For the 14.6 μM **5**, 1.0 mM NTA, and 10.0 mM $CaCl_2$ solution, 1.0 mL of stock **5** solution, 10.0 mL of stock NTA solution, 25.0 mL of stock 0.04 M $CaCl_2$ solution, and 9.0 mL of methanol were combined in a 100 mL volumetric flask. The solution was then dilute with 7.0 pH HEPES buffer to fill. The working solution containing 14.6 μM **5** and 1.0 mM NTA was made in the same fashion excluding the addition of any $CaCl_2$ solution. For both working solutions a 1:9 ratio of methanol: HEPES aqueous solution was maintained.

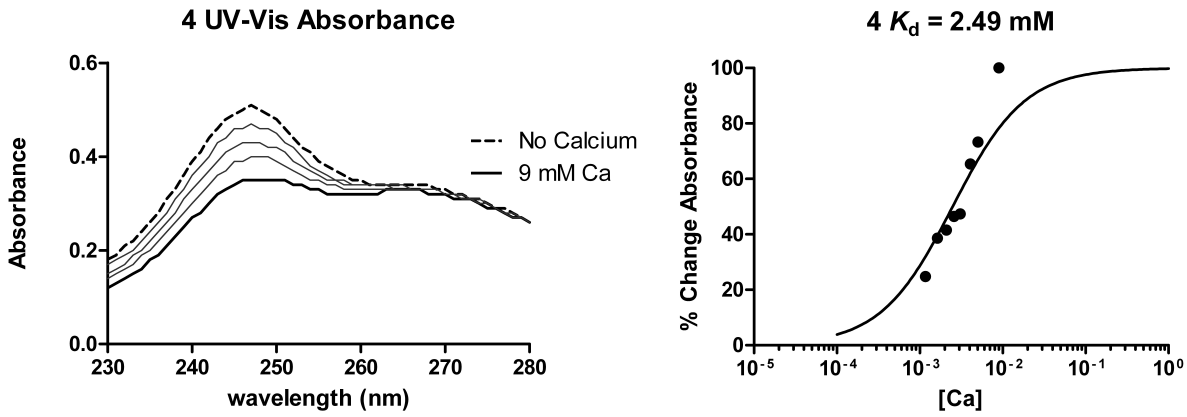

Method for determining magnesium binding dissociation constants (K_d): The free concentration of magnesium dication in solution was determined (equation 2). The total concentration of magensium in a measured solution was varied by combining different ratios of magnesium-containing solution and those without magnesium. The wavelength displaying the largest absorbance change was converted to percent change in absorbance and plotted versus the log of the concentration of free zinc. The K_d of the analog was then determined from the inflection point of the curve.

Solutions used for determination of magnesium binding dissociation constant (K_d):

Stock solution of magnesium: A stock solution of magnesium chloride hexahydrate (2.033 g, 10.0 mmol) was made in 7.0 pH HEPES buffer (250.0 mL) to form a magnesium chloride concentration of 0.04 M.

7.0 pH HEPES buffer solution: The 7.0 pH HEPES buffer was made from enzyme grade HEPES (23.83 g, 0.1 mol) in nano-pure water (1.0 L). The pH of the HEPES buffer was adjusted with sodium hydroxide (5.0 M) to 7.0 pH. The pH was measured using a probe, calibrated with 4.0 pH stock buffer solutions and 6.88 pH stock buffer solutions.

Stock solution of N-(hydroxyethyl)-ethylenediaminetriacetic acid: A solution of N-(hydroxyethyl)-ethylenediaminetriacetic acid (HEDTA, 181.1 mg, 1.00 mmol) was made in 7.0 pH HEPES buffer (100.0 mL) solution to form a HEDTA concentration of 10.0 mM.

Solutions of 4-((8-hydroxyquinolin-7-yl)(phenyl)methylamino)benzoic acid (1): A stock solution of NSC 1011 (9.3 mg, 25 μmol) was made in methanol (25.0 mL) to form a 1.0 mM concentration. From this stock solution two working solutions were prepared via dilutions. For the 10.0 μM **1**, 1.0 mM HEDTA, and 10.0 mM $MgCl_2$ solution, 1.0 mL of stock **1** solution, 10.0

mL of stock HEDTA solution, 25.0 mL of stock 0.04 M $MgCl_2$ solution, and 9.0 mL of methanol were combined in a 100 mL volumetric flask. The solution was then dilute with 7.0 pH HEPES buffer to fill. The working solution containing 10.0 μM **1** and 1.0 mM HEDTA was made in the same fashion excluding the addition of any $MgCl_2$ solution. For both working solutions a 1:9 ratio of methanol: HEPES aqueous solution was maintained.

Solutions of 4-((8-hydroxyquinolin-7-yl)(pyridin-2-yl)methylamino)benzoic acid (2): A stock solution of **2** (9.3 mg, 25 μmol) was made in methanol (25.0 mL) to form a 1.0 mM concentration. From this stock solution two working solutions were prepared via dilutions. For the 10.0 μM **2**, 1.0 mM HEDTA, and 10.0 mM $MgCl_2$ solution, 1.0 mL of stock **2** solution, 10.0 mL of stock HEDTA solution, 25.0 mL of stock 0.04 M $MgCl_2$ solution, and 9.0 mL of methanol were combined in a 100 mL volumetric flask. The solution was then dilute with 7.0 pH HEPES buffer to fill. The working solution containing 10.0 μM **2** and 1.0 mM HEDTA was made in the same fashion excluding the addition of any $MgCl_2$ solution. For both working solutions a 1:9 ratio of methanol: HEPES aqueous solution was maintained.

Solutions of 4-((8-hydroxyquinolin-7-yl)(*p*-tolyl)methylamino)benzoic acid (4): A stock solution of **4** (9.6 mg, 25 μmol) was made in methanol (25mL) to form a 1.0 mM concentration. From this stock solution two working solutions were prepared via dilutions. For the 10.0 μM **4**, 1.0 mM HEDTA, and 10.0 mM $MgCl_2$ solution, 1.0 mL of stock **4** solution, 10.0 mL of stock HEDTA solution, 25.0 mL of stock 0.04 M $MgCl_2$ solution, and 9.0 mL of methanol were combined in a 100 mL volumetric flask. The solution was then dilute with 7.0 pH HEPES buffer to fill. The working solution containing 10.0 μM **4** and 1.0 mM HEDTA was made in the same

fashion excluding the addition of any $MgCl_2$ solution. For both working solutions a 1:9 ratio of methanol: HEPES aqueous solution was maintained.

Solutions of 4-((4-bromophenyl)(8-hydroxyquinolin-7-yl)methylamino)benzoic acid (5): A stock solution of **5** (8.2 mg, 18 μmol) was made in methanol (25.0 mL) to form a 0.73 mM concentration. From this stock solution two working solutions were prepared via dilutions. For the 14.6 μM **5**, 1.0 mM HEDTA, and 10.0 mM $MgCl_2$ solution, 1.0 mL of stock **5** solution, 10.0 mL of stock HEDTA solution, 25.0 mL of stock 0.04 M $MgCl_2$ solution, and 9.0 mL of methanol were combined in a 100 mL volumetric flask. The solution was then dilute with 7.0 pH HEPES buffer to fill. The working solution containing 14.6 μM **5** and 1.0 mM HEDTA was made in the same fashion excluding the addition of any $MgCl_2$ solution. For both working solutions a 1:9 ratio of methanol: HEPES aqueous solution was maintained.

Method for determining manganese binding dissociation constants (K_d): The free concentration of manganese dication in solution was determined (Equation 2). The total concentration of manganese in a measured solution was varied by combining different ratios of manganese-containing solution and those without manganese. The UV-Vis absorption spectrum from 350 – 200 nm was obatined for each solution. The wavelength displaying the largest absorbance change was converted to percent change in absorbance and plotted versus the log of the concentration of free zinc. The K_d of the analog was then determined from the inflection point of the curve.

Solutions used for determination of manganese binding dissociation constant (K_d):

Stock solution of manganese: A stock solution of manganese chloride tetrahydrate (1.979 g, 10.0 mmol) was made in 7.0 pH HEPES buffer (250.0 mL) to form a manganese chloride concentration of 0.04 M.

7.0 pH HEPES buffer solution: The 7.0 pH HEPES buffer was made from enzyme grade HEPES (23.83 g, 0.1 mol) in nano-pure water (1.0 L). The pH of the HEPES buffer was adjusted with sodium hydroxide (5.0 M) to 7.0 pH. The pH was measured using a probe, calibrated with 4.0 pH stock buffer solutions and 6.88 pH stock buffer solutions.

Stock solution of nitriloacetic acid: A solution of nitrilotriacetic acid (NTA, 181.1 mg, 1.00 mmol) was made in 7.0 pH HEPES buffer (100.0 mL) solution to form a NTA concentration of 10.0 mM.

Solutions of 4-((8-hydroxyquinolin-7-yl)(phenyl)methylamino)benzoic acid (1): A stock solution of **1** (9.3 mg, 25 μmol) was made in methanol (25.0 mL) to form a 1.0 mM concentration. From this stock solution two working solutions were prepared via dilutions. For

the 10.0 μM **1**, 1.0 mM NTA, and 10.0 mM $MnCl_2$ solution, 1.0 mL of stock NSC 1011 solution, 10.0 mL of stock NTA solution, 25.0 mL of stock 0.04 M $MnCl_2$ solution, and 9.0 mL of methanol were combined in a 100 mL volumetric flask. The solution was then dilute with 7.0 pH HEPES buffer to fill. The working solution containing 10.0 μM **1** and 1.0 mM NTA was made in the same fashion excluding the addition of any $MnCl_2$ solution. For both working solutions a 1:9 ratio of methanol: HEPES aqueous solution was maintained.

Solutions of 4-((8-hydroxyquinolin-7-yl)(pyridin-2-yl)methylamino)benzoic acid (2): A stock solution of **2** (9.3 mg, 25 μmol) was made in methanol (25.0 mL) to form a 1.0 mM concentration. From this stock solution two working solutions were prepared via dilutions. For the 10.0 μM **2**, 1.0 mM NTA, and 10.0 mM $MnCl_2$ solution, 1.0 mL of stock **2** solution, 10.0 mL of stock NTA solution, 25.0 mL of stock 0.04 M $MnCl_2$ solution, and 9.0 mL of methanol were combined in a 100 mL volumetric flask. The solution was then dilute with 7.0 pH HEPES buffer to fill. The working solution containing 10.0 μM **2** and 1.0 mM NTA was made in the same fashion excluding the addition of any $MnCl_2$ solution. For both working solutions a 1:9 ratio of methanol: HEPES aqueous solution was maintained.

Solutions of 4-((8-hydroxyquinolin-7-yl)(*p*-tolyl)methylamino)benzoic acid (4): A stock solution of **4** (9.6 mg, 25 μmol) was made in methanol (25mL) to form a 1.0 mM concentration. From this stock solution two working solutions were prepared via dilutions. For the 10.0 μM **4**, 1.0 mM NTA, and 10.0 mM $MnCl_2$ solution, 1.0 mL of stock **4** solution, 10.0 mL of stock NTA solution, 25.0 mL of stock 0.04 M $MnCl_2$ solution, and 9.0 mL of methanol were combined in a 100 mL volumetric flask. The solution was then dilute with 7.0 pH HEPES buffer to fill. The working solution containing 10.0 μM **4** and 1.0 mM NTA was made in the same fashion

excluding the addition of any $MnCl_2$ solution. For both working solutions a 1:9 ratio of methanol: HEPES aqueous solution was maintained.

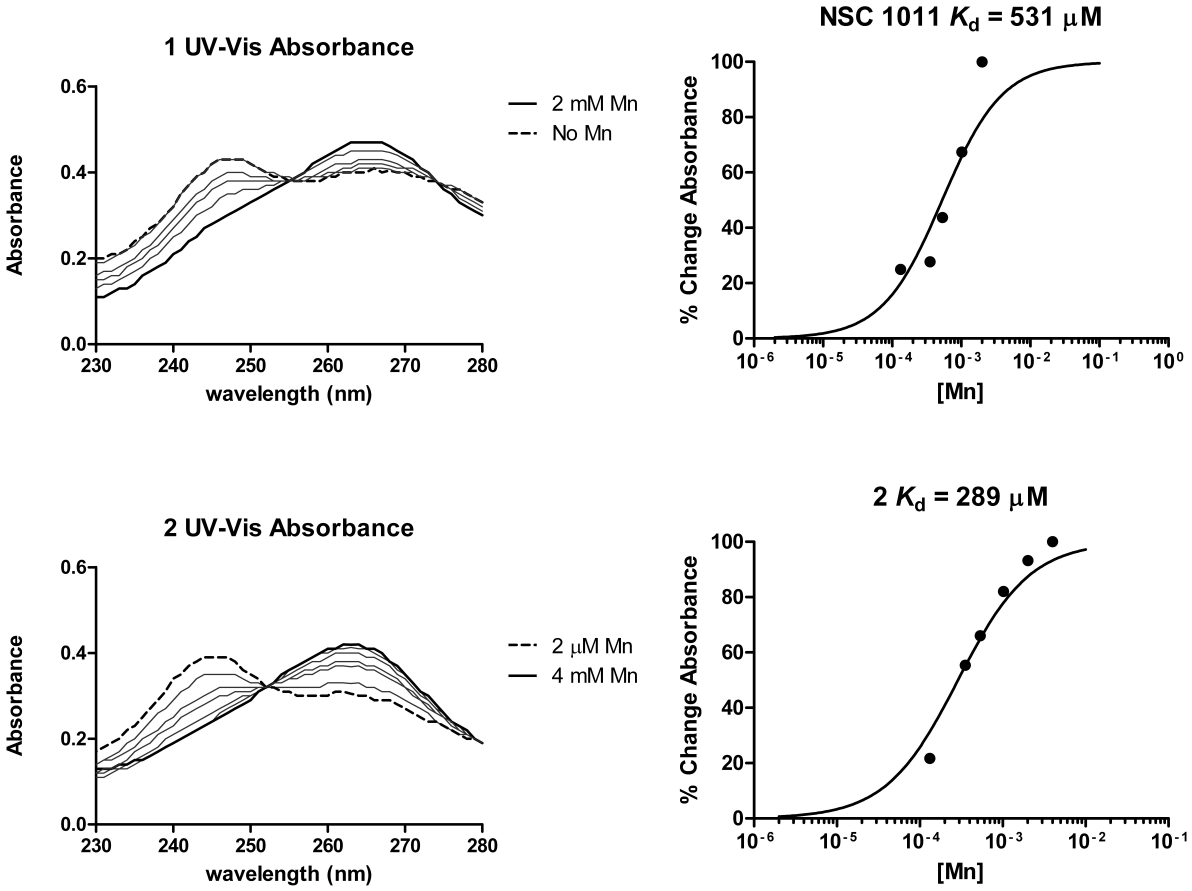

REFERENCES

(1) Adekoya, O. A.; Sylte, I., The Thermolysin Family (M4) of Enzymes: Therapeutic and Biotechnological Potential. *Chem. Biol. Drug Des.* **2009,** *73*, 7-16.

(2) Dangle, P. P.; Zaharieva, B.; Jia, H.; Pohar, K. S., Ras-MAPK pathways as a therapeutic target in cancer - emphasis on bladder cancer. *Recent Pat. Anti-Cancer Drug Discovery* **2009,** *4*, 125-136.

(3) Winter-Vann, A. M.; Casey, P. J., Post-prenylation-processing enzymes as new targets in oncogenesis. *Nat. Rev. Cancer* **2005,** *5*, 405-412.

(4) Konstantinopoulos, P. A.; Karamouzis, M. V.; Papavassiliou, A. G., Post-translational modifications and regulation of the RAS superfamily of GTPases as anticancer targets. *Nat. Rev. Drug Discovery* **2007,** *6*, 541-555.

(5) Tidyman, W. E.; Rauen, K. A., The RASopathies: developmental syndromes of Ras/MAPK pathway dysregulation. *Curr. Opin. Genet. Dev.* **2009,** *19*, 230-236.

(6) Takai, Y.; Sasaki, T.; Matozaki, T., Small GTP-binding proteins. *Physiol. Rev.* **2001,** *81*, 153-208.

(7) Eastburn, D. J.; Han, M., Ras signaling in C. elegans: a genetic overview. *Proteins and Cell Regul.* **2006,** *4*, 199-255.

(8) Young, A.; Lyons, J.; Miller, A. L.; Phan, V. T.; Alarcon, I. R.; McCormick, F., Ras signaling and therapies. *Adv. Cancer Res.* **2009,** *102*, 1-17.

(9) Voet, D.; Voet, J. G., *Biochemistry*. 3rd ed.; John Wiley & Sons, INC.: 2004.

(10) Mokry, D. Z.; Manandhar, S. P.; Chicola, K. A.; Santangelo, G. M.; Schmidt, W. K., Heterologous Expression Studies of *Saccharmoyces cerrevisiae* Reveal Two Distinct Tyrpanosomatid CaaX protease Activities and Identify Their Potential Targets. *Eukaryot. Cell* **2009,** *8*, 1891-1900.

(11) Young, S. G.; Ambroziak, P.; Kim, E.; Clarke, S., Postisoprenylation protein processing: CXXX (CaaX) endoproteases and isoprenylcysteinecarboxyl methyltransferase. In *The Enzymes*, Tamanoi, F.; Sigman, D. S., Eds. Academic Press: New York, 2001; pp 155–213.

(12) Reid, T. S.; Terry, K. L.; Casey, P. J.; Beese, L. S., Crystallographic Analysis of CaaX Prenyltransferases Complexed with Substrates Defines Rules of Protein Substrate Selectivity. *J. Mol. Biol.* **2004,** *343*, 417-433.

(13) Casey, P. J.; Seabra, M. C., Protein Prenyltransferases. *J. Biol. Chem.* **1996,** *271*, 5289-5292.

(14) Boyartchuk, V. L.; Ashby, M. N.; Rine, J., Modulation of Ras and a-Factor Function by Carboxyl-Terminal Proteolysis. *Science* **1997,** *275*, 1796-1800.

(15) Tam, A.; Nouvet, F. J.; Fujimura-Kamada, K.; Slunt, H.; Sisodia, S. S.; Michaelis, S., Dual roles for Ste24p in yeast a-factor maturation: NH_2-terminal proteolysis and COOH-terminal CAAX processing. *J. Cell Biol.* **1998,** *142*, 635-649.

(16) Sapperstein, S.; Berkower, C.; Michaelis, S., Nucleotide sequence of the yeast STE14 gene, which encodes farnesylcysteine carboxyl methyltransferase, and demonstration of its essential role in a-factor export. *Mol. Cell. Biol.* **1994,** *14*, 1438-1449.

(17) Dai, Q.; Choy, E.; Chiu, V.; Romano, J.; Steitz, S. R.; Steitz, S. A.; Michaelis, S.; Philips, M. R., Mammalian prenylcysteine carboxyl methyltransferase is in the endoplasmic reticulum. *J. Biol. Chem.* **1998,** *273*, 15030-15034.

(18) Michaelson, D.; Ali, W.; Chiu, V. K.; Bergo, M.; Silletti, J.; Wright, L.; Young, S. G.; Philips, M., Postprenylation CAAX processing is required for proper localization of Ras but not Rho GTPases. *Mol. Biol. Cell* **2005,** *16*, 1606-1616.

(19) Fehrenbacher, N.; Philips, M., Intracellular Signaling: Peripatetic Ras. *Curr. Biol.* **2009,** *19*, R454-R457.

(20) Saini, D. K.; Chisari, M.; Gautam, N., Shuttling and translocation of heterotrimeric G proteins and Ras. *Trends Pharmacol. Sci.* **2009,** *30*, 278-286.

(21) Sebti, S. M.; Hamilton, A. D., Farnesyltransferase and geranylgeranyltransferase I inhibitors and cancer therapy: lessons from mechanism and bench-to-bedside translational studies. *Oncogene* **2000,** *19*, 6584-6593.

(22) Bonne, G.; Di Barletta, M. R.; Varnous, S.; Becane, H.-M.; Hammouda, E.-H.; Merlini, L.; Muntoni, F.; Greenberg, C. R.; Gary, F.; Urtizberea, J.-A.; Duboc, D.; Fardeau, M.; Toniolo, D.; Schwartz, K., Mutations in the gene encoding lamin A/C cause autosomal dominant Emery-Dreifuss muscular dystrophy. *Nat. Genet.* **1999,** *21*, 285-288.

(23) Sullivan, T.; Escalante-Alcalde, D.; Bhatt, H.; Anver, M.; Bhat, N.; Nagashima, K.; Stewart, C. L.; Burke, B., Loss of A-type lamin expression compromises nuclear envelope integrity leading to muscular dystrophy. *J. Cell Biol.* **1999,** *147*, 913-919.

(24) Raharjo, W. H.; Enarson, P.; Sullivan, T.; Stewart, C. L.; Burke, B., Nuclear envelope defects associated with LMNA mutations cause dilated cardiomyopathy and Emery-Dreifuss muscular dystrophy. *J. Cell Sci.* **2001,** *114*, 4447-4457.

(25) Li, T.; Sparano, J. A., Farnesyl Transferase Inhibitors. *Cancer Invest.* **2008,** *26*, 653-661.

(26) Hrycyna, C. A.; Sapperstein, S. K.; Clarke, S.; Michaelis, S., The Saccharomyces cerevisiae STE14 gene encodes a methyltransferase that mediates C-terminal methylation of a-factor and RAS proteins. *EMBO J.* **1991,** *10*, 1699-1709.

(27) Bergo, M. O.; Gavino, B. J.; Hong, C.; Beigneux, A. P.; McMahon, M.; Casey, P. J.; Young, S. G., Inactivation of Icmt inhibits transformation by oncogenic K-Ras and B-Raf. *J. Clin. Invest.* **2004,** *113*, 539-550.

(28) Bergo, M. O.; Leung, G. K.; Ambroziak, P.; Otto, J. C.; Casey, P. J.; Young, S. G., Targeted inactivation of the isoprenylcysteine carboxyl methyltransferase gene causes mislocalization of K-Ras in mammalian cells. *J. Biol. Chem.* **2000,** *275*, 17605-17610.

(29) Schmidt, W. K.; Tam, A.; Fujimura-Kamada, K.; Michaelis, S., Endoplasmic reticulum membrane localization of Rce1p and Ste24p, yeast proteases involved in carboxyl-terminal CAAX protein processing and amino-terminal a-factor cleavage. *Proc. Natl. Acad. Sci. U. S. A.* **1998,** *95*, 11175-11180.

(30) Kim, E.; Ambroziak, P.; Otto, J. C.; Taylor, B.; Ashby, M.; Shannon, K.; Casey, P. J.; Young, S. G., Disruption of the mouse Rce1 gene results in defective Ras processing and mislocalization of Ras within cells. *J. Biol. Chem.* **1999,** *274*, 8383-8390.

(31) Bergo, M. O.; Lieu, H. D.; Gavino, B. J.; Ambroziak, P.; Otto, J. C.; Casey, P. J.; Walker, Q. M.; Young, S. G., On the Physiological Importance of Endoproteolysis of CAAX

Proteins: Heart-specific Rce1 knockout mice develop a lethal cardiomyopathy. *J. Biol. Chem.* **2004,** *279*, 4729-4736.

(32) Bergo, M. O.; Gavino, B.; Ross, J.; Schmidt, W. K.; Hong, C.; Kendall, L. V.; Mohr, A.; Meta, M.; Genant, H.; Jiang, Y.; Wisner, E. R.; Van Bruggen, N.; Carano, R. A. D.; Michaelis, S.; Griffey, S. M.; Young, S. G., Zmpste24 deficiency in mice causes spontaneous bone fractures, muscle weakness, and a prelamin A processing defect. *Proc. Natl. Acad. Sci. U. S. A.* **2002,** *99*, 13049-13054.

(33) Pendas, A. M.; Zhou, Z.; Cadinanos, J.; Freije, J. M. P.; Wang, J.; Hultenby, K.; Astudillo, A.; Wernerson, A.; Rodriguez, F.; Tryggvason, K.; Lopez-Otin, C., Defective prelamin A processing and muscular and adipocyte alterations in Zmpste24 metalloproteinase-deficient mice. *Nat. Genet.* **2002,** *31*, 94-99.

(34) Bergo, M. O.; Ambroziak, P.; Gregory, C.; George, A.; Otto, J. C.; Kim, E.; Nagase, H.; Casey, P. J.; Balmain, A.; Young, S. G., Absence of the CAAX endoprotease Rce1: effects on cell growth and transformation. *Mol. Cell. Biol.* **2002,** *22*, 171-181.

(35) Plummer, L. J.; Hildebrandt, E. R.; Porter, S. B.; Rogers, V. A.; McCracken, J.; Schmidt, W. K., Mutational Analysis of the Ras Converting Enzyme Reveals a Requirement for Glutamate and Histidine Residues. *J. Biol. Chem.* **2006,** *281*, 4596-4605.

(36) Ma, Y. T.; Gilbert, B. A.; Rando, R. R., Inhibitors of the isoprenylated protein endoprotease. *Biochemistry* **1993,** *32*, 2386-2393.

(37) Chen, Y.; Ma, Y.-t.; Rando, R. R., Solubilization, partial purification, and affinity labeling of the membrane-bound isoprenylated protein endoprotease. *Biochemistry* **1996,** *35*, 3227-3237.

(38) Dolence, J. M.; Steward, L. E.; Dolence, E. K.; Wong, D. H.; Poulter, C. D., Studies with Recombinant *Saccharomyces cerevisiae* CaaX Prenyl Protease Rce1p. *Biochemistry* **2000,** *39*, 4096-4104.

(39) Mitchell, J. K.; Pitcher, D.; McArdle, B. M.; Alnefelt, T.; Duffy, S.; Avery, V.; Quinn, R. J., Identifying common metalloprotease inhibitors by protein fold types using Fourier Transform Mass Spectrometry. *Bioorg. Med. Chem. Lett.* **2007,** *17*, 6521-6524.

(40) Zuniga, J. E.; Schmidt, J. J.; Fenn, T.; Burnett, J. C.; Araç, D.; Gussio, R.; Stafford, R. G.; Badie, S. S.; Bavari, S.; Brunger, A., A Potent Peptidomimetic Inhibitor of Botulinum Neurotoxin Serotype A Had a Very Different Conformation than SNAP-25 Substrate. *Structure* **2008,** *16*, 1588-1597.

(41) Pei, J.; Grishin, N. V., Type II CAAX prenyl endopeptidases belong to a novel superfamily of putative membrane-bound metalloproteases. *Trends Biochem. Sci.* **2001,** *26*, 275-277.

(42) Chen, Y., Inhibition of K-ras-transformed rodent and human cancer cell growth via induction of apoptosis by irreversible inhibitors of ras endoprotease. *Cancer Lett.* **1998,** *131*, 191-200.

(43) Chen, Y., Selective inhibition of ras-transformed cell growth by a novel fatty acid-based chloromethyl ketone designed to target ras endoprotease. *Ann. N. Y. Acad. Sci.* **1999,** *886*, 103-108.

(44) Matthews, B. W., Structural Basis of the Action of Thermolysin and Related Zinc Peptidases. *Acc. Chem. Res.* **1988,** *21*, 333-340.

(45) Gaucher, J. F.; Selkti, M.; Tiraboschi, G.; Prangé, T.; Roques, B. P.; Tomas, A.; Fournié-Zaluski, M. C., Crystal Structures of α-Mercaptoacyldipeptides in the Thermolysin Active Site: Structural Parameters for a Zn Monodentation or Bidentation in Metalloendopeptidases. *Biochemistry* **1999,** *38*, 12569-12576.

(46) Ksander, G. M.; de Jesus, R.; Yuan, A.; Ghai, R. D.; Trapani, A.; McMartin, C.; Bohacek, R., Ortho-Substituted Benzofused Macrocyclic Lactams as Zinc Metalloprotease Inhibitors. *J. Med. Chem.* **1997,** *40*, 495-505.

(47) Manandhar, S. P.; Hildebrandt, E. R.; Schmidt, W. K., Small-molecule inhibitors of the Rce1p CaaX protease. *J. Biomol. Screen* **2007,** *12*, 983-993.

(48) Dolence, E. K.; Dolence, J. M.; Poulter, C. D., Solid-Phase Synthesis of a Farnesylated CaaX Peptide Library: Inhibitors of the Ras CaaX Endoprotease. *J. Comb. Chem.* **2000,** *2*, 522-536.

(49) Craig, K. S.; Williams, D. E.; Hollander, I.; Frommer, E.; Mallon, R.; Collins, K.; Wojciechowicz, D.; Tahir, A.; Van Soest, R.; Andersen, R. J., Novel sesterterpenoid and norsesterterpenoid RCE-protease inhibitors isolated from the marine sponge *Hippospongia* sp. *Tetrahedron Lett.* **2002,** *43*, 4801-4804.

(50) Schlitzer, M.; Winter-Vann, A.; Casey, P. J., Non-peptidic, non-prenylic inhibitors of the prenyl protein-specific protease Rce1. *Bioorg. Med. Chem. Lett.* **2001,** *11*, 425-427.

(51) Porter, S. B.; Hildebrandt, E. R.; Breevort, S. R.; Mokry, D. Z.; Dore, T. M.; Schmidt, W. K., Inhibition of the CaaX proteases Rce1p and Ste24p by peptidyl (acyloxy)methyl ketones. *Biochim. Biophys. Acta* **2007,** *1773*, 853-862.

(52) Wu, X.; Fang, G.; Liu, Q.; Wang, J.; Wu, S., Synthesis of L-651582. *Zhongguo Yiyao Gongye Zazhi* **2006,** *37*, 147-149.

(53) Desai, A. A.; Innocenti, F.; Janisch, L.; DeMario, M.; Shepard, D.; Ramirez, J.; Fleming, G. F.; Ratain, M. J., A phase I trial of pharmacokinetic modulation of carboxyamidotriazole (CAI) with ketoconazole in patients with advanced cancer. *Cancer Chemother. Pharmacol.* **2004,** *54*, 377-384.

(54) Ge, S.; Rempel, S. A.; Divine, G.; Mikkelsen, T., Carboxyamido-triazole induces apoptosis in bovine aortic endothelial and human glimoa cells. *Clin. Cancer Res.* **2000,** *6*, 1248-1254.

(55) Kohn, E. C.; Sandeen, M. A.; Liotta, L. A., In vivo efficacy of a novel inhibitor of selected signal transduction pathways including calcium, arachidonate, and inositol phosphates. *Cancer Res.* **1992,** *52*, 3208-3212.

(56) Felder, C. C.; Ma, A. L.; Liotta, L. A.; Kohn, E. C., The antiproliferative and antimetastatic compound L651582 inhibits muscarinic acetylcholine receptor-stimulated calcium influx and arachidonic acid release. *J. Pharmacol. Exp. Ther.* **1991,** *257*, 967-971.

(57) Kohn, E. C.; Liotta, L. A., L651582: a novel antiproliferative and antimetastasis agent. *J. Natl. Cancer Inst.* **1990,** *82*, 54-60.

(58) Hupe, D. J.; Boltz, R.; Cohen, C. J.; Felix, J.; Ham, E.; Miller, D.; Soderman, D.; Van Skiver, D., The inhibition of receptor-mediated and voltage-dependent calcium entry by the antiproliferative L-651,582. *J. Biol. Chem.* **1991,** *266*, 10136-10142.

(59) Bond, A.; Reichert, Z.; Stivers, J. T., Novel and specific inhibitors of a poxvirus type I topoisomerase. *Mol. Pharmacol.* **2006,** *69*, 547-557.

(60) Phillips, J. P.; Barrall, E. M., Betti reactions of some phenols. *J. Org. Chem.* **1956,** *21*, 692-694.

(61) Betti, M., Condensation between beta-naphthol, aldehydes, and amines. II. Synthesis of oxazine derivatives. *Gazz. Chim. Ital.* **1901,** *31*, 377-393.

(62) Brode, W. R.; Littman, J. B., Condensations of secondary amines with naphthols and aldehydes. II. *J. Am. Chem. Soc.* **1931,** *53*, 1531-1532.

(63) Littman, J. B.; Brode, W. R., Condensation of secondary amines with aldehydes and naphthols. *J. Am. Chem. Soc.* **1930,** *52*, 1655-1659.

(64) Sharma, P. K.; Khanna, R. N., Photo-*Fries* Rearrangement: Rearrangement of Benzoyloxy Compounds. *Monatsh. Chem.* **1985,** *116*, 353-356.

(65) Gholizadeh, M., A Study of Probing the Mechanism of Acylation Reactions and Fries Rearrangement by Polyphosphoric acid (PPA). *Int. J. Appl. Chem.* **2007,** *3*, 139-144.

(66) Phillips, J. P., The Reactions of 8-Quinolinol. *Chem. Rev.* **1956,** *56*, 271-297.

(67) Deraeve, C.; Maraval, A.; Vendier, L.; Faugeroux, V.; Pitié, M.; Meunier, B., Preparation of New Bis(8aminoquinoline) Ligands and Comparison with Bis(8-hydroxyquinoline) Ligands on Their Ability to Chelate Cu^{II} and Zn^{II}. *Eur. J. Inorg. Chem.* **2008**, 5622-5631.

(68) Sugawara, K. F.; Weetall, H. H.; Schucker, G. D., Preparation, Properties, and Applications of 8-Hydroxyquinoline Immobilized Chelate. *Anal. Chem.* **1974,** *46*, 489-492.

(69) Pierre, J.-L.; Baret, P.; Serratrice, G., Hydroxyquinolines as Iron Chelators. *Curr. Med. Chem.* **2003,** *10*, 1077-1084.

(70) Tsien, R. Y., New Calcium Indicators and Buffers with High Selectivity against Magnesium and Protons: Design, Synthesis, and Properties of Prototype Structures. *Biochemistry* **1980,** *19*, 2396-2404.

(71) Melton, J. R.; Kantzas, A.; Langford, C. H., Nuclear magnetic resonance relaxometry as a spectroscopic probe of the coordination sphere of a paramagnetic metal bound to a humic acid mixture. *Anal. Chim. Acta* **2007,** *605*, 46-52.

(72) Jensen, M. R.; Hass, M. A. S.; Hansen, D. F.; Led, J. J., Investigating metal-binding in proteins by nuclear magnetic resonance. *Cell. Mol. Life Sci.* **2007,** *64*, 1085-1104.

(73) Tsien, R. Y., New calcium indicators and buffers with high selectivity against magnesium and protons: design, synthesis, and properties of prototype structures. *Biochemistry* **1980,** *19*, 2396-2404.

(74) Nowicka-Jankowska, T., Some Properties of Isosbestic Points. *J. Inorg. Nucl. Chem.* **1971,** *33*, 2043-2050.

(75) Izumi, S.; Urano, Y.; Hanaoka, K.; Terai, T.; Nagano, T., A Simple and Effective Strategy To Increase the Sensitivity of Fluorescence Probes in Living Cells. *J. Am. Chem. Soc.* **2009,** *131*, 10189-10200.

(76) Hollander, I.; Frommer, E.; Mallon, R., Human Ras-Converting Enzyme (hRCE1) Endoproteolytic Activity on K-Ras-Derived Peptides. *Anal. Biochem.* **2000,** *286*, 129-137.